

Fall 2012

Quantitation and identification of protein S-nitrosylation: Implication for the progression of Alzheimer's disease

Siyang Wang

Follow this and additional works at: <https://digitalcommons.latech.edu/dissertations>

 Part of the [Biomedical Engineering and Bioengineering Commons](#)

**QUANTITATION AND IDENTIFICATION OF PROTEIN
S-NITROSYLATION: IMPLICATION FOR THE
PROGRESSION OF ALZHEIMER'S DISEASE**

by

Siyang Wang, B.S., M.S.

A Dissertation Presented in Partial Fulfillment
of the Requirements of the Degree
Doctor of Philosophy

COLLEGE OF ENGINEERING AND SCIENCE
LOUISIANA TECH UNIVERSITY

November 2012

UMI Number: 3536679

All rights reserved

INFORMATION TO ALL USERS

The quality of this reproduction is dependent upon the quality of the copy submitted.

In the unlikely event that the author did not send a complete manuscript and there are missing pages, these will be noted. Also, if material had to be removed, a note will indicate the deletion.



UMI 3536679

Published by ProQuest LLC 2013. Copyright in the Dissertation held by the Author.

Microform Edition © ProQuest LLC.

All rights reserved. This work is protected against unauthorized copying under Title 17, United States Code.



ProQuest LLC
789 East Eisenhower Parkway
P.O. Box 1346
Ann Arbor, MI 48106-1346

LOUISIANA TECH UNIVERSITY

THE GRADUATE SCHOOL

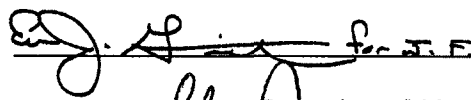
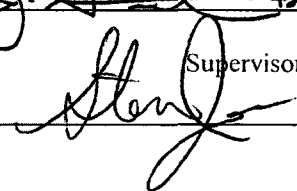
JULY 23, 2012

Date

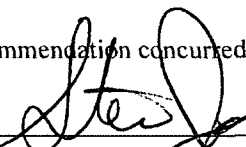


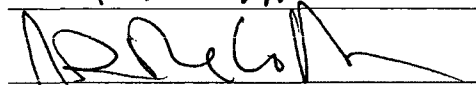
We hereby recommend that the Dissertation prepared under our supervision by
Siyang Wang, B. S., M. S.

Entitled Quantitation and Identification of Protein S-Nitrosylation: Implication
for the Progression of Alzheimer's Disease

be accepted in partial fulfillment of the requirements for the Degree of
Ph. D. in Biomedical Engineering

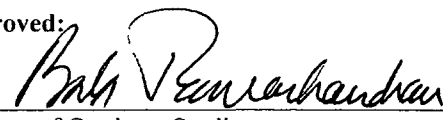

Supervisor of Dissertation Research

Head of Department
Department

Recommendation concurred in:

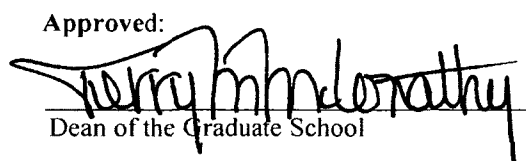





Advisory Committee

Approved:


Director of Graduate Studies

Approved:


Dean of the Graduate School


Dean of the College

ABSTRACT

Protein S-nitrosylation, the covalent modification of a cysteine sulfhydryl group by nitric oxide (NO), plays a critical role in post-translational modification (PTM) that regulates a large variety of cellular functions and signalling events. The nitrosylation state changes with oxidative damage and is involved in variety of cancers and neurodegeneration diseases.

Three technologies were developed for nitrosylated protein detection and identification. Capillary gel electrophoresis with laser induced fluorescence (CGE-LIF) detection was used for the detection and quantitation of nitrosylated proteins. A two-dimensional micro-electrophoresis (2D μ -CE) separations system was also built to detect nitrosylated proteins via poly (methylmethacrylate) microchips. Proteomics following nitrosylated proteins enrichment was used for identification of protein S-nitrosylation.

The CGE-LIF method, with a limit detection of 1.3 picomolar (pM) concentration of nitrosothiols in nanograms of proteins, is the lowest limit of detection of nitrosothiols reported to date. Dylight 488 maleimide was used to specifically label thiol group (SH) after switching the S-nitrosothiol (S-NO) to SH in cysteine using the “fluorescence switch” assay. *In vitro* nitrosylation model-BSA subjected to S-nitrosoglutathione (GSNO) optimized the labeling reactions and characterized the response of the LIF detector. The direct application of this method was demonstrated in monitoring protein nitrosylation damage in menadione (MQ) mediated human colon adenocarcinoma cells

(HT-29). The nitrosothiol amounts in 200 μ M MQ treated and untreated cells are 14.8 ± 0.2 and 10.4 ± 0.5 pmol/mg of proteins, respectively. In addition, also depicted are nitrosylated protein electrophoretic profiles of brain cerebrum of five-month-old AD transgenic (Tg) mice model. In the Tg mice brain, 15.5 ± 0.4 pmol of nitrosothiols/mg of proteins was quantified while the wild type contained 11.7 ± 0.3 pmol/mg proteins. The methodology is validated to quantify low levels of S-nitrosylated protein in complex protein mixtures from both physiological and pathological conditions.

Compared with the conventional protein separation method, microfluidics has been widely used for development of novel tools for separation of protein mixtures. Sodium dodecyl sulphate micro-capillary gel electrophoresis (SDS μ -CGE) and microemulsion electrokinetic chromatography (MEEKC) were used for the 1D and 2D separations, respectively. The effective separation lengths for both dimensions were ten mm, and electrokinetic injection was used with field strength at 200V/cm. After 80 seconds separation in the 1D CGE, fractions were successfully transferred to a second MEEKC dimension for a short ten-seconds separation. This 2D μ -CE separation was first demonstrated by resolving five standard proteins with a molecular weight (MW) ranging from 20 to 64 kDa. A high peak capacity 3D landscape image of nitrosylated proteins from HT-29 cells before and following MQ treatment to induce oxidative stress is also presented. Additionally, to illustrate the potential of the 2D μ -CE separation method for rapid profiling of oxidative stress-induced biomarkers implicated in AD disease, the nitrosylated protein fingerprints from 11-month-old AD transgenic mice brain and its age matched control were also generated. This is the first known report on 2D profiling of nitrosylated proteins in the biological samples on the microchip. The

characteristics of this biomarker profiling will potentially serve as the screening for early detection of AD.

The proteomics study revealed protein S-nitrosylation in the MQ treated human colon adenocarcinoma, HT-29 cells. Its profile of S-nitrosylated proteins was compared to a control cell line not exposed to MQ. A total of 20 proteins were modified by nitrosylation in MQ-treated HT-29 cells and at least ten nitrosylated proteins were increased by exposure to MQ. Seventeen of the 20 proteins are novel targets of S-nitrosylation not previously reported. These proteins include cytoskeletal and signaling proteins, metabolic enzymes, chaperones, and redox-and differentiation-related proteins. These results broaden knowledge of therapy targets.

APPROVAL FOR SCHOLARLY DISSEMINATION

The author grants to the Prescott Memorial Library of Louisiana Tech University the right to reproduce, by appropriate methods, upon request, any or all portions of this Dissertation. It is understood that "proper request" consists of the agreement, on the part of the requesting party, that said reproduction is for his personal use and that subsequent reproduction will not occur without written approval of the author of this Dissertation. Further, any portions of the Dissertation used in books, papers, and other works must be appropriately referenced to this Dissertation.

Finally, the author of this Dissertation reserves the right to publish freely, in the literature, at any time, any or all portions of this Dissertation.

Author Siggy Wgy

Date 10/23/2012

DEDICATION

This dissertation is dedicated to my parents, Lijun Wang and Lijuan Song.

TABLE OF CONTENTS

ABSTRACT.....	iii
DEDICATION.....	vii
LIST OF TABLES.....	xiii
LIST OF FIGURES.....	xiv
ACKNOWLEDGMENTS.....	xvi
CHAPTER 1 INTRODUCTION.....	1
1.1 Central Hypothesis.....	1
1.2 Aims.....	2
1.3 Outline.....	3
CHAPTER 2 BACKGROUND.....	4
2.1 Protein S-nitrosylation.....	4
2.1.1 Post-translational Modifications.....	4
2.1.2 Formation of Protein S-nitrosothiols.....	4
2.1.3 Techniques for Measuring Protein S-nitrosothiols.....	5
2.1.4 Techniques for Identification of Nitrosylated Proteins.....	7
2.2 Protein Separation.....	10
2.2.1 Capillary Gel Electrophoresis for Analysis of Proteins.....	10
2.2.2 Microchip Separation.....	10
2.3 Protein Identification.....	11
2.3.1 Top-Down Strategy.....	12

2.3.2	Bottom-Up Strategy	12
2.3.3	Peptide Preparation	13
2.3.4	Mass Spectrometry Analysis.....	13
CHAPTER 3 HIGHLY SENSITIVE DETECTION OF S-NITROSYLATED PROTEINS BY CAPILLARY GEL ELECTROPHORESIS WITH LASER INDUCED FLUORESCENCE.....		15
3.1	Introduction.....	15
3.2	Material and Methods	17
3.2.1	Materials and Reagents	17
3.2.2	Capillary Electrophoresis with Laser Induced Fluorescence Detection	18
3.2.3	<i>In Vitro</i> Nitrosylation of BSA and SNO quantification by Saville-Griess Assay.....	18
3.2.4	Cell Culture and Incubation with MQ	19
3.2.5	Protein Extraction from MQ Treated Cells.....	19
3.2.6	Isolation of Brain Cerebrum from AD Transgenic Mice Model	20
3.2.7	Fluorescence Switch Assay.....	20
3.2.8	Data Analysis for CE	22
3.2.9	Validation of Nitrosylated Proteins CE Peaks Using Proteomics	22
3.3	Results and Discussion	24
3.3.1	Fluorescence Switch Assay Coupled with CGE-LIF.....	24
3.3.2	Selectivity and Specificity of the Fluorescence Switch Assay	26
3.3.3	Calibration of CGE-LIF Method with Nitrosothiol BSA Standard	28
3.3.4	Monitoring Nitrosylation in MQ-mediated Cells	29
3.3.5	Monitoring Nitrosylation in AD Tg Mice Brain.....	31
3.3.6	Detection of S-nitrosylated Proteins in HT-29 Cells	33
3.3.7	Repeatability and Precision of CGE-LIF	35

3.4	Conclusions.....	38
CHAPTER 4 TWO-DIMENSIONAL NITROSYLATED PROTEIN FINGERPRINTING BY USING POLY (METHYLMETHACRYLATE) CHIPS.....		
4.1	Introduction.....	39
4.2	Material and Methods	42
4.2.1	Materials and Reagents	42
4.2.2	Microchip Fabrication.....	43
4.2.3	LIF Detection and Data Acquisition	44
4.2.4	Standard Proteins Fluorescence Labelling.....	46
4.2.5	Isolation of Brain Tissue from AD Transgenic Mice Model	46
4.2.6	Fluorescence Switch Assay.....	47
4.2.7	μ -CE (1D) Microchip Operation	47
4.3	Results and Discussion	49
4.3.1	Assessment of Sample Transfer Starting Time and CGE-to-MEEKC Transfer Cycles.....	50
4.3.2	μ -CGE (1D) and μ -MEEKC (1D) Separation of Standard Proteins.....	51
4.3.3	μ -CGE/MEEKC Separation (2D) of Standard Proteins	53
4.3.4	μ -CGE (1D) of Nitrosylated Proteins from HT-29 Cells	55
4.3.5	μ -CGE/ μ -MEEKC (2D) Nitrosylated Protein Fingerprint from HT-29 Cells.....	56
4.3.6	Nitrosylated Protein Fingerprint (2D) from 11-month-old AD Mice Brain.....	59
4.4	Conclusions.....	62
CHAPTER 5 IDENTIFICATION OF S-NITROSYLATED PROTEINS AFTER EXPOSURE OF HUMAN COLON ADENOCARCINOMA CELLS TO MENADIONE.....		
5.1	Introduction.....	64

5.2	Material and Methods	68
5.2.1	Materials and Reagents	68
5.2.2	<i>In Vitro</i> Nitrosylation of BSA and SNO Quantification by Saville-Griess Assay.....	70
5.2.3	Labelling of S-nitrosylated Proteins by the Biotin Switch Assay.....	69
5.2.4	Purification of S-nitrosylated Proteins for Proteomics	70
5.2.5	Analysis by LC-MS/MS	71
5.3	Results.....	72
5.3.1	Proteomic Analysis of S-nitrosylated Proteins in MQ Treated HT-29 Cells.....	73
5.3.2	Identification of Biotin Modification Sites in MQ Treated HT-29 Cells	77
5.4	Discussion.....	82
5.4.1	Signaling Proteins	84
5.4.2	Chaperones.....	85
5.4.3	Metabolism	85
5.4.4	Post-translational Modification.....	86
5.4.5	Translation	87
5.4.6	Regulation of the Colloidal Osmotic Pressure of Blood.....	87
5.4.7	Cytoskeleton Proteins	88
5.5	Conclusions.....	88
CHAPTER 6 CONCLUSIONS AND FUTURE WORK		89
6.1	Conclusions.....	89
6.2	Future Work	90
6.2.1	PCA Analysis for Future Direction.....	91
6.2.2	Estimating S-Nitrosylation Levels by Fluorescence Imaging	91
6.2.3	Integrated Microfluidic Systems with Proteomics.....	92

REFERENCES 93

LIST OF TABLES

Table 3-1: S-nitrosylated proteins from MQ treated HT-29 cells identified by (ESI) MS/MS.	34
Table 4-1: Summary of high-voltage protocol for 2D separations on a PMMA microchip	49
Table 5-1: S-nitrosylated proteins identified by LC-MS/MS in HT-29 cells preincubated with MQ.	73
Table 5-2: S-nitrosylated proteins identified by LC-MS/MS analysis in untreated HT-29 cells.....	76
Table 5-3: S-nitrosylated proteins identification of biotin modification sites in MQ treated HT-29 cells.	78

LIST OF FIGURES

Figure 1-1:	The general goals and specific aims for this dissertation.....	2
Figure 2-1:	Four major mechanisms to form protein S-nitrosylation.....	5
Figure 3-1:	Schematic of fluorescence switch assay coupled with CGE-LIF for detecting and quantifying S-nitrosylated proteins. Fluorescence switch assay (Steps 1-3) includes blocking thiol group by MMTS, reducing nitrosothiol group with ascorbate and labeling reduced free thiol by Dylight 488 maleimide. Finally, labeled proteins are separated and analyzed by CGE-LIF.	22
Figure 3-2:	CGE-LIF separation of nitrosylated BSA labeled with Dylight 488 maleimide. Separation, -570V/cm; hydrodynamic injection, 11kpa, 4s; sieving matrix, 20mM Tris, 20mM Tricine, 0.5% SDS, 15% dextran (65.5kDa), pH 8. Top trace and middle trace are offset on the y-axis for clarity. * — Dylight 488 maleimide, ^ — nitrosylated BSA.....	26
Figure 3-3:	Electropherograms of a series of dilution (1-, 2-, 4-, 10-fold) of nitrosylated BSA labeled with Dylight 488 maleimide. Other conditions are the same as in Figure 3-2. *—Dylight 488 maleimide, ^—nitrosylated BSA.	28
Figure 3-4:	Electropherograms of extracted proteins from HT29 cells after fluorescence switch assay. Top and bottom traces represent MQ treated and untreated, respectively. All the experimental conditions are the same as in Figure3-2. Top trace is offset in the y-axis for the clarity. *—Dylight 488 maleimide; migration window between a and b indicated nitrosylated proteins.	30
Figure 3-5:	Electropherograms of cerebrum from five-month-old transgenic (upper trace) and wild type (bottom trace) mice brain tissue. All the experimental conditions are the same as in Figure3-2. Top trace is offset in the y-axis for the clarity. *—Dylight 488 maleimide; migration window between a and b indicated nitrosylated proteins.....	31
Figure 3-6:	MS/MS peptide spectra of nucleolin (a and b) and isoform 1 of vinculin (c and d).	37

Figure 4-1: Topography of the micro-electrophoresis chip used for the 2D separations.....	43
Figure 4-2: Diagram of the in-house constructed LIF system used for these dissertation.	45
Figure 4-3: Background signal generated by Dylight 488 maleimide.....	45
Figure 4-4: 1D separation (SDS μ -CGE) of dye (Dylight 488 maleimide) using the PMMA microchip.	51
Figure 4-5: Plot of the logarithm of molecular mass versus corresponding migration times of the SDS μ -CGE separation of five standard proteins ranging in MW from 20-66 kDa.	52
Figure 4-6: MEEKC separation of five standard proteins.	53
Figure 4-7: Landscape image from five standard proteins. (A) Contour image for the microchip 2D SDS μ -CGE $\times\mu$ -MEEKC separation profile of five standard proteins. The density in this plot is proportional to the fluorescence intensity. (B) Corresponding microchip 2D SDS μ -CGE $\times\mu$ -MEEKC separation. The height of the peak is proportional to the fluorescence intensity.....	54
Figure 4-8: SDS μ -CGE analysis (1D separation) of HT-29 cells using a PMMA microchip.	56
Figure 4-9: Protein landscape image from HT-29 cells. Panel A is the contour image from 2D separation profile of nitrosylated protein extracted from HT-29 cells. Panel B presents the corresponding 3D landscape image for the 2D contour image. Panels C and D show the corresponding 2D protein nitrosylation separation images from cells that had been treated with 200 μ M MQ for 30 min.....	51
Figure 4-10: 2D separation landscape images of the nitrosylated proteins from AD transgenic mice and age matched wild type control. Panels A and B were generated from 11-month-old AD transgenic mouse brain tissues. Panels C and D were generated from age related wild type control.	60
Figure 5-1: The potential damage MQ induced in cells.	68
Figure 5-2: Schematic of the biotin switch assay technique following the track of protein S-nitrosylation.	70
Figure 5-3: The MS/MS spectra of protein S100 A10.....	79

Figure 5-4: The MS/MS spectra of Glutathione S transferase.....	79
Figure 5-5: The MS/MS spectra of Enlogation factor 2.....	80
Figure 5-6: The MS/MS spectra of Putative heat shock 70 kDa protein 7.....	80
Figure 5-7: The MS/MS spectra of 40S ribosomal protein S20.....	80
Figure 5-8: The MS/MS spectra of Serum albumin (Human).....	81
Figure 5-9: The MS/MS spectra of Heterogeneous nuclear ribonucleoprotein U.....	81
Figure 5-10: The MS/MS spectra of L lactate dehydrogenase A chain.....	81
Figure 5-11: The MS/MS spectra of Actin cytoplasmic 1.....	82
Figure 5-12: The MS/MS spectra of Phosphoglycerate kinase 1.....	82
Figure 6-1: General picture of the protein S-nitrosylation study in AD Tg mice brain tissue and MQ treated HT-29 cells.	92

ACKNOWLEDGMENTS

First, I would like to express my profound appreciation to my advisor, Dr. June Feng, who has offered me the golden opportunity to do research with her guidance, support and wisdom. During the past three years, her willingness to try new things provided me the opportunity to apply a variety of important tools of modern biomedical engineering. Without working in her group, I could hardly imagine learning all of these techniques in a single laboratory.

Second, I thank my parents, Lijun Wang and Lijuan Song, for their love and support in my quest for higher education and pursuit of my goals. My special thanks go to my husband, Gang Chen, for his love and endless support in my life and my professional growth.

Third, I am grateful to work with all the collaborators in my research career. I learned cell culture and western blot techniques in Dr. Tak Y. Aw's lab (LSUHSC, Shreveport). Also, I learned how to set up the 2D μ -CE system in Dr. Steven A. Soper's lab (LSU, Baton Rouge) during the two-month summer research program. Dr. Indu Kheterpal (LSU, Baton Rouge) helped us do the mass spectrometry analysis for our samples. Without their technical support and suggestions, my research would have been nearly unbearable and impractical.

Fourth, I thank all my group members, Drs. Bryant C. Hollins, Cheng Zhang and Hui Xia, who were willing to share my frustration and joys during the past three years.

Finally, I acknowledge all of the Department of Biomedical Engineering faculty members, especially my committee members, Drs. Mark A. Decoster, Steven A. Jones and Eric J. Guilbeau for their guidance and for serving on my advisory committee for this dissertation.

CHAPTER 1

INTRODUCTION

1.1 Central Hypothesis

The central hypothesis in this dissertation is that oxidative-stress induced protein S-nitrosylation profiling increases in both biological brain tissues and cells. A corollary is that an increase in nitrosylated protein levels is higher in Alzheimer's disease (AD) transgenic mice brain tissues than in the wide type controls. A second corollary is that MQ-treated HT-29 cells show more protein S-nitrosylation than untreated cells.

First, the hypothesis was tested using AD transgenic mice model (B6Cg-Tg). Carrying both the Swedish amyloid precursor protein mutation (APP) and exon 9 deletion of the PSEN1 gene, the B6Cg-Tg mouse is a valuable model to study the pathological alterations in AD. It always develops amyloid plaques at six to seven months of age. Second, oxidative protein nitrosylation damage mediated by menadione (MQ), a redox cycling quinone in human colon adenocarcinoma cells (HT-29) was monitored.

Three technology needs were addressed: (i) Detecting and quantifying nitrosylated proteins by capillary gel electrophoresis with laser induced fluorescence detection (CGE-LIF), (ii) Using the 2D micro-electrophoresis method for the separation of complex protein samples and detection of nitrosylated protein biomarkers using a poly (methylmethacrylated) (PMMA) microchip, and (iii) Identifying of nitrosylated proteins.

1.2 Aims

The overall goal of this dissertation was to quantify and identify the major nitrosylated proteins as oxidative stress biomarkers in Alzheimer's disease (AD) transgenic mice model (B6Cg-Tg) and HT-29 cells. Specifically, this goal could be divided into three main specific aims (Figure 1-1):

(i) Develop a quantitative method to detect and quantify nitrosylated proteins (S-NO) from MQ-treated HT-29 cells and AD transgenic mice cerebrum using the CGE-LIF instrument.

(ii) Perform 2D separation of nitrosylated proteins from MQ-treated HT-29 cells and AD transgenic mice brain tissue by using in-house laser-induced fluorescence detection system.

(iii) Identify nitrosylated proteins of MQ-treated HT-29 cells via a proteomic method.

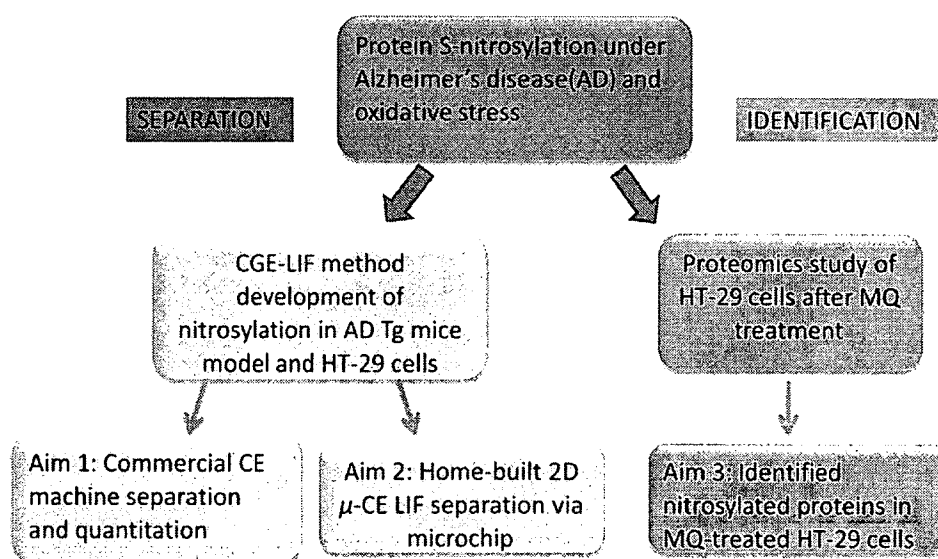


Figure 1-1: The general goals and specific aims.

1.3 Outline

This dissertation consists of six chapters. Background (Chapter 2) reviews the general understanding of different areas, including free radical theory, protein S-nitrosylation, analytical techniques, and mass spectrometry. In Chapter 3, a quantitative method was developed to detect the nitrosothiol content in biological samples based on capillary gel electrophoresis with laser induced fluorescence detection (CGE-LIF). Chapter 4 describes an in-house built LIF system to detect S-nitrosothiols in complex biological samples. This separation is based on 2D micro-electrophoresis method by using PMMA microchips. Chapter 5 describes a proteomic strategy, based on affinity enrichment of nitrosylated proteins to identify protein S-nitrosothiols in the MQ-treated HT-29 cells. Results found ten nitrosylated proteins increasing in the MQ-treated HT-29 cells compared to the untreated ones. Finally, Chapter 6 summarizes the findings of Chapters 3, 4, and 5. It also makes suggestions for future directions in oxidative stress induced biomarker development.

CHAPTER 2

BACKGROUND

2.1 Protein S-nitrosylation

2.1.1 Post-translational Modifications

Post-translational modifications (PTMs) are defined as the series of chemical reactions whereby a newly synthesized polypeptide chain is converted to a functional protein. A common characteristic of PTMs is that the accompanying change in amino acid structure produces the corresponding change in the formula weight of that amino acid relative to the original, unmodified residue.

Protein S-nitrosylation is one of the most commonly studied post-translational modifications. Nitrosylated proteins have become the biomarkers of oxidative damage under conditions of oxidative stress, aging and disease.

Researchers have shown that protein S-nitrosothiols content has been previously reported in organs, including brain tissue, kidney, liver, lung [1-4]. Other reports identify nitrosylated proteins in different types of cells, such as mesangial, vascular smooth muscle, endothelial and HeLa cells [5-8].

2.1.2 Formation of Protein S-nitrosothiols

There are four major mechanisms to potentially form the nitrosothiol (SNO) group in a biological system (Figure 2-1): (1) Nitric oxide (NO) can react with O₂ to

form dinitrogen trioxide (N_2O_3), which is considered to be the main S-nitrosylating species due to its powerful electrophilicity[9]. (2) Peroxynitrite (ONOO^-), the product between NO and superoxide (O_2^-), can react with thiols to form S-nitrosothiols [10, 11]. (3) Transnitrosylation between glutathione (GSH) and RSNO leads to the formation of S-nitrosogluthathione (GSNO) [11-13]. (4) S-Nitrosothiols can be formed from the reaction of nitrous acid (HONO) with thiols in an acidic environment, potentially occurring in the gastro-intestinal tract [14, 15]. However, it is not clear which of these mechanisms more closely resembles *in vivo* physiological S-nitrosylation [16].

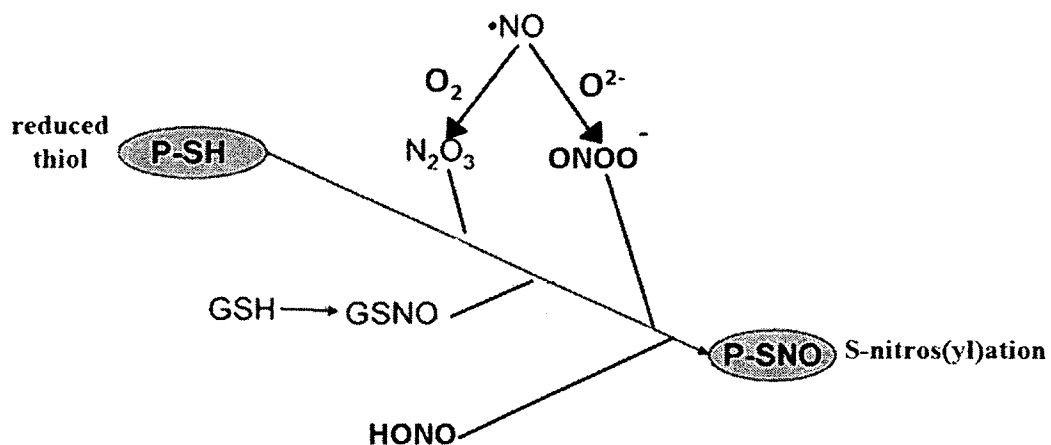


Figure 2-1: Four major mechanisms to form protein S-nitrosylation.

2.1.3 Techniques for Measuring Protein S-nitrosothiols

Currently, a number of “indirect” methods are used for the quantitative measurement of nitrosothiols, which either requires cleavage of the S-NO bond, followed with NO level measurement or replacement of the S-NO with another detectable tag. One widely utilized method is the colorimetric Saville assay [17]. NO^+ is displaced from the thiol by mercuric chloride in the presence of sulphanilamide and then reacts with N-(1-

naphyl)-ethylenediamine. The reaction product, a colored azo dye, can be detected spectrophotometrically at 540 nm. This method has a limit of detection (LOD) around 500 nM [18]. However, this LOD is above physiological levels of nitrosothiols, which limits the application of the technique to quantitative studies of nitrosothiols from biological samples.

Chemiluminescence assay has also been developed for S-NO measurement [19]. After cleavage of the S-NO bond through either photolysis or chemical reduction, the released NO reacts with ozone to form NO_2^* , which decays to NO_2 with the production of light. This method has good sensitivity with an LOD of 2 picomoles [19]. However, the technical challenges lie in the equal mixing of the test gas flow with the ozone [18]. Additionally, although the photolysis method consistently gives quantitative measures, the NO yields by chemical tri-iodide reduction chemiluminescence assay are generally low and difficult to reproduce [20].

A fluorescence method for the indirect detection of SNOs using spectrofluorometry to measure the status of NO has also been reported [21, 22]. The S-NO bonds are cleaved with HgCl_2 , and the newly formed NO is monitored from its reaction with 4, 5-diaminofluorescein (DAF) to yield a fluorescent triazolofluorescein (excitation/emission=485/520 nm) [19]. The LOD of this method reaches 5nM [21].

All the methods described above are not compatible with the analysis of small or biological samples, such as those obtained from needle biopsies, single cells or tissues. In order to detect and quantitate nitrosothiols from these samples, a more sensitive method with lower LOD is required. The method developed will be discussed in Chapter 3. This new method may aid in developing methods for rapid analysis of protein S-nitrosylation

in smaller or biological samples. In addition, microfluidics have been widely used for the development of novel tools for separation of protein mixtures. To resolve more nitrosylated proteins in the biological samples, the 2D electrophoresis separation method will be discussed in Chapter 4.

2.1.4 Techniques for Identification of Nitrosylated Proteins

In addition to measuring the protein S-nitrosylation amount, it is also important to identify nitrosylated proteins and the sites at which nitrosylation occurs. Nitrosylated proteins have been identified in several ways. These approaches can be generally divided into two branches: direct methods and indirect methods.

Direct detection of protein S-nitrosylation involves immunohistochemistry by the use of an SNO-specific antibody to detect *in vivo* protein S-nitrosylation [23]. Conventional methods such as immunoprecipitation, 2D-gel electrophoresis or western blot are generally not preferable for protein S-nitrosylation because the S-NO bond is degraded in the SDS-PAGE step [24]. However, the use of a biotin switch assay coupled with these methods can indirectly detect the changes in the protein S-nitrosylation status under different biological conditions [25].

Recently, more “indirect” methods are being developed for the quantitation of nitrosothiols. These methods measure either the newly formed NO level after the S-NO bond is cleaved, or another detectable tag which replaces the S-NO group. One widely utilized method is the Saville assay [17]. The mechanism of this method is to replace NO^+ from the thiol group by mercuric chloride in the presence of sulphamylamide and then react with N-(1-naphyl)-ethylenediamine. The reaction product, a colored azo dye, can be detected by spectrophotometrically at 540nm [20]. Biotin switch assay (BSA) is

another widely used methods for detecting protein S-nitrosylation [25]. It utilizes a sulphhydryl-specific biotinylating agent to react with free cysteine that is created from nitrosothiol group (S-NO) to form the biotin tag. Then, this method can couple with immunoblotting, 2D-gel electrophoresis, or fluorescence gel electrophoresis to detect changes in protein S-nitrosylation status under different biological conditions. Such methods can effectively determine the total level of protein S-nitrosylation present in the biological sample, but they are unable to identify specific S-nitrosylated proteins.

For the identification of nitrosylated proteins sites in the complex biological samples, approaches based on mass spectrometry (MS) are required. Due to the lability to this type of modification, the direct detection of MS is still quite problematic. A couple of indirect methods have been developed for protein identification. The previously widely used method is the biotinylated proteins purified by avidin affinity chromatography after BSA and then followed by 2D-gel electrophoresis for MS analysis [5, 7, 26-30]. Few S-nitrosylation proteins have been identified by this approach due to its low abundance and to the low recovery of S-nitrosylated peptides from in-gel digestion. A new method, SNO Site Identification (SNO), introduced a proteolytic digestion step before avidin capture [31]. It allows the selective isolation of peptides that previously contained S-nitrosylated Cys residues and 68 S-nitrosylated peptides from 56 rat cerebellar proteins that were identified in this study. In this way, only the modified peptides are enriched and eluted for the following identification by MS: this is fundamental improvement because only the localization of the modified residue can confer high confidence in the results. However, two disadvantages are shown in this method. First, the identification of a protein depends on MS/MS-based sequence information inferred from a single peptide ion. Second, a

relative large amount (1g) of starting tissue/cells is required. Camerini et al. used an N-terminally modified His-tag to selectively label the thiol group (SH) reduced by nitrosothiol group (SNO) instead of biotin tag [32]. From this approach, the author got 28 modified Cysteine moieties from 19 proteins. Forrester et al. recently developed a method named S-nitrosothiol resin-assisted capture (SNO-RAC), which requires fewer steps because it combines the “labeling ” and “pull down” steps from the BSA into one step [33]. This approach can detect 44 novel SNO sites in *E. coli* [33]. The author pointed out that this method appeared to be more sensitive than the BSA for high mass proteins, and at least as sensitive as the BSA for proteins smaller than 100 kDa. However, Liu et al. revealed that both the BSA and RAC approaches were not effective at S-nitrosylation site identification [24]. They did not address the issue of accurate site localization, especially when more than one cysteine was present in an identified peptide sequence. They presented a novel and robust method for site-specific high-throughput identification of protein S-nitrosylation (SHIPS) in complex protein mixtures. The SHIPS approach utilized a cysteinyl affinity resin to pull down ascorbate reduced S-nitrosylated peptides, rather than S-nitrosylated proteins. Two commonly used alkylation agents, acrylamide and iodoacetamide, were employed to differentiate free and disulfide-bonded cysteine form reduced S-nitrosylated cysteine [24]. A total of 162 S-nitrosylation sites were identified and an S-nitrosylation motif was revealed in this study.

Even though all these studies successfully identified nitrosylated proteins, none of them identified the oxidative stress induced nitrosylation in HT-29 cells. This dissertation developed a proteomic strategy to identify nitrosylated proteins in HT-29 cells before and

after MQ treatment. The strategy allowed identifying the proteins that are truly affected by oxidative protein nitrosylation damage mediated by MQ.

2.2 Protein Separation

Protein separation involves reducing the complexity of the protein mixture by sorting them into smaller purified protein compartments. The goal is to obtain individual protein plugs or spots, so that each protein can be easily identified without interference from another protein. Separating a complex protein mixture into individual proteins is usually impractical, especially when dealing with a complex proteome that contains numerous proteins.

2.2.1 Capillary Gel Electrophoresis for Analysis of Proteins

In order to quantitate nitrosothiol levels of proteins, the previous methods for measuring protein S-nitrosylation discussed in Section 2.1.2 are not sensitive enough for investigation of biological samples. With a highly sensitive detection system such as laser-induced fluorescence (LIF), capillary electrophoresis is chosen because of the low limits of detection (LOD) achieved.

2.2.2 Microchip Separation

The conventional method of 2D separation involves a charge-based separation where proteins are separated based on their isoelectric points followed by a size-based separation, where proteins are separated according to their molecular weight [34]. This technique has capability of resolving 5000 proteins [34, 35], and 10,000 proteins can be resolved by large sized 2D-gels [36]. However, this method has some major issues, such

as poor reproducibility, and time consuming and labor-intensive experimental procedures.

Microchips offer various advantages, such as short analysis times, minimal sample volumes, reduced dead volumes, high peak capacities and easy coupling of multiple separation channels [37]. Although the common modes of protein CE separation have been adapted to the chip format, the multidimensional approaches are still in progress. Numerous groups have reported different microchip 2D systems for protein separations. In the former, Soper and co-workers employed SDS micro-capillary gel electrophoresis (SDS μ -CGE) and μ -MEKC electrophoresis in the 1D and 2D, respectively, reporting to sort ten model proteins [38] and serum proteins [39] using a PMMA microchip. The 2D electrophoresis system could generate a peak capacity of $\sim 2,600$ in fewer than 30 minutes for proteins isolated from fetal calf serum (FCS). The same group also combined the SDS μ -CGE with micro-emulsion electrokinetic chromatography (μ -MEEKC) and reported μ -MEEKC in the 2nd dimension was found to produce higher peak capacities (481 ± 18) compared to μ -MEKC (332 ± 17) [40].

2.3 Protein Identification

Proteomics is the study of the entire proteins in a given organism, whereas the proteome is a catalogue of the proteins in a specific organism that are coded by the genome. Proteomics is concerned with the determination of structures, expressions, interactions, and functions, which includes activities, roles and locations of proteins in an organism. The original definition of the proteome views the proteome as the protein complement of the genome; therefore, it does not account for the numerous post-translational modifications and the ever-changing state of proteins. Proteomics can then

be defined as the comprehensive analysis, including the determination of structure, modifications, expression levels, localization and protein-protein interactions, within a given organism, tissue, cell, or biological fluid at a specified time.

In general, two approaches for protein identification in proteomics are recognized, namely, bottom-up and top-down strategies. The top-down and bottom-up strategies are complementary to each other in terms of proteomic coverage.

2.3.1 Top-Down Strategy

In the top-down strategy, the intact protein mixture is directly subjected to a proteolytic digestion without protein separation followed by separation of the peptides with the isolated peptides submitted for mass analysis. The main advantage of this method is a protein mixture is digested to generate peptides, which are easier to analyze compared to a complex protein sample that contains a mixture of very small or very large proteins. The main disadvantage of this methodology is its lower efficiency in protein identification since it lacks an efficient protein separation technology that can be easily interfaced to the mass spectrometer.

2.3.2 Bottom-Up Strategy

In the bottom-up strategy, first, a protein mixture is separated. Then the resolved proteins are enzymatically broken into peptides before being sent into a mass spectrometer for mass analysis. There are several advantages to using this strategy. First, proteins can be visualized immediately after gel separation before the protein digestion. Second, protein profiles of the sample can be generated since a gel separation is performed. Third, fewer peptides are fed into the MS, resulting in simple peptide mass spectra compared to the MS spectra obtained from a top-down strategy.

2.3.3 Peptide Preparation

The most basic task of proteomics is the detection and identification of proteins from a biological sample. In this dissertation, the top-down strategy was used for nitrosylated proteins identification. It began with the protein digestion after protein purification with “biotin switch assay” method, followed by nitrosylated proteins enrichment and mass analysis typically by liquid chromatography-tandem mass spectrometry (LC-MS/MS).

For protein digestion, trypsin is used to convert proteins to peptides. After this step, the peptides are always separated and go to MS analysis. SDS-PAGE is often used to separate complex protein mixtures. Slices can be excised from the whole lane of gel, and proteins from each gel slice can be analyzed separately by high performance liquid chromatography followed by mass spectrometry (HPLC-MS). Alternately, gel-free MS-based proteomics, such as affinity chromatography, are occupying a central role in biological research. In this dissertation, streptavidin agarose was used to enrich biotinylated nitrosylated proteins after trypsin digestion.

2.3.4 Mass Spectrometry Analysis

Mass spectrometry has been widely used as an analytical technique since its establishment more than one hundred years ago. Currently, many laboratories are experimenting with the application of MS as an instrumental tool for analytical and structural studies of proteins.

Ionization source, analyser, detector, data processor and vacuum pumps are the main components in a mass spectrometer. The analyser and the detector must be under vacuum. In the late 1980s, two new ionization techniques, electrospray ionization (ESI)

and matrix-assisted laser desorption/ionization (MALDI), were developed for the first time for the acquisition of mass spectra with minute quantities of peptides and proteins. In ESI, ions are formed at atmospheric pressure, while ions in MALDI may be generated either at atmospheric pressure or under vacuum conditions. ESI is commonly used for the top-down strategy. The reason for that is liquid chromatography (LC), used in the separation of the peptides, couples naturally to ESI due to the ability of continuous sample infusion into the ES ion source.

The analyser is the part of the mass spectrometer where the separation process takes place. A mass spectrometer may be constructed with multiple analysers, depending on the task they will be used for. Instruments composed of two or more mass analysers coupled together are known as tandem mass spectrometers.

CHAPTER 3

HIGHLY SENSITIVE DETECTION OF S-NITROSYLATED PROTEINS BY CAPILLARY GEL ELECTROPHORESIS WITH LASER INDUCED FLUORESCENCE

3.1 Introduction

S-nitrosylation (also referred to as nitrosation) of protein is a post translational modification (PTM) of thiols on cysteines [41]. It is essential in cellular function and signaling regulation [9, 11, 42-44] and serves as a biomarker in many diseases including Alzheimer's disease, Parkinson's disease, Huntington's disease, diabetes, and stroke [1, 45-48].

Accurate and sensitive methods to detect and quantify low levels of S-nitrosylated proteins in complex protein mixtures from both physiological and pathological conditions are required in order to fully understand the range and extent of this modification. In this paper, a new quantitative method to detect SNOs by capillary gel electrophoresis with laser induced fluorescence detection (CGE-LIF) is developed. Among the commercial detection modes developed for CE, LIF is one of the most sensitive detection techniques [49]. Here, a fluorescence switch method derived from the biotin switch assay is used to label the nitrosothiols [50, 51]. The procedure consists of the derivatization of nitrosothiols into free sulfhydryl groups followed by specific labeling of sulfhydryl-containing proteins with Dylight 488 maleimide (Ex/Em = 493/528 nm). The

derivatization process includes alkylation with methyl-methanethiosulfonate (MMTS) to block all sulfhydryl groups followed by the reduction of nitrosothiols to newly formed sulfhydryl groups. Then the Dylight 488 fluorophore labels nitrosylated proteins, which are monitored using CGE-LIF. This procedure proves to be adequate for analyzing nanogram numbers in protein samples with picomolar levels of nitrosothiols in less than 15 minutes.

This study also demonstrates the direct application of the above mentioned method in monitoring oxidative protein nitrosylation damage mediated by menadione (MQ), a redox cycling quinone in human colon adenocarcinoma cells (HT29). MQ has the redox-cycling capacity to acrylate cellular nucleophiles such as DNA and proteins, with mitochondrion considered as the main redox site. MQ can mediate apoptosis through formation of the toxic species, the semiquinone (SQ[•]) radical, which is formed by mitochondrial NADPH-ubiquinone oxidoreductase (ubQO) through one-electron metabolism. The SQ[•] can then participate in redox cycling through reaction with O₂ to generate the superoxide anion (O₂^{•-}) and concomitantly regenerate MQ[52-54]. The electropherogram results indicated that a wide distribution of molecular weight (MW) of proteins were nitrosylated. In addition, it is observed that exposure to MQ caused an increase in protein nitrosylation damage.

Also examined was the nitrosylation level in a minuscule amount of brain cerebrum tissue from an Alzheimer's disease (AD) transgenic mice model (B6Cg-Tg). Carrying both the Swedish amyloid precursor protein mutation (APP) and exon 9 deletion of the PSEN1 gene, the B6Cg-Tg mouse is a valuable model to study the pathological alterations in AD. These results not only depicted an electrophoretic profile of

nitrosylated proteins in brain tissue, but also proved capable of analyzing a minuscule amount of tissue using the CGE-LIF method.

3.2 Material and Methods

3.2.1 Materials and Reagents

sodium dodecyl sulfate (SDS), 2-[4-(2-hydroxyethyl)piperazin-1-yl] ethanesulfonic acid (HEPES), tris (hydroxymethyl)-aminomethane, tricine, (+)-sodium L-ascorbate, ethylenediaminetetraacetic acid (EDTA), albumin bovine serum (BSA), methanol, sodium hydroxide, hydrochloric acid, neocuproine, S-methyl methanethiosulfonate (MMTS), dextran from *Leuconostocmesenteroides* (average MW 64,000-76,000), trichloroacetic acid (TCA), menadione (2-methyl-1,4-naphthoquinone; MQ) were all purchased from Sigma. Amicon ultra-4 (MW cutoff of 3000 Da) was from Millipore. DyLight 488 Maleimide and dimethyl sulfoxide (DMSO) was from Thermo Scientific. Ultra Trol Dynamic Pre-Coat LN was obtained from Target Discovery. Sulphanilamide was purchased from Alfa Aesar. N-1-Naphthylethylenediamine hydrochloride was obtained from TCI. S-Nitrosoglutathione (GSNO) was purchased from Calbiochem. The bicinchoninic acid (BCA) assay was from Pierce. HEN buffer was composed of 250 mM HEPES, 1 mM EDTA, and 0.1 mM neocuproine at pH 7.7. HENS buffer was prepared in HEN buffer with the addition of 1% SDS. The separation buffer consisted of 20 mM Tris, 20 mM Tricine, 0.5% SDS at pH 8. The sieving matrix buffer was prepared in the separation buffer with 15% dextran.

3.2.2 Capillary Electrophoresis with Laser Induced Fluorescence Detection

A commercial capillary electrophoresis instrument, Beckman Coulter P/ACE MDQ system (Fullerton, CA), was used for the analysis of protein nitrosylation. For excitation, the LIF detector used an argon-ion laser (488 nm line, 3 MW) that was directed to a detector window in the capillary using fiber optics. A 520DF20 bandpass filter (~510-530 nm) was used to select the Dylight 488 fluorescence before the photomultiplier tube (PMT). The PMT output signals were sampled at 4 Hz.

Separations were carried out using a 31-cm-long, 50- μm -i.d., 361- μm -outer-o.d. fused-silica capillary. UltraTrol LN, a class of linear polyacrylamide made of *N*-substituted acrylamide copolymers, was used for precoating the capillary walls. This procedure decreases the electroosmotic flow (EOF) and inhibits protein binding to the inner wall of the capillary. The sample was injected hydrodynamically at 11kPa for 4 seconds into the capillary containing the sieving matrix buffer. Separations were performed at -570 V/cm. The capillary was reconditioned between consecutive runs with sequential pressure-driven flushes (20 psi) of 0.5 M sodium hydroxide for five minutes, H₂O for three minutes, the dynamic coating reagent UltraTrol LN for two minutes, the separation buffer for two minutes, and the sieving matrix buffer for four minutes [55, 56].

3.2.3 In Vitro Nitrosylation of BSA and SNO quantification by Saville-Griess Assay

GSNO can react with thiol groups to yield nitrosothiols. Briefly, the BSA solution (7.5 mg/mL) was incubated with the NO donor GSNO (500 μM) in darkness for 30 minutes with constant rotating [8]. Nitrosylated protein level from the *in vitro* BSA test model was quantified using Saville-Griess assay. Briefly, mercury displacement of NO

from nitrosylated BSA was achieved by ten minutes of incubation with 100 μ M mercury chloride. The remaining GSNO was removed via Slide-A-Lyzer Dialysis Cassettes (10K MWCO, Pierce) overnight. The buffer for dialysis was BupHTM Borate buffer Pack (Pierce). Nitrite levels were determined spectrophotometrically after reaction with 100 μ L of Griess reagent (1:1 mixture of 3% sulfanilamide in 0.4 M HCl and 0.1% *N*-(1-naphthyl) ethylenediamine in 0.4 M HCl) and quantified using absorbance at 540 nm and extinction coefficient of 51 $\text{mM}^{-1}\text{cm}^{-1}$ [57, 58].

3.2.4 Cell Culture and Incubation with MQ

The human colon epithelial adenocarcinoma cell line HT-29 was purchased from the American Type Culture Collection (Manassas, VA, USA). HT-29 cells were grown in McCoy's medium supplemented with 10% fetal bovine serum, penicillin (100 units/mL), and streptomycin (100 units/mL). HT-29 cells were maintained at 37°C in 5% CO₂ humidified incubator. One day prior to experimentation, HT-29 cells were plated in T75 flasks and exposed to a final concentration of 200 μ M MQ (freshly prepared) for 30 minutes in serum-free DMEM (Dulbecco's Modified Eagle's medium). Thereafter, cells were washed and scraped into cold-PBS. The resulting pellet obtained upon centrifugation at 1000 rpm (Centrifuge 5804 R, Eppendorf) was immediately frozen in liquid nitrogen and used for further analysis of nitrosylated proteins.

3.2.5 Protein Extraction from MQ Treated Cells

The pellets of HT-29 cells prepared from Section 3.2.4 were washed five times with phosphate-buffered saline (PBS) and resuspended in 100 μ L water. The cells were sonicated for 20 s in the power level of 4 (550 Sonic Dismembrator from Fisher Scientific). The suspension was centrifuged at 600 \times g (Centrifuge 5804 R, Eppendorf) for

ten minutes. A 40 μL aliquot of the supernatant was then used for “fluorescence switch” assay. The untreated HT-29 cells followed the same procedure. The protein concentration was measured by the BCA assay.

3.2.6 Isolation of Brain Cerebrum from AD Transgenic Mice Model

The cerebrum was isolated from the brain of five-month old transgenic mice (B6Cg-Tg) and its age-matched wild type (WT) control. Briefly, the cerebrum was minced with scissors and suspended in isolation buffer (320 mM Sucrose, 10 mM Hepes, 1 mM EDTA). The minced tissue was homogenized and 100 μL homogenate of each sample (Tg and WT) was added with 40 μL 20% TCA followed with incubation for ten minutes at 4 °C. After that, the solution was centrifuged at 10000 $\times g$ (Labnet PrismTM R Refrigerated Microcentrifuge) for five minutes at 4 °C and the supernatant was discarded. The protein pellet was mixed with 50 μL HENS buffer.

3.2.7 Fluorescence Switch Assay

Figure 3-1 shows the schematic of fluorescence switch assay. This procedure consists of the derivatization of SNOs into free sulfhydryl groups followed with highly sensitive specific labeling of sulfhydryl-containing proteins with Dylight 488 maleimide. As the S-NO bond is light sensitive, all the experimental procedures were conducted in the dark [8, 11, 59]. Briefly, for the labeling reaction, a volume of 5 μL nitrosylated BSA prepared in Section 3.2.3 was incubated with 20 μL blocking buffer (nine volumes of HEN buffer, one volume of 25% SDS, 0.1 volumes of 2 M MMTS stock solution in N, N-dimethylformamide) at 50°C for 30 minutes with frequent rotating. To remove the excess MMTS, an Amicon Ultra-4 centrifugal filter unit (3000 MW cut-off) was used. The sample was centrifuged for three times at 4500 $\times g$ for 20 minutes with the washing

solvent, HEN buffer. The final volume after wash was around 60 μL . Then 2 μL freshly prepared 50 mM ascorbate was added to reduce the nitrosothiol groups to thiols and the incubation lasted for one hour at room temperature. For labeling the newly reduced free thiol groups generated from the last reduction step, 4 μL of 12.5 mM Dylight 488 maleimide was added into the solution, and the reaction proceeded overnight at room temperature.

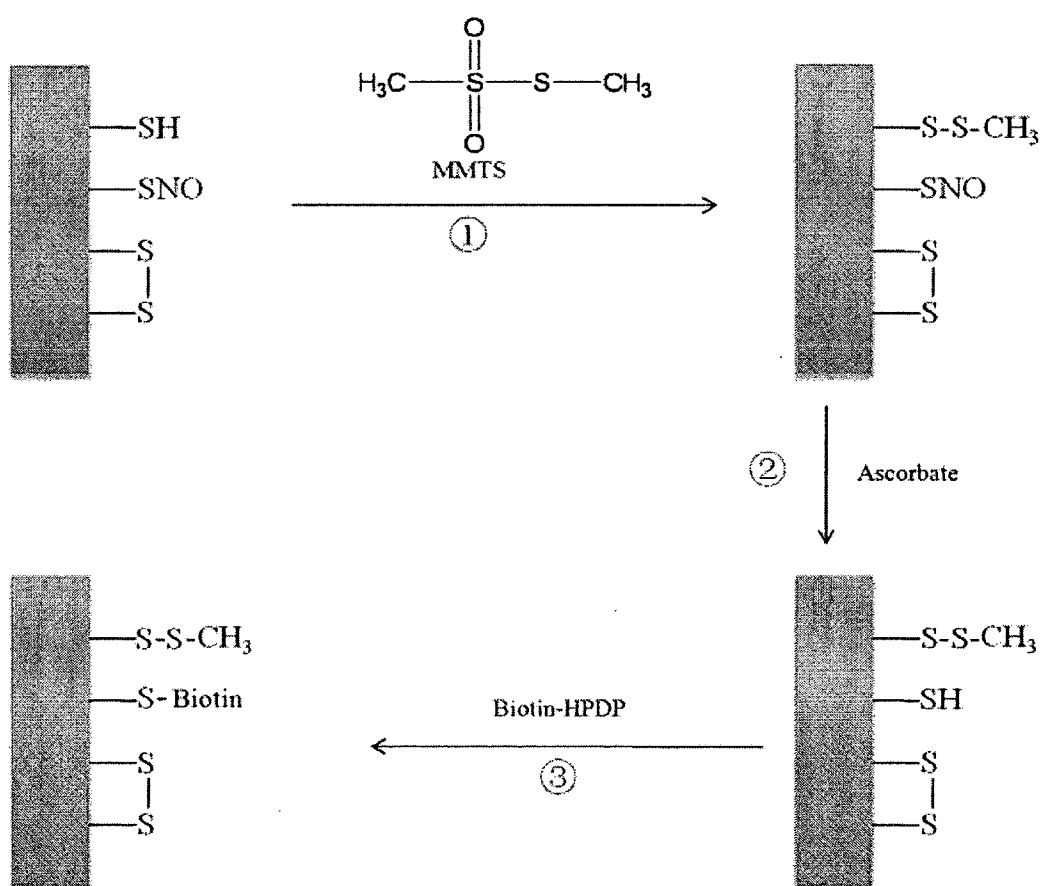


Figure 3-1: Schematic of fluorescence switch assay coupled with CGE-LIF for detecting and quantifying S-nitrosylated proteins. Fluorescence switch assay (Steps 1-3) includes blocking thiol group by MMTS, reducing nitrosothiol group with ascorbate and labeling reduced free thiol by Dylight 488 maleimide. Finally, labeled proteins are separated and analyzed by CGE-LIF.

To remove the unreacted Dylight 488 maleimide dye from the sample, the sample was centrifuged for a total of six times at $4500\times g$ for 20 minutes using the Amilcon filter with 3000 MW cut-off [25, 60]. The washing solvent was the CE separation buffer. After removal of excessive dye, 5 μL of 20% SDS in separation buffer was added into a final volume around 100 μL to saturate proteins. The derivatized and fluorophore labeled solution was then diluted to 1, 0.5, 0.25, and 0.1 fold of the original concentration with separation buffer.

The procedure for nitrosylation labeling in HT-29 cells and B6Cg-Tg mice with Dylight 488 maleimide was basically the same as the nitrosylated BSA, except for the use of 40 μL of from both HT-29 cells and B6Cg-Tg mice cerebrum. The selectivity of labeling nitrosothiols using this fluorescence switch assay was studied by incubating nitrosylated BSA with mercury chloride to displace the NO group prior to the procedure of the assay. Also, fluorescence switch assay without proteins and untreated BSA as a negative control was performed individually with fluorescence switch assay and CGE-LIF to validate the specificity of the assay to SNOs.

3.2.8 Data Analysis for CE

Igor Pro software (Wavemetrics, Lake Oswego, OR) was used to analyze electropherograms, which provides intensity values at each migration time point. The integrated fluorescence peak areas were measured to calculate the nitrosylated protein amounts using the in-house-written Igor procedure, Wide Peak Analysis [55].

3.2.9 Validation of Nitrosylated Proteins CE Peaks Using Proteomics

The biotin switch assay was performed as described by Jaffrey and Snyder [25]. Briefly, the protein concentration was adjusted to 0.8 $\mu\text{g}/\mu\text{L}$ using HEN Buffer (250 mM

Hepes/NaOH pH 7.7, 1 mM EDTA, 0.1 mM neocuproine) and then incubated at 50 °C for 30 minutes in blocking buffer (9 volumes of HEN buffer, 1 volume of SDS (25% w/v in H₂O) and MMTS added to a final concentration of 20 mM) with frequent vortexing. Acetone precipitation was performed to remove MMTS. The protein pellet was resuspended in 0.1 mL HENS solution (HEN Buffer in 1% SDS) per mg protein, followed by incubation with 2 mM biotin-HPDP and 2 mM ascorbate for 1h at 25 °C. After biotinylation to label S-nitrosylated proteins, biotin-HPDP was removed by acetone precipitation and centrifugation, and the pellet was resuspended in HENS buffer as above. The proteins were then trypsin digested overnight, and the resulting peptides were desalted in a mixed-mode cation exchange column (MCX; Waters) followed by Sep-Pak reverse-phase extraction prior to LC-electrospray ionization (ESI) MS/MS analysis [61].

For identifying nitrosylated proteins, the sample was divided into three equal portions and analyzed by LC-MS/MS. Peptide mixtures were first separated on an Agilent 1200 Capillary Series liquid chromatograph (Agilent Technologies, Palo Alto, California, CA), and identified via μ LC-ESI MS/MS on a hybrid linear ion trap-Orbitrap mass spectrometer (LTQ-Orbitrap XL; Thermo Electron, San Jose, CA). MS/MS spectra were acquired in a data-dependent acquisition mode that automatically selected and fragmented the five most intense peaks by higher-energy collisional dissociation (HCD) from each MS spectrum generated.

MS/MS spectra were searched using human International Protein Index protein sequence data base (version 3.74, 39,906 protein sequences; European Bioinformatics Institute). The dataset, built from the Swiss-Prot, TrEMBL, Ensembl and RefSeq databases, offers complete nonredundant data sets representing a set of human proteomes

[62]. The database searching was performed using Proteome Discovery (version 1.0, Thermo Fisher, San Jose, CA) and Mascot (version 2.2.02, Matrix Science, London, UK) with the following parameters: trypsin as digestion enzyme; Methylthiolation (C), Oxidation (M) and Biotin-HPDP (C) were set as variable modifications.

3.3 Results and Discussion

3.3.1 Fluorescence Switch Assay Coupled with CGE-LIF

The Dylight 488 maleimide was used to label the reduced nitrosothiol group after blocking the free thiols in the nitrosylated proteins. The mechanism of this method resembles biotin switch assay, which is widely used in the study of nitrosylation proteomics using mass spectrometry [25]. One possible question in fluorescence switch assay is the possibility of nonspecific reduction of SNOs by ascorbate. In this regard, Giustarini *et al.* have expressed concern that the ascorbate treatment may reduce 5,5'-dithiobis (2-nitrobenzoic acid) (DTNB) and the protein mixture, giving rise to a significant false-positive signal [63]. However, most recently Forrester *et al.* challenged this opinion with the following reasons: first, DTNB is not representative of biological disulfides since its disulfide bonds are highly electrophilic. The high electrophilic bonds can be facilitated by ascorbate [64]. Second, ascorbate could not reduce intramolecular protein disulfides under denaturing conditions, even if protein mixture disulfides may be cleaved by ascorbate [63]. Third, the reduction of disulfide bonds by ascorbate is highly thermodynamically unfavorable since the oxidation-reduction potential of cysteine (CSH)/cystine (CSSC) is found to be -220 mV and that of the ascorbic acid is 70 mV [65, 66]. Lastly, Giustarini *et al.* did not perform the biotin switch assay. However, Forrester *et*

al. revealed that the reduction of ascorbate to the S-NO bond is unique among Cys oxidation products after biotin switch, and the authors conclude that this reaction confers specificity to the biotin switch assay [67], as evidenced by previous reports [42, 64]. Therefore, ascorbate does not significantly influence the selectivity of this method. In addition, ascorbate is unstable, and the dehydroascorbate that forms by oxidation rapidly decomposes to small sugars, such as trioses. Hence, freshly prepared ascorbate solution was used to remove the nitrosothiols for sample preparation [68].

We also performed a simple calculation to check whether derivatization would cause any significant change in the protein mobility. After derivatization, Dylight 488 maleimide was labeled to the nitrosylated proteins, causing only an 800 Da molecular weight (MW) shift due to the MW of the dye. The mobility will not be altered much with this minimum MW shift when considering the average molecular weights of proteins such as BSA (MW = 63 kDa).

In order to distinguish the peaks of the fluorescence dye itself from those of the nitrosylated proteins, the electropherogram of the Dylight 488 maleimide alone, which exhibits multiple peaks appearing from 200 s to 400 s, is shown in Figure 3-2 (bottom Trace 1). More than one fluorescence peak was observed since this reagent is an isomeric mixture.

In vitro nitrosylated BSA was used as a model to test the reactivity of Dylight 488 maleimide toward SNOs in treated BSA. After the fluorescence switch assay and removal of excessive dye, a representative electropherogram of nitrosylated BSA was shown in Trace 2 of Figure 3-2. It depicts that the nitrosylated BSA appears approximately at 690 s. A series of peaks (200-400 s) occurring before the nitrosylated BSA is attributed to the

residual Dylight 488 maleimide. However, the control of just the dye (Trace 1 in Figure 3-2) has three well defined peaks in this range, whereas the nitrosylated BSA derivatized with the dye has a wide range of peaks in this window. In order to validate that the wide range of peaks are indeed from residual dye instead of SNOs, and further understand why this visual disparity exists, various controls were used, including untreated BSA, mercury chloride treated nitrosylated BSA, and the fluorescence switch assay with no protein.

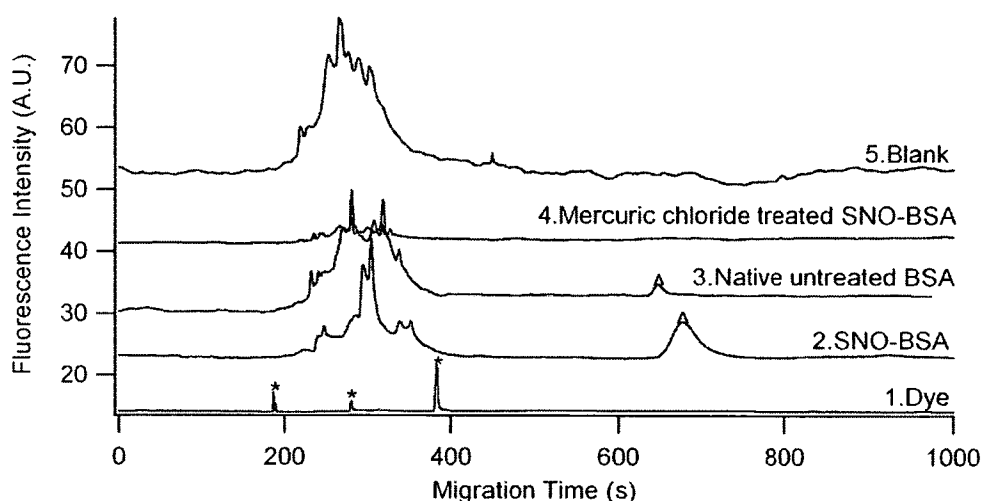


Figure 3-2: CGE-LIF separation of nitrosylated BSA labeled with Dylight 488 maleimide. Separation, -570V/cm ; hydrodynamic injection, 11kpa, 4s; sieving matrix, 20mM Tris, 20mM Tricine, 0.5% SDS, 15% dextran (65.5kDa), pH 8. Top trace and middle trace are offset on the y-axis for clarity. * — Dylight 488 maleimide, ^ — nitrosylated BSA.

3.3.2 Selectivity and Specificity of the Fluorescence Switch Assay

After the derivatization of untreated BSA with the fluorescence switch assay and injecting the samples to CE, a significantly smaller peak was detected around 690 s for SNOs. It was initially expected that no peak for SNOs in the commercial BSA would be detected. The fluorescence switch S-nitrosylation assay is based on the assumption that only the S-nitrosylated cysteine residues will be derivatized and fluorescently labeled. If

the free thiols of the cysteine residues have not all been successfully blocked with MMTS, then the nonblocked cysteines may produce a fluorescence signal in the electropherogram. To rule out this possibility, MMTS with a high concentration of 100 mM was used for blocking. Hence, it is believed that the little peak (Trace 3 in Figure 3-2) was from the SNOs in the commercial BSA, which were previously indicated in other studies [69, 70].

The primary structure of BSA has 35 cysteines. Among them, 34 cysteine residues form disulphide bridges and only one 'free' cysteine residue, Cys34 exists [71]. Consistently, the thiol group in native untreated BSA measured by Ellman's assay showed average values of 0.55 free -SH per mol of BSA instead of one -SH group as expected [70]. This suggested that commercially available BSA is already oxidized at residue Cys34 [69, 70]. They could form a disulfide bond with several compounds like cysteine or glutathione, or undergo nitrosylation of Cys34 by nitric oxide [72]. Hence, this significantly smaller peak compared with the one from nitrosylated BSA indicates a small fraction of SNO in commercial BSA.

The selectivity of labeling nitrosothiols using Dylight 488 maleimide was also studied by incubating nitrosylated BSA with mercuric chloride before the fluorescence switch procedure. Mercuric chloride (HgCl_2) can break the S-NO bond, and the newly formed nitrosonium ion (NO^+) can undergo rapid hydration to produce NO_2^- at neutral pH [10]. So it was reasonable to see the decreased intensity of the SNOs signal for the HgCl_2 treated nitrosylated BSA. In fact, no obvious peak was observed in Trace 4 in Figure 3-2, confirming the selective Dylight 488 maleimide labeling of nitrosylated BSA after derivatization.

Additionally, the fluorescence switch assay was conducted using a sample without proteins. No peaks at 690 s in the protein migration time window were observed, while the same wide peaks existed ranging from 200 to 400s (shown in Trace 5 of Figure 3-2). Altogether, these studies further validate that these wide peaks were neither protein nor SNOs based. Currently it is speculated that this wide range of peaks preceding the protein peak might be due to hydrolysis of Dylight 488 maleimide.

3.3.3 Calibration of CGE-LIF Method with Nitrosothiol BSA Standard

BSA subjected to RSNO was used as a test model to optimize the derivatization and labeling procedures and to characterize the response of the LIF detector. The standard curve was made by a series of dilutions of nitrosylated BSA using CGE-LIF (Figure 3-3). The NO donor, GSNO, created 76 pmol nitrosothiol/mg of BSA determined by Saville assay. This result is in close agreement with the published data [73].

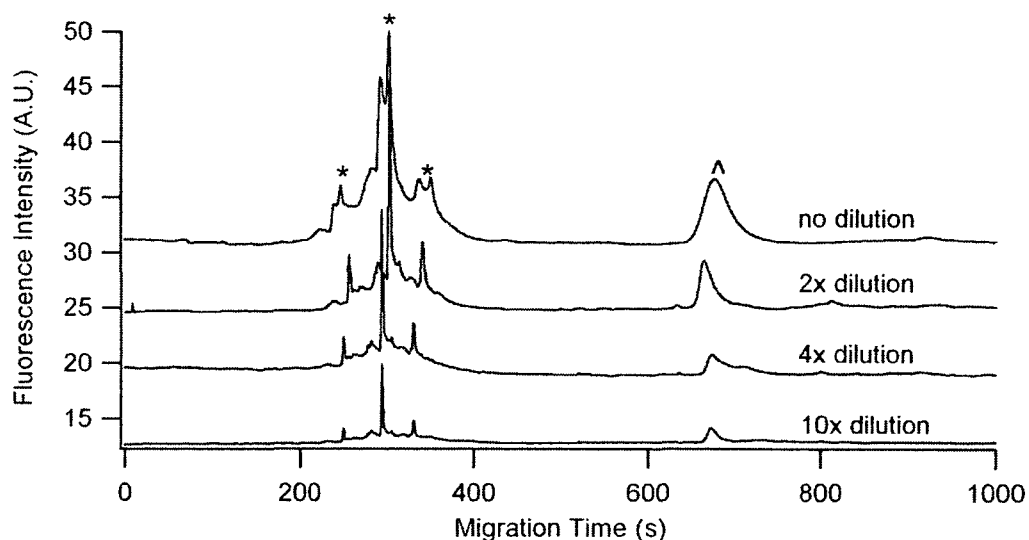


Figure 3-3: Electropherograms of a series of dilution (1-, 2-, 4-, 10-fold) of nitrosylated BSA labeled with Dylight 488 maleimide. Other conditions are the same as in Figure 3-2. *—Dylight 488 maleimide, ^—nitrosylated BSA.

Four dilutions of Dylight 488 labeling nitrosylated BSA were run in CGE-LIF in triplicate. The injection volume is 1.1 nL, which is calculated based on the radius (25.1 μm) and length (31 cm) of capillary, viscosity of sample (0.02 kg/m \cdot sec), injection pressure (11 kpa) and time (4 s). The calibration curve was made by the fluorescence peak area (y) of nitrosothiols on BSA and the corresponding moles of nitrosothiol (x), given by the following equation:

$$y = (1 \pm 0.13) \times 10^{19} x - (4.58 \pm 15.53); R^2 = 0.97. \quad \text{Eq. 3-1}$$

In the above calibration curve generated from nitrosothiol BSA standard, the slope has 13% error; and the error in the intercept is not significant for quantifying nitrosothiols amount because the slope is to the nineteenth power. The Saville assay can detect 500 nM of nitrosothiol proteins. So far, the lowest reported limit of nitrosothiol detection based on DAF fluorescence assay was 5 nM [21]. The limit of detection (LOD) in this CGE-LIF method determined by the above equation was 1.3 pM, which is the lowest LOD reported to date. Speculatively, it is proposed that the dynamic range can reach 4.2 pM (limit of quantification) at the lowest limit. Theoretically, the upper limit of range occurs when signals are sufficient enough to saturate detectors. However, biological samples do not typically have high levels of SNO, so this value is ignored.

3.3.4 Monitoring Nitrosylation in MQ-mediated Cells

The direct application of this CGE-LIF method in biological systems was demonstrated in the nitrosylation profiling of MQ-treated HT-29 cells. After extracting the proteins from the MQ-treated HT-29 cells, the proteins were treated with fluorescence switch assay prior to labeling with Dylight 488 maleimide. Figure 3-4 shows the electropherograms resulting from the hydrodynamic injection of Dylight 488 maleimide

labeled proteins of MQ-treated HT-29 cells (upper trace) and untreated samples (bottom trace). The labeled HT-29 cell proteins were detected between 420 and 880s, which are denoted by “a” and “b” in Figure 3-4. This indicates a wide MW range of proteins that are susceptible to nitrosylation.

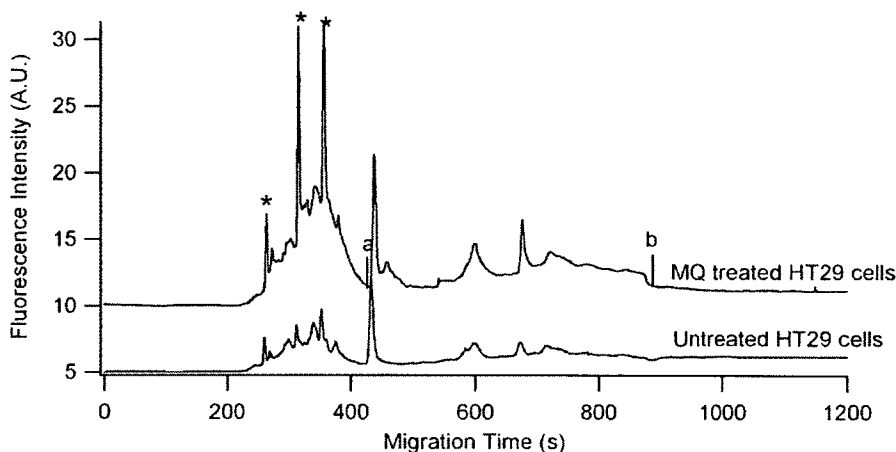


Figure 3-4: Electropherograms of extracted proteins from HT29 cells after fluorescence switch assay. Top and bottom traces represent MQ treated and untreated, respectively. All the experimental conditions are the same as in Figure3-2. Top trace is offset in the y-axis for the clarity. *—Dylight 488 maleimide; migration window between a and b indicated nitrosylated proteins.

Based on the previous equation, the total nitrosothiol content detected in each electropherogram for MQ-treated and untreated HT-29 cells (cf. Figure 3-4) were 65.5 ± 0.9 amol and 45.9 ± 2.4 amol (average \pm SD; three injections), respectively. Based on the BCA analysis of the same preparation (4.04 mg protein/mL for the MQ treated HT29 cells and 3.92 mg protein/mL for the untreated one) and a 1.1 nL injection (11 kPa, 4 s) per electropherogram, the total protein content was 4.44 ng for the MQ treated HT 29 cells and 4.31ng for the untreated one. Therefore, the untreated cells contained a low level of SNO (10.4 ± 0.5 pmolnitrosothiol/mg protein), and treatment with MQ resulted in a 1.5-fold increase in SNO content (14.8 ± 0.2 pmolnitrosothiol/mg protein). These results

are consistent with other reported values (from 100 nmol/mg of protein to 10 pmol/mg of protein) for nitrosothiols in various biological tissues [74-76].

3.3.5 Monitoring Nitrosylation in AD Tg Mice Brain

Another direct biological application of this CGE-LIF method was demonstrated in analyzing nitrosylation in very small amounts of the cerebrum of five-month-old AD transgenic B6Cg-Tg mice. Figure 3-5 shows electropherograms of five-month-old B6Cg-Tg mice cerebrum labeled with Dylight 488 maleimide. The fluorescence of Dylight 488 maleimide-labeled SNOs was detected between 500 and 1248s (indicated by “a” and “b”, respectively) in both Tg and WT cerebrum. The region between a and b were included in the calculation of the total area for nitrosothiol determination.

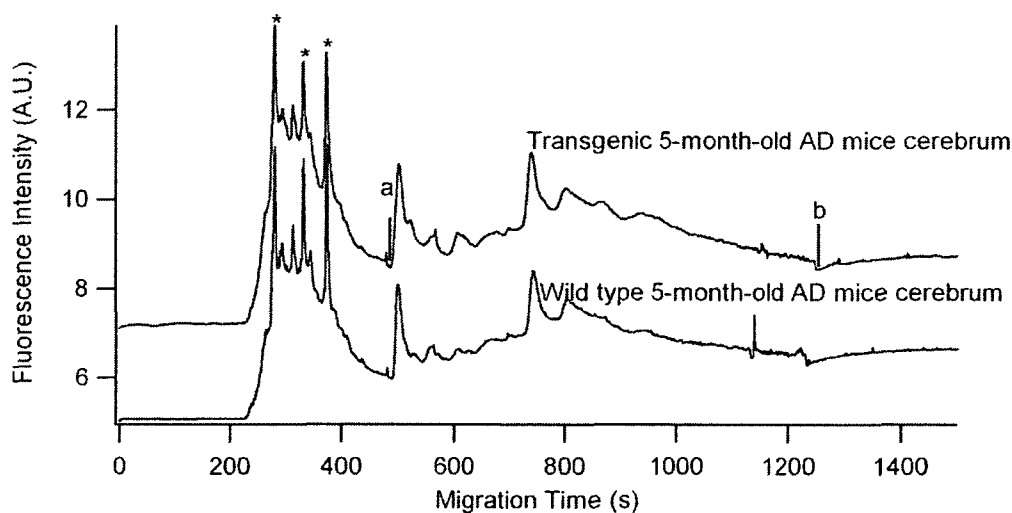


Figure 3-5: Electropherograms of cerebrum from five-month-old transgenic (upper trace) and wild type (bottom trace) mice brain tissue. All the experimental conditions are the same as in Figure 3-2. Top trace is offset in the y-axis for the clarity. *— Dylight 488 maleimide; migration window between a and b indicated nitrosylated proteins.

Based on the Eq. 3-1, the total nitrosothiol content detected in each electropherogram for Tg and WT (*cf.* Figure 3-5) was 71.2 ± 2 and 62.3 ± 1.7 amol (average

\pm SD; three injections), respectively. The total injected protein content was 4.58 ng and 5.38 ng for Tg and WT, respectively based on injected volume of 1.1 nL. Thus, the concentration of nitrosylated protein in the five-month-old transgenic B6Cg-Tg mice was 15.5 ± 0.4 (average \pm SD; three injections) pmol/mg, while WT cerebrum was 11.7 ± 0.3 (average \pm SD; three injections) pmol/mg. This preliminary result of just one animal pair indicates a small difference in brain SNOs expression at five months old, a time stage right before the amyloid plaque onset in this AD B6Cg mice model. Although a conclusive assessment of the S-nitrosothiols abundance in this Tg mice cannot be made based on this initial application, we have demonstrated the capability of this CGE-LIF method for monitoring nitrosylation electrophoretic profiles in the AD Tg mouse brain. This assay will be valuable in further studies for (i) monitoring 11-month-old AD Tg mouse brain tissue and WT control; (ii) characterizing SNO MW profiling in various brain tissues and other biological tissues, such as blood plasma; and (iii) monitoring longitudinal SNO changes in AD progression.

This newly developed CE-LIF method monitoring nitrosylated proteins in analysis of biological samples has several advantages, such as its low LOD, fast analysis time, high accuracy, and potential for pattern classification. Currently, many assay techniques for measuring biological SNOs are used near the limit of detection [18]. The currently developed method allowed only nanogram amount of protein and it reached the limit of SNO detection of 1.3 pM, which is 10^5 fold less than the conventional Saville assay. This CGE-LIF adds great advantages for detecting low abundance of nitrosothiols in complex biological samples.

Additionally, the results from biological samples indicate a wide MW range of proteins that are susceptible to nitrosylation. Although individual protein types were not fully resolved by CGE, a profile of nitrosylated proteins was obtained in under 15 minutes, much faster than SDS-PAGE requiring six hours of analysis. This short analysis time makes this method potentially useful as a prescreening tool in proteomics studies aimed at discovering proteins susceptible to nitrosylation.

Also, because CGE can separate samples by size, it can distinguish the interfering residual fluorescent dye from the SNOs peaks. This further eliminates the false positive signals from excessive dye and enhances accuracy compared with other spectrofluorometric assays.

CE-LIF also helps to obtain a molecular weight distribution profile of nitrosylated proteins. In future studies based on the data points from electropherograms, this work can potentially be used to investigate genotype-related and age-dependent changes in protein nitrosothiols in mice AD brain using chemometric techniques such as principal component analysis [55].

3.3.6 Detection of S-nitrosylated Proteins in HT-29 Cells

To prove the selectivity of CGE-LIF method, the desired peaks in the electropherograms were also confirmed. S-nitrosylated proteins in HT-29 cells were detected and identified using the biotin-switch assay developed by Jaffrey et al., which is based on the labeling of S-nitrosylated cysteine on targeted proteins with a biotin moiety [25]. This method contains three essential steps: blocking the free thiols with a thiol-specific methylthiolating reagent (MMTS), reducing the S-nitrosothiols to free thiols specifically by ascorbate, and labeling the thiols from the previous step with biotin-

HPDP. Detection of biotinylated proteins was performed by liquid chromatography and electrospray ionization tandem mass spectrometry (LC-ESI MS/MS) analysis after a series of purification steps. The result from HT-29 cells (Figure 3-2) indicates a wide molecular weight (Mw) range of protein peaks (from 420 s to 880 s) that are susceptible to nitrosylation. Although the individual protein peaks were not fully resolved by the CGE-LIF method, the nitrosylated proteins from the wide Mw range of peaks were identified by the LC-electrospray ionization (ESI) MS/MS. The data in Table 3-1 shows 24 nitrosylated proteins were identified in HT-29 cells, and the wide Mw range of the identified proteins was from 11 kDa to 300 kDa. These proteins include cell membrane proteins, nucleus proteins, cytoskeleton proteins, cell cycle proteins, signaling proteins, redox-related proteins, and folding-related proteins. The representative MS/MS peptide spectra of nucleolin and isoform 1 of vinculin are shown in Figure 3-6.

Table 3-1: S-nitrosylated proteins from MQ treated HT-29 cells identified by (ESI) MS/MS.

Number	Identified protein (HT-29 cell)	Accession number (IPI)	Molecular weight (kDa)
Redox-related proteins			
1	Protein disulfide-isomerase A4	IPI00009904.1	72.9
Transcription factors			
2	Isoform B of GC-rich sequence DNA-binding factor 1	IPI00069267.2	93.1
Nucleus protein			
3	Histone H1.2	IPI00217465.5	21.4
4	Histone H4	IPI00453473.6	11.4

Table 3-1 (continued): S-nitrosylated proteins from MQ treated HT-29 cells identified by (ESI) MS/MS.

5	Histone H2B type 2-E	IPI00003935.6	13.9
6	Lamin A/C	IPI00514204.3	53.2
7	Nucleolin	IPI00604620.3	76.6
8	Isoform 5 of Treacle protein	IPI00555853.2	96.7
9	Putative uncharacterized protein DKFZp779G118 (Fragment)	IPI00744556.1	14.5
Chaperones			
10	HSPA5 protein	IPI00003362.2	72.4
Cytoskeleton proteins			
11	Isoform 3 of Microtubule-associated protein 4	IPI00043863.2	88.2
12	Isoform 3 of CAP-Gly domain-containing linker protein 1	IPI00217113.1	157.7
13	cDNA FLJ53327, highly similar to Gelsolin	IPI00796316.4	77.7
14	Putative uncharacterized protein TPM3	IPI00966664.1	11.0
Receptors and membrane proteins			
15	Isoform 1 of Vinculin	IPI00291175.7	116.6
16	p180/ribosome receptor	IPI00856098.1	165.6
Signaling proteins			
17	FYN-binding protein	IPI00446986.3	85.3
18	cDNA: FLJ22670 fis, clone HSI08684	IPI00018624.3	15.6
19	Isoform Short of Adenomatous polyposis coli protein	IPI00215877.2	300.1

Table 3-1 (continued): S-nitrosylated proteins from MQ treated HT-29 cells identified by (ESI) MS/MS.

Protein synthesis factors			
20	EEF1A protein (Fragment)	IPI00382804.1	24.1
Cell cycle			
21	Invadolysin	IPI00925115.1	68.2
Protein folding			
22	Putative uncharacterized protein FRMD4B	IPI00946418.1	18.7
Others			
23	cDNA FLJ53328, highly similar to Methylcrotonoyl-CoA carboxylase subunit alpha, mitochondrial	IPI00789136.2	52.6
24	cDNA FLJ51535, highly similar to Phosphatidylethanolamine-binding protein 1	IPI00908746.1	17.3

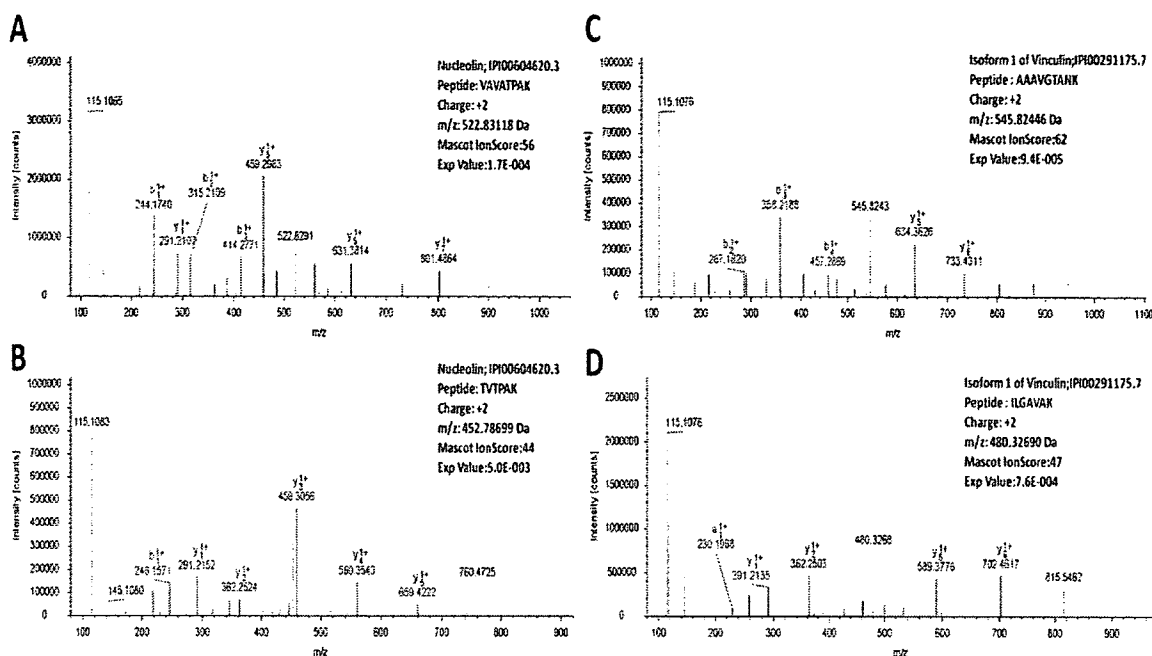


Figure 3-6: MS/MS peptide spectra of nucleolin (**a** and **b**) and isoform 1 of vinculin (**c** and **d**).

3.3.7 Repeatability and Precision of CGE-LIF

The repeatability and precision of the method was determined by performing injection repeatability and analysis repeatability in replicate ($n=5$) injection of the BSA standard solutions [77]. Injection repeatability was measured by performing five replicate injections of the BSA standard solutions; analysis repeatability was measured by the injection of five different samples prepared by the same sample preparation procedure. The relative standard deviation (RSD) values for migration time and peak area were 0.3 and 4.2 %, respectively. The RSD values for migration time and peak area were 0.4 and 1.4 % in the measurement of analysis repeatability. From the data, it was observed that the RSD value of the peak area in analysis repeatability was a little higher than in the injection repeatability. This may suggest the importance of the freshly prepared samples.

In injection repeatability, the SNOs in samples may decrease with each replicate.

However, the analysis repeatability has the advantage of freshly prepared samples, thus leading to lower RSD value.

The precision of the method was determined by performing intra-day and day-to-day assays by replicate (n=5) injection of the mixed standard solution. Intra-day assay precision was done by measuring the BSA standard solutions during the same day, whereas day-to-day precision measured the same BSA standard solutions for five consecutive days. For intra-day precision, the RSD values of migration time and peak area was 0.2 and 3.2 %, respectively; for day-to-day precision, the corresponding values were 0.2 and 2.7 %. The data suggests similar precision for intra-day and day-to-day assays. These results demonstrate that CGE-LIF method can be regarded as repeatable and precise since the RSD values for the migration time and peak areas are all < 5.0%.

3.4 Conclusions

A method for detection and quantification of nitrosylated proteins using fluorescence switch assay coupled with CGE-LIF was developed. This method can detect 1.3 pM concentration of nitrosylated proteins in nanogram amounts of proteins, which is the lowest LOD reported to date. This method also demonstrated its capability in monitoring nitrosylation in both cell culture and tissue systems. Due to the small sample need, it is envisioned that the method can be extended to investigate protein nitrosylation profiles in minuscule brain tissues and/or blood plasma in the disease progression of AD transgenic mouse models.

CHAPTER 4

TWO-DIMENSIONAL NITROSYLATED PROTEIN FINGERPRINTING BY USING POLY (METHYLMETHACRYLATE) MICROCHIPS

4.1 Introduction

Protein S-nitrosylation, the covalent modification of a cysteine sulfhydryl group by nitric oxide (NO), plays a critical role in post-translational modification (PTM) that regulates a large variety of cellular functions and signalling events [44]. The increasing evidence shows this redox-based modification is a biomarker in many diseases, including Alzheimer's disease (AD), Parkinson's disease (PD), Huntington's disease, diabetes, and stroke [1, 45-48]. AD is the most common type of dementia in the elderly population [45]. Previously, an ultrasensitive method of coupling fluorescence switch assay with CGE-LIF system to detect the S-nitrosothiols in biological sample was developed [78]. The fluorescence switch assay procedure consists of the derivatization of nitrosothiols into free sulfhydryl groups followed by specific labelling of sulfhydryl-containing proteins with Dylight 488 maleimide (Ex/Em = 493/528 nm). This procedure proved to be adequate for analyzing nanogram protein samples with picomolar levels of nitrosothiols in less than 15 minutes in a capillary format. However, this one dimensional (1D) gel electrophoresis was unable to separate all individual nitrosylated protein components in the complex biological samples with high dynamic range due to its

relatively poor peak capacities [79]. For this reason, the development of multi-dimensional techniques is necessary for analyzing complex biological samples.

2D separation techniques have been developed for the analysis of complex biological samples [80]. Conventional 2D-gel electrophoresis is one of the most widely used methods, which is a combination of isoelectric focusing (IEF) in the 1st dimension followed by sodium dodecyl sulphate polyacrylamide gel electrophoresis (SDS-PAGE) in the 2nd dimension [34]. This technique has the capability of resolving 5000 proteins [34, 35], and 10,000 proteins can be resolved by large sized 2D-gels [36]. However, this method has some major issues, such as poor reproductibility, time consumption and labour-intensive experimental procedures.

Microchips offer various advantages, such as short analysis times, minimal sample volumes, reduced dead volumes, high peak capacities and easy coupling of multiple separation channels [37]. Although the common modes of protein CE separation have been adapted to the chip format, the multidimensional approaches are still in progress. If the separation mechanisms are orthogonal, the peak capacity of a multidimensional separation is the product of the individual peak capacities obtained from each individual separation [81].

Several groups have explored the application of electrokinetically driven separation techniques on different 2D microchip systems to illustrate multidimensional peptide and protein separations [82]. Li *et al.* described a 2D-CE plastic microfluidic network system for IEF and SDS-PAGE analysis [83]. Yang and co-workers reported a 2D IEF/PAGE separation of *E. coli* proteins using a poly (methylmethacrylate) (PMMA) microchip [84]. However, IEF as the 1st dimension in the microchip separation contains

two drawbacks. First, IEF increases the overall development time of the 2D separation, resulting from an equilibration step prior to the focusing step [84]. Second, IEF is not compatible with highly hydrophobic proteins since they are not compatible with the aqueous IEF buffers typically used [39].

To avoid the drawbacks of IEF, micromicellar electrokinetic chromatography (μ -MEKC) [85, 86] and open-channel electrochromatography (OCEC) [87] have been coupled with capillary electrophoresis on a microfluidic device for the 2D separation of trypsin-digested peptides. Soper and co-workers employed SDS micro-capillary gel electrophoresis (SDS μ -CGE) and μ -MEKC electrophoresis in the 1st and 2nd dimensions, respectively, reporting to sort ten model proteins [38] and serum proteins [39] using a PMMA microchip. The 2D electrophoresis system could generate a peak capacity of ~2,600 in less than 30 minutes for proteins isolated from fetal calf serum (FCS). The same group also combined the SDS μ -CGE with micro-emulsion electrokinetic chromatography (μ -MEEKC) and reported that μ -MEEKC in the 2nd dimension was found to produce higher peak capacities (481 ± 18) compared to μ -MEKC (332 ± 17) [40].

However, many of the multi-dimensional micro-electrophoresis techniques primarily demonstrated their proof-of-concept separation using several model proteins, with only few applied to the true biological samples. To date, no known group has investigated profiling of oxidatively stress-induced biomarkers for disease phenotypes using the 2D μ -CE. This application could help in fingerprinting a panel of electrophoretically separated biomarkers associated with diseases and further act as a tool to distinguish various phenotypes. To address this issue, a 2D micro-electrophoresis

method for the separation of complex protein samples and detection of nitrosylated protein biomarkers using a PMMA microchip has been developed. The 1st dimensional separation contained SDS μ -CGE, which separated proteins based on molecular weight. The 2nd dimension consisted of a fast μ -MEEKC separation, which sorted proteins based on the difference in analytes retention between an aqueous phase and charged oil droplets. Effluents from the SDS μ -CGE dimension were sequentially transferred onto the MEEKC dimension using a pulse sample transfer technique. Laser-induced fluorescence (LIF) was used at MEEKC channel for detecting the fluorophore-labelled nitrosylated proteins. This work presents the use of the discussed 2D μ -CE system to characterize the nitrosylated protein expression in both native and oxidant MQ treated HT-29 cells. The 2D electrophoretic analysis of nitrosylated protein in 11-month-old AD transgenic mice brain tissues and their age-matched wild-type controls are also reported. For future study, nitrosylated proteins in five-month-old AD transgenic mice brain tissues will be compared to their age-matched wild-type controls.

4.2 Material and Methods

4.2.1 Materials and Reagents

Methyl hydroxyethyl cellulose (MHEC), 1X PBS (pH 7.2), tris (hydroxymethyl)-aminomethane, heptanes (>99%), 1-butanol (>99%), ovalbumin, avidin, trypsin inhibitor, glyceraldehyde 3-phosphate dehydrogenase (GAPDH) were all purchased from Sigma. The MEEKC buffer contained 12 mM Tris-HCl, 8 mM heptanes, 90 mM 1-butanol, 0.5% SDS and also 0.05% MHEC at pH 8.5. Prior to rinsing the microfluidic devices, all the buffer solutions were filtered using a 0.2 μ m Acrodisc syringe filter (Pall Corp., East Hills, NY). Other chemicals used in this chapter were described in Section 3.2.1.

4.2.2 Microchip Fabrication

PMMA was used as the substrate for micro-electrophoresis devices because of its high thermal conductivity, separation efficiency, good migration time reproducibility, low cost and ease of fabrication [88, 89]. The microfluidic chip layout is shown in Figure 4-1. Six fluid reservoirs contained sample (A), sample waste (B), buffer 1 (C), buffer waste 1 (D), buffer 2 (E), and buffer waste 2 (F). High voltages were applied to these reservoirs using an independently controlled, programmable six-electrode power supply. The power supply was controlled by a computer with an I/O board (PCI 1200, National Instruments, Austin, TX) and an in-house-written LabVIEW 6.1 (National Instruments) program.

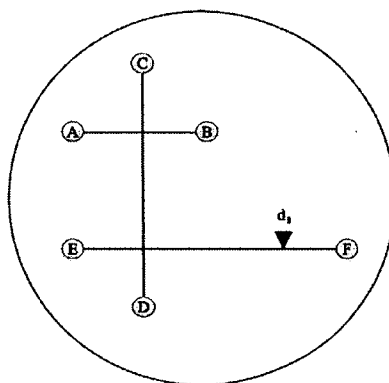


Figure 4-1: Topography of the micro-electrophoresis chip used for the 2D separations.

Channel lengths were ten mm for injection channel, 20 mm for both the SDS μ -CGE (C-D channel) and μ -MEEKC separation (E-F channel) dimensions. All channels were 15 μ m wide and 30 μ m deep. Microfluidic chips were designed using AutoCAD 2010 (Autodesk Inc., San Rafael, CA) and fabricated by following the procedure described previously [39]. Briefly, microfluidic features were fabricated into a brass plate using a micromilling machine (Kern Micro und Feinwerktechnik GmbH and Co., KG,

Murnau, Germany). Then this brass plate was used to produce PMMA (MSC, Melville, NY) chips by hot embossing. A PHI Precision Press model TS-21-H-C (4A)-5 (City of Industry, CA, USA) was used, and the molding tools were heated to 160 °C for pressing the brass plate into the PMMA plate with a pressure of 1100 psi for ~410 s [89].

Following the embossing, the PMMA substrate was cooled to room temperature and removed from the molding die. The embossed PMMA substrate was cleaned with 50% isopropanol in ultrapure water. Finally, a PMMA cover plate (0.25 mm) was bonded via thermal fusion to the substrate by heating in a temperature programmable furnace to 110 °C for 20 minutes.

4.2.3 LIF Detection and Data Acquisition

Fluorescence detection was set up using an in-house constructed laser induced fluorescence (LIF) system (Figure 4-2). A schematic diagram of this detection system has been described previously [39]. A 500 mW, 488 nm blue laser (Coherent, Chicago, IL) was used as the excitation source. A density filter collimated the light from the laser to the 500 nm long pass (LP) dichroic filter. A 40×, NA=0.65 microscopic objective was employed to focus the excitation beam onto the microchip at point d_1 in MEEKC channel (see Figure 4-1). The emission of the sample passed through the 500 nm LP dichroic mirror to the second 540 nm LP dichroic mirror. The resulting Dylight 488 emission was then spatially filtered through a 1 mm pinhole and spectrally filtered using a band-pass filter (520DF5). To reduce background noise, the whole detection setup was contained in a black box, and special care was taken to reduce the scattered light within the box.

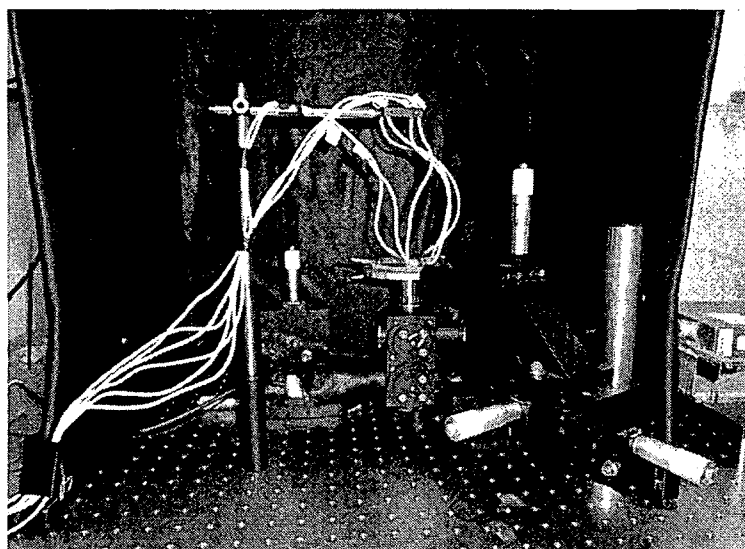
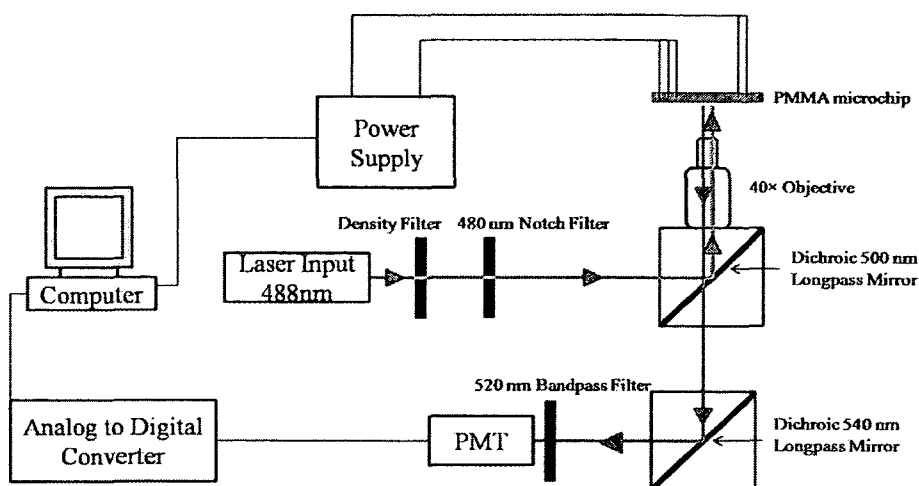


Figure 4-2: Diagram (top) and picture (bottom) of the in-house constructed LIF system.

The data acquisition and control of the high voltage power supplies were created by LabVIEW 6.1 software (National Instruments, Austin, TX, USA). The resulting signal was digitized by an I/O board (PCI-6602, National Instruments). The raw data collected from LabVIEW 6.1 was further analyzed by Igor Pro software (Wavemetrics, Lake Oswego, OR). A custom Igor procedure was created to generate the 3D map analysis of the fluorescence peaks.

4.2.4 Standard Proteins Fluorescence Labelling

A mixture of five proteins (bovine serum albumin, ovalbumin, avidin, trypsin inhibitor, glyceraldehyde 3-phosphate dehydrogenase) was prepared at 5 mg/mL concentration (in deionized water solution) for each protein without further purification. Proteins were fluorescent-tagged according to manufacturer's guidelines of Dylight 488 maleimide (Pierce). Dylight 488 maleimide was used to react with thiols of cysteine residues in these model proteins, creating a highly fluorescent product. Briefly, the proteins' disulphide bond was reduced to generate more thiol groups on cysteine residues by adding tris-(2-carboxyethyl) phosphine (TCEP) into the sample solution. Cysteines then reacted with the Dylight 488 maleimide in an approximate 1:10 molar ratio for at least two hours at room temperature. To remove the unreacted Dylight 488 maleimide dye from the sample, the sample was centrifuged six times at 4500×g (Centrifuge 5804 R, Eppendorf) for 20 minutes each using the Amicon filter with 3000 MW cut-off [25, 60]. The washing solvent was the μ -CE separation buffer. After removal of excessive dye, 5 μ L of 20% SDS in separation buffer was added to a final volume around 100 μ L to denature proteins. The final solution was centrifuged for five minutes at 6000 rpm (Centrifuge 5804 R, Eppendorf) to remove any particles.

4.2.5 Isolation of Brain Tissue from AD Transgenic Mice Model

Double hemizygous AD-Tg mice (B6.Cg-Tg, stock no. 005864, Jackson Laboratory, Bar Harbor, ME) with over expression of mutated forms of Swedish amyloid precursor (A β PP^{swe}), presenilin (PSEN1^{dE9}) and their wild type littermate were used. Since the AD-Tg mice start to develop amyloid plaques at five to six months old, a pair of 11-month old transgenic mice (B6Cg-Tg) and their age-matched wild type (WT)

controls were used to study the expression of nitrosylation long after the pathological plaque manifestation. Mouse gender was not taken into consideration in this research.

The detailed protocol is the same as Section 3.2.6.

4.2.6 Fluorescence Switch Assay

To detect a trace amount of nitrosylated proteins in biological samples (oxidant mediated cell culture and AD brain homogenate), targeted nitrosylated proteins were derivatized and fluorescently labelled for their subsequent electrokinetic separation on chips. The detailed procedure of fluorescently labeling of nitrosylated proteins was described in Section 3.2.7.

The untreated HT-29 cells, 11-month-old Tg B6Cg-Tg mice brain tissues and their age-matched controls followed the same procedure.

4.2.7 μ -CE (2D) Microchip Operation

The procedure for running the 2D micro-electrophoresis separation was as follows: First, prior to the electrophoretic separation, MHEC was dissolved in PBS (pH 7.2) to a concentration of 5mg/mL. This solution was injected at reservoir C to flush the entire microfluidic channel for at least ten minutes. The MHEC was used as a dynamic coating to control electroosmotic flow (EOF) and reduce protein adsorption to channel walls. Next, the 1st dimension channel was filled with a CGE sieving matrix. The gel filling was monitored by bright field microscopy to make sure the gel was allowed to fill the chip exactly at the intersection of the first and the 2nd dimensions of the channels. The 2nd dimension was then filled with the MEEKC buffer. Reservoir A was emptied and subsequently filled with 2 μ L fluorescently labelled samples. After the sample was loaded, a field strength of 200 V/cm was applied for 30 seconds to move the proteins to

the intersection of channels A-B and C-D. The electric field was generated by applying a positive potential at waste reservoir B while grounding the sample reservoir (A). The 2nd dimension separation was programmed to start after an 80 second electrophoresis run time in the 1st dimension.

The SDS μ -CGE separation was carried out at 350 V/cm in the 1st dimensional channel (CD channel) by administering a positive voltage at reservoir D while grounding reservoir C. Then the pull back voltages (0.07 kV) were applied to both sample and waste reservoirs (A and B). The 2nd dimensional MEEKC cycle consisted of a ten second run operated at field strength of 400 V/cm (see Table 4-1). This amount of time was found to be sufficient to assure that all of the components injected into the 2nd dimension reached the LIF detection zone. After a ten second separation, voltage was turned off at F, and the 1st dimensional separation was resumed for one second to move more proteins into the MEEKC channel. This was followed by a ten second separation in the EF channel. The process was repeated until all proteins were transferred from the 1st dimension to the 2nd dimension. Pullback voltage was applied throughout entire experiment. The LIF detector was positioned at point d₁ (10 mm from the intersection of channels CD and EF) on EF channel.

Table 4-1: Summary of high-voltage protocol for 2D separations on a PMMA microchip

Step	Applied voltages (kV) in reservoirs					
	A	B	C	D	E	F
Injection	Grounded	+0.20	Floating	Floating	Floating	Floating
SDS μ -CGE	+0.07	+0.07	Grounded	+0.07	Floating	Floating
Second MEEKC cycle	+0.07	+0.07	Floating	Floating	Grounded	+0.08
1D to 2D sample transfer	+0.07	+0.07	Grounded	+0.07	Floating	Floating

4.3 Results and Discussion

4.3.1 Assessment of Sample Transfer Starting Time and CGE-to-MEEKC Transfer Cycles

Since the dye in the fluorescence switch assay may not be removed completely [90], the 1D separation and detection of the fluorophore dye, Dylight 488 maleimide was examined first. This study also helped in distinguishing the peaks of the fluorescence dye itself from those of the nitrosylated proteins. Figure 4-3 shows the electropherogram of the Dylight 488 maleimide alone, which exhibits multiple peaks. More than one fluorescence peak is observed since this reagent is an isomeric mixture.

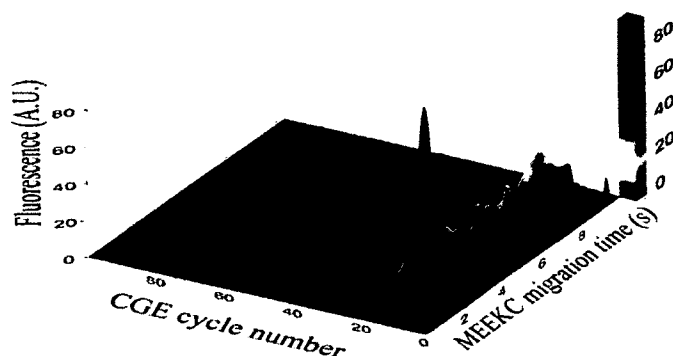


Figure 4-3: Background signal generated by Dylight 488 maleimide.

The time to start transferring migrating components from the 1st dimension (CGE) to the 2nd dimension (MEEKC) in this study depended on the migration time of the 1st peak in the SDS μ -CGE dimension. The Dylight 488 maleimide, a small molecule compared to proteins, showed up as the first peak after 80 s in the 1st dimension (Figure 4-4). Hence we started the 1st-to-2nd dimension transfer at 80 s. To assure all the peaks in the 1st CGE dimension would be transferred and sampled in the 2nd MEEKC dimension, the total number of required cycles was determined according to the transfer time of one second and the last band migration time determined experimentally in the 1st dimension.

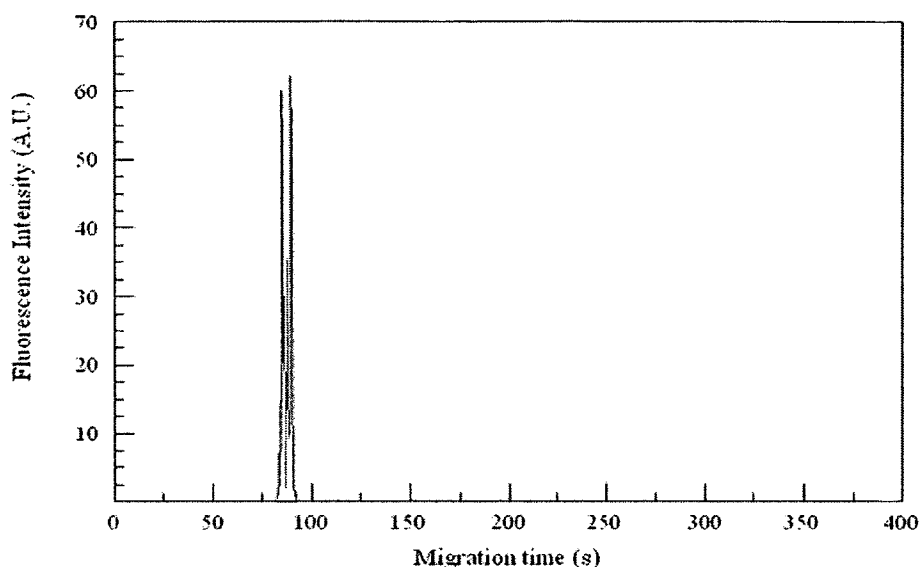


Figure 4-4: 1D separation (SDS μ -CGE) of dye (Dylight 488 maleimide) using the PMMA microchip.

4.3.2 μ -CGE (1D) and μ -MEEKC (1D) Separation of Standard Proteins

Five model proteins consisting of bovine serum albumin (BSA) (66,000 Da), ovalbumin (43,000 Da), avidin (64,000 Da), trypsin-inhibitor (20,000 Da) and glyceraldehyde 3-phosphate dehydrogenase (GAPDH) (36,000 Da) were employed for demonstration of 1D separations in μ -CGE and 1D MEEKC chip.

CGE mode is perhaps mostly employed in microchips for protein separation. Because a pullback voltage is applied during 1D separation, only the proteins in the channel intersection are injected. Therefore, a total volume of 6.75 pL of solution is analyzed in this study. Hence, 33.75 pg of each protein was detected based on the concentration of 5 mg/mL for each standard protein. The limit of detection for this dimension was estimated as 4.53 attomole when signal-to-noise ratio was set at 3. A linear plot of logarithmic molecular mass-log (MW) versus the corresponding migration

times (MT) was constructed for SDS μ -CGE separation (Figure 4-5), and an equation was obtained as follows

$$\log(MW) = 3 \times 10^{-3}MT + 3.948.$$

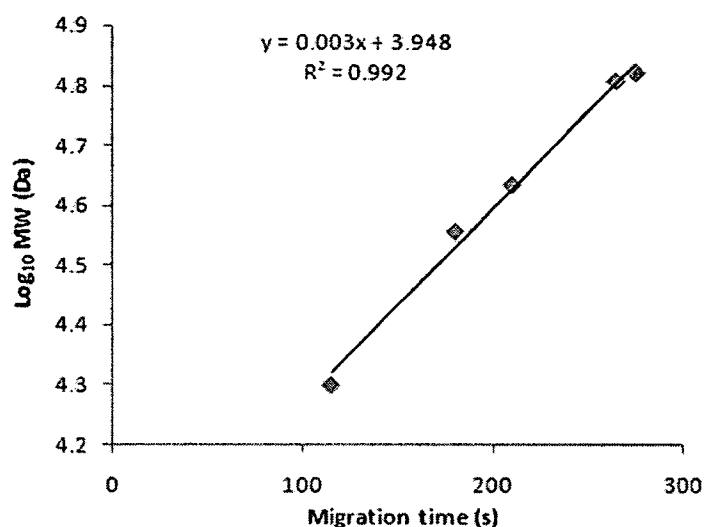


Figure 4-5: Plot of the logarithm of molecular mass versus corresponding migration times of the SDS μ -CGE separation of five standard proteins ranging in MW from 20-66 kDa.

The plot shows good linearity ($R^2=0.992$) across the molecular weight range studied (20,000-66,000 Da). The sieving electrophoresis dimension of the 1D separation provides an estimate of molecular weight similar to that provided by other sieving electrophoresis methods, such as conventional CE separation [56].

From the SDS μ -CGE separation, the size-based μ -CGE separation was unable to resolve all five standard proteins since BSA and avidin have similar molecular weight. However, all five model proteins were successfully resolved in phase retention based MEEKC separation (Figure 4-6).

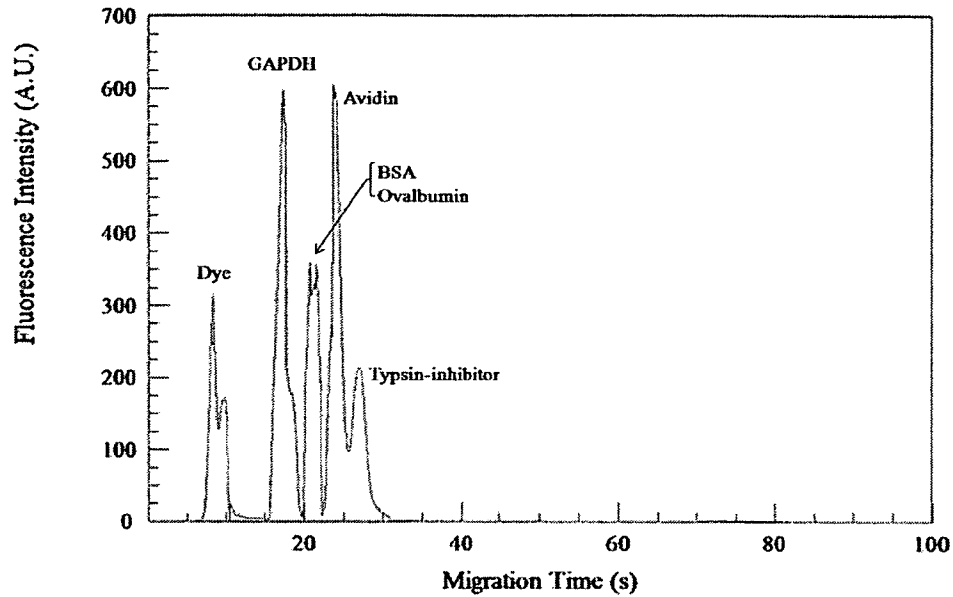


Figure 4-6: MEEKC separation of five standard proteins.

Peak capacities were then calculated for individual peak profiles from the CGE and MEEKC separations [86]. A peak capacity of 48 in the first CGE separation was estimated by assuming a span of migration time that peaks appear over an average separation baseline width of five seconds. For MEEKC, the model protein produced an average separation baseline width of two seconds over a separation window of 16 seconds, which resulted in a peak capacity of eight. With the orthogonal micro-electrophoresis chip design of CGE and MEEKC, the overall peak capacity in the current protein separation platform was estimated to be around 304 (48 and eight in the 1st and 2nd dimension, respectively).

4.3.3 μ -CGE/MEEKC Separation (2D) of Standard Proteins

A set of five standard proteins was analyzed with the 2D- μ CE system. A set of five spots was observed in Figure 4-7. In this study, SDS μ -CGE was selected as the 1st

dimension because of the rapid separation and easy diffusion of the protein samples into the MEEKC channel. To completely transfer the protein plug from the 1st CGE dimension to the 2nd MEEKC dimension, the electrokinetic-based technique was employed to inject effluent every one second.

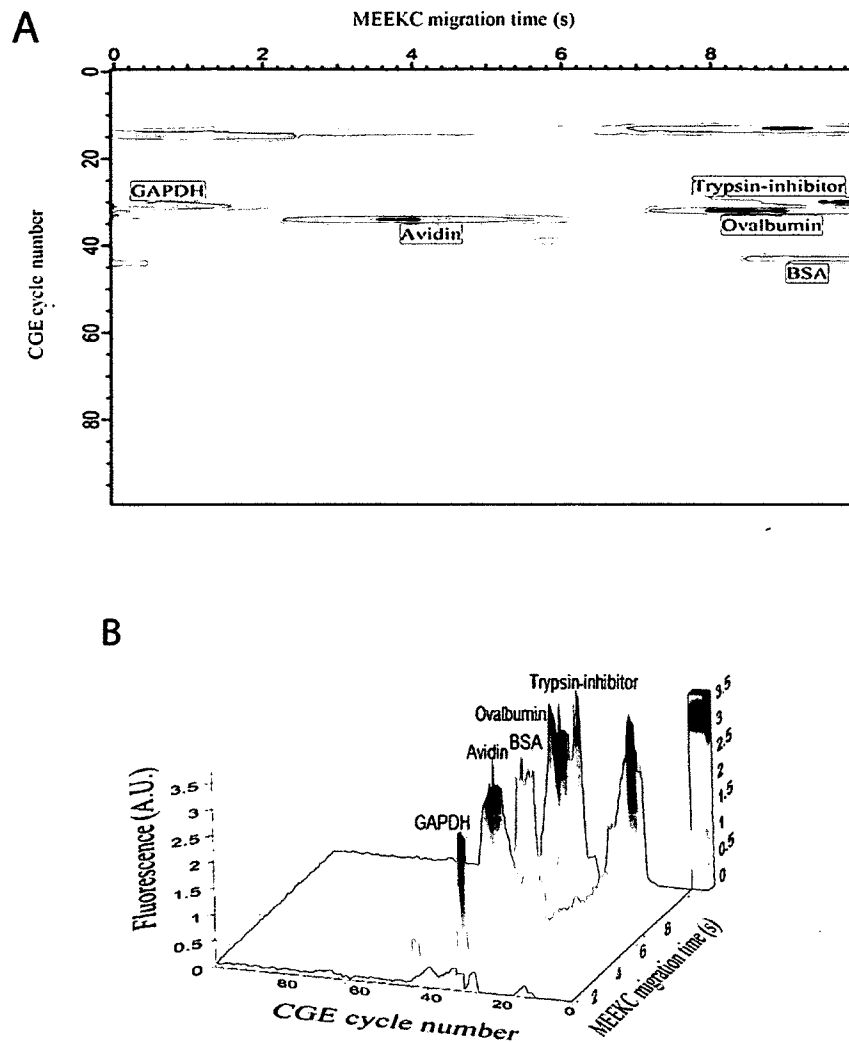


Figure 4-7: Landscape image from five standard proteins. (A) Contour image for the microchip 2D SDS μ -CGE \times μ -MEEKC separation profile of five standard proteins. The density in this plot is proportional to the fluorescence intensity. (B) Corresponding microchip 2D SDS μ -CGE \times μ -MEEKC separation. The height of the peak is proportional to the fluorescence intensity.

The gel/MEEKC buffer solution interface helped isolate these two separation media and further provided protein stacking during electrokinetic transfer between the coupled separation dimensions.

In the future, each protein should be run individually to correspond to the mixed sample.

4.3.4 μ -CGE (1D) of Nitrosylated Proteins from HT-29 Cells

To demonstrate the detection of nitrosylated proteins after nitrosothiol derivatization and fluorescence labelling, the 1D μ -CGE separation of proteins from the human colon epithelial adenocarcinoma cell line HT-29 was first investigated (Figure 4-8). Approximately, 50 peaks were counted with different levels of resolution and width. These differences resulted from protein peaks overlapping at a close range of MW. The first and last migration components have migration times of 125 seconds and 450 seconds, respectively. Based on this defined migration window and the average separation baseline width estimated as 5 seconds, a peak capacity of 65 was generated in the 1-D μ -CGE separation of nitrosylated proteins in HT-29 cells. The widely used formula ($N=5.545 t_R^2/w_{1/2}^2$) was used to calculate the theoretical number in the 1st dimensional separation of nitrosylated proteins isolated from HT-29 cells. The separation efficiency amounts to up to 2.81×10^5 theoretical plates generated from the half height peak width of 2 s ($w_{1/2}$) and retention time of 450 s (t_R) [91]. Since the peaks displayed in Figure 4-8 are too complex, protein purification and pre-separation need further study.

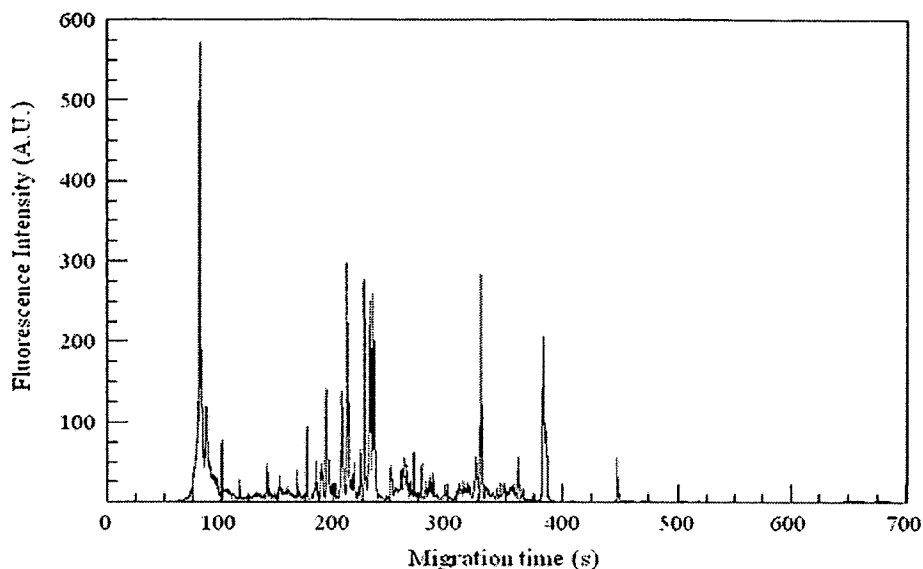


Figure 4-8: SDS μ -CGE analysis (1D separation) of HT-29 cells using a PMMA microchip.

4.3.5 μ -CGE/ μ -MEEKC (2D) Nitrosylated Protein Fingerprint from HT-29 Cells

Figure 4-9 presents the 2D image and the corresponding 3D landscape image of nitrosylated proteins from HT-29 cells. Figures 4-9 A and B present the data from HT-29 cells. The z-axis (fluorescence signal) at each point is proportional to the nitrosylation abundance. The data consists of some peak clusters around the 320th cycle. These clusters undoubtedly consist of a number of proteins that co-migrate. The signals from these components are out of range of the photomultiplier tube, which demonstrates the sensitivity of the instrument. Since most of the signals were saturated, in the future samples should be diluted before 2D separation.

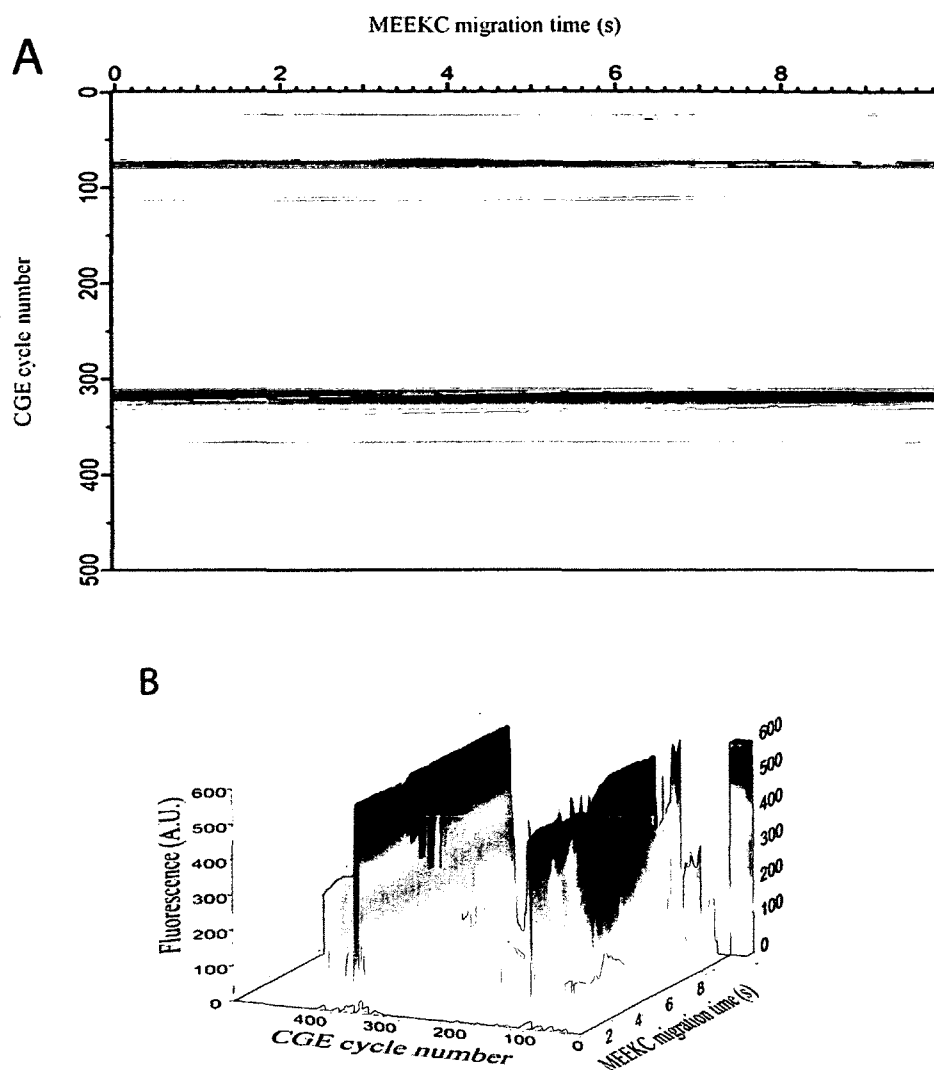


Figure 4-9: Protein landscape image from HT-29 cells. Panel A is the contour image from 2D separation profile of nitrosylated protein extracted from HT-29 cells. Panel B presents the corresponding 3D landscape image for the 2D contour image.

Figures 4-9 C and D present the 3D landscape of nitrosylated proteins from HT-29 cells that were treated with menadione (MQ). MQ is a redox cycling quinone that has the redox-cycling capability to acrylate cellular nucleophiles, such as DNA and proteins, in mitochondrion, considered as the main redox site [52-54]. HT-29 cells treated with MQ demonstrate an altered cellular phenotype with more peaks appearing. Furthermore, MQ-treated HT-29 cells generated much larger signals than the untreated cells between

the 350th and 440th cycles. Therefore, it is concluded that exposure to MQ caused an increase in protein nitrosylation damage. However, we can see that even the 2nd dimensional separation could not resolve the complex protein mixture in the biological samples with a separation length of 10 mm. To increase the peak capacity of this 2D separation format, the effective separation channel length could be potentially increased in the future separation [39].

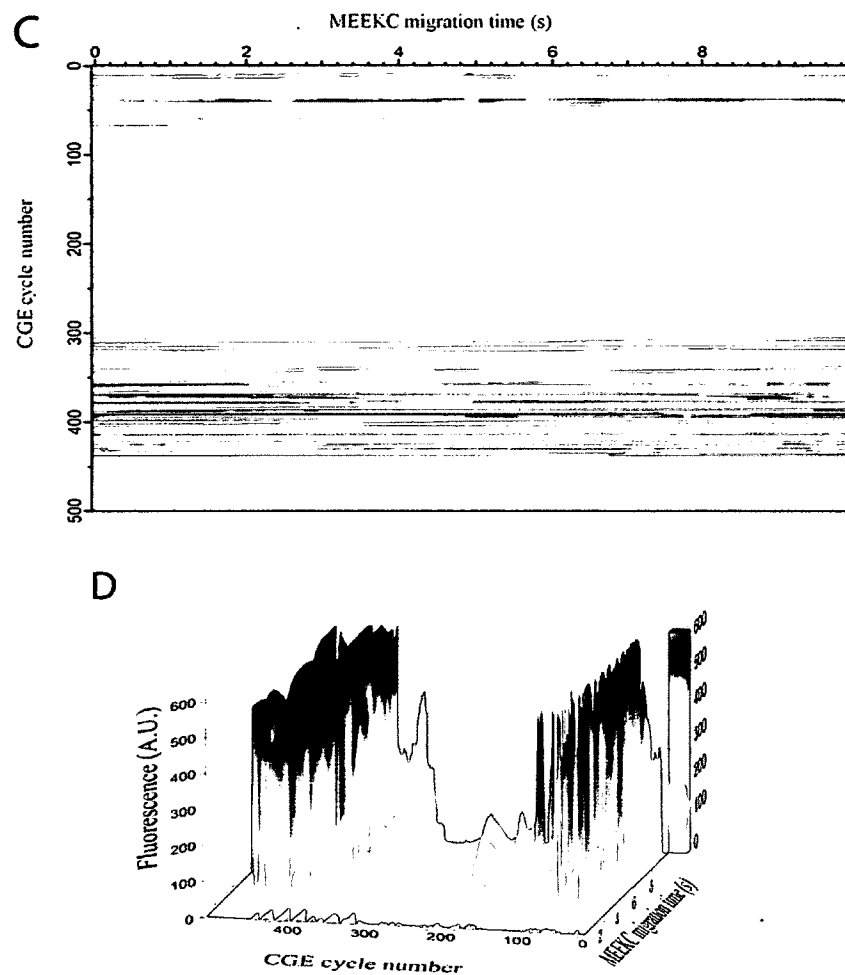


Figure 4-9 (continued): Protein landscape image from HT-29 cells. Panels C and D show the corresponding 2D protein nitrosylation separation images from cells that had been treated with 200 μ M MQ for 30 minutes.

Additionally, based on the linearity between the logarithm of molecular weight and electrophoretic mobility (Figure 4-5), these nitrosylated HT-29 cell proteins were estimated to be in the range from 20 kDa to 300 kDa. Since this range is beyond the one used in the calibration curve, bigger range of standard proteins will be used to confirm this result.

Since the average separation baseline width was determined in the 1D μ -CE to be around five seconds, the fraction transfer time was intentionally set at one second leading to five times of the second MEEKC separation upon transfer for each peak. This frequent sampling actually helped eliminate band aliasing artifacts and further improve 2D profiling accuracy [87, 92].

In order to completely sample all components migrating from the 1st dimension to the 2nd dimension, at least a total of 450 cycles were required with ten seconds separation in each MEEKC run after one second per transfer. When considering the 80 seconds runtime in the 1st CGE dimension, the total development time for the full 2D separation was around 84 minutes.

4.3.6 Nitrosylated Protein Fingerprint (2D) from 11-month-old AD Mice Brain

As a second example, Figure 4-10 presents 2D experiments for the protein nitrosylation fingerprinting from 11-month-old transgenic mice (B6Cg-Tg) and their age-matched wild type (WT) controls.

Carrying both APP and exon 9 deletion of the PSEN1 gene, the B6Cg-Tg mouse is a valuable model to study the pathological alterations in AD.

A 2D separation of the nitrosylated proteins in AD transgenic mice (Figure 4-10 A and B) produced higher peak signals when compared to the wild type controls (Figures 4-10

C and D) around 165th and 190th cycles. The total 2D separation with LIF detection was completed in 36 minutes.

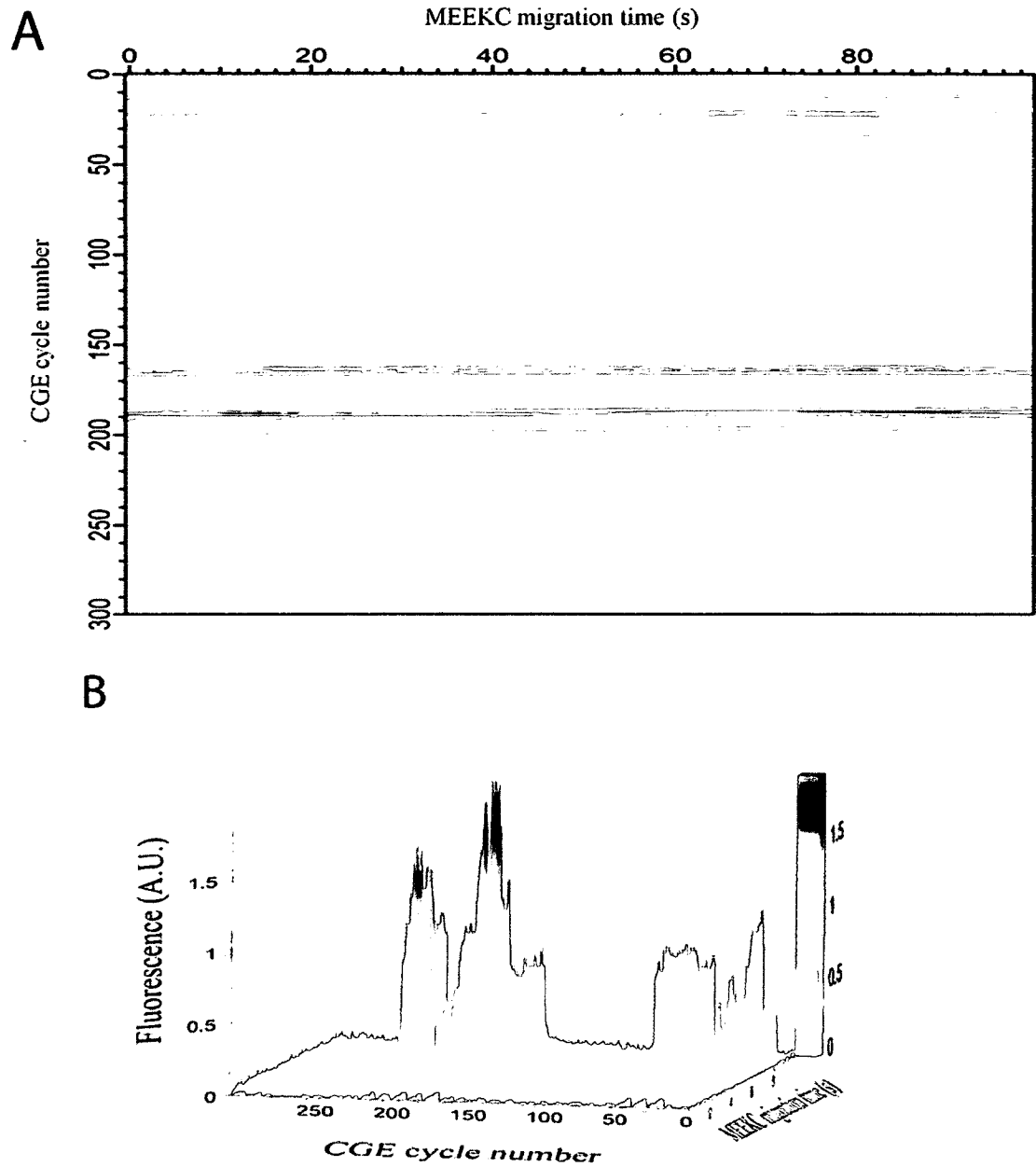


Figure 4-10: 2D separation landscape images of the nitrosylated proteins from AD transgenic mice and age matched wild type control. Panels A and B were generated from 11-month-old AD transgenic mouse brain tissues.

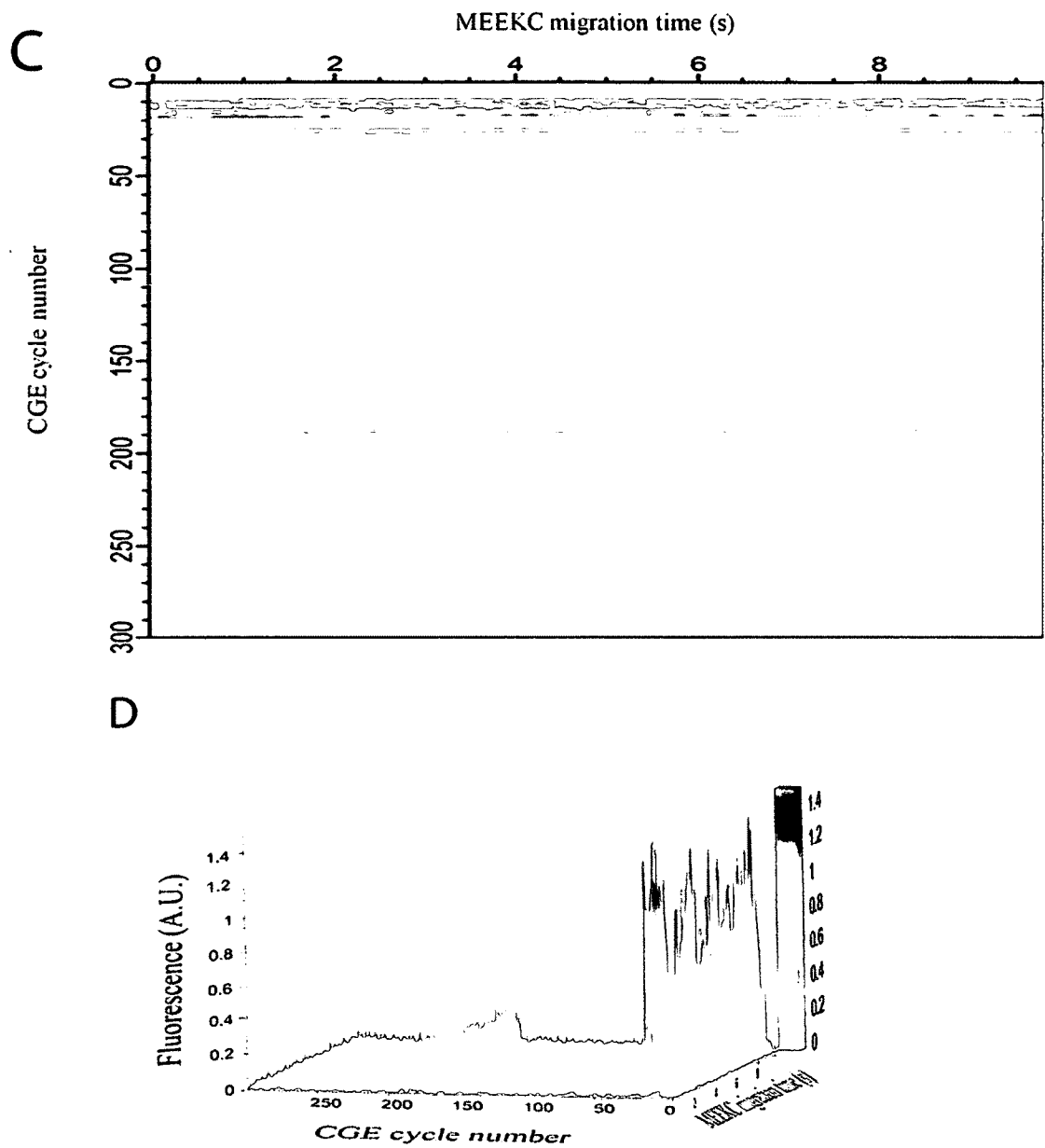


Figure 4-10 (continued): 2D separation landscape images of the nitrosylated proteins from AD transgenic mice and age matched wild type control. Panels C and D were generated from age related wild type control.

Additionally, these AD brain proteins, which are most susceptible to oxidative damage, particularly nitrosylation, were estimated to have a MW between 35 kDa and 65 kDa.

While 2D separation occurs, 1D is placed in a standing state. It is not known what effect a long standing state has on the pre-separated protein bands. However, results indicate a clear separation of these proteins in the 2D. Therefore, it is concluded that the separation efficiency in the 2nd dimension is great enough to overcome any possible protein diffusion.

4.4 Conclusions

A complex sub-population of proteome, nitrosylated proteins was studied, profiling it using a 2D μ -CGE/MEEKC polymer microchip and monitoring its expression using a LIF detector. The 2D μ -CE device achieved high peak capacity, which allows the separation of a panel of nitrosylated proteins. In addition, the ultrasensitive assay of nitrosothiol derivatization and labelling allowed monitoring these biomarkers even at a low abundance level. First, *in-vitro* nitrosylated proteins were used, including BSA, avidin, avabumin, GAPDH, trypsin inhibitor, ranging in size from 20 to 66 kDa, as the model to test the performance of the 2D microchip separation and fluorescence detection. All of the five standard nitrosylated proteins were detected using LIF with excitation/emission at 493/518 nm. Additionally, high peak capacity 2D maps of complex nitrosylated protein mixtures were generated from MQ-treated HT-29 cells and 11-month-old AD transgenic mouse brain. Finally, the rapid profiling of oxidative stress-related protein biomarkers was demonstrated in a complex biological mixture using 2D micro-electrophoresis. Altogether, oxidative-stress induced biomarker profiling was

generated. This application could further serve as fingerprints to determine AD disease phenotypes from biological samples.

CHAPTER 5

IDENTIFICATION OF S-NITROSYLATED PROTEINS AFTER EXPOSURE OF HUMAN COLON ADENOCARCINOMA CELLS TO MENADIIONE

5.1 Introduction

Protein S-nitrosylation, the covalent modification of a cysteine sulfhydryl group with nitric oxide (NO), plays an essential role in posttranslational modification (PTM) that regulates a large variety of cellular functions and signaling events [44]. Most organisms are exposed to oxygen specials that may influence the structural configuration and integrity of proteins and modulate their function and eventually influence cell survival. The nitrosylation state changes with oxidative damage and is involved in variety of cancers and neurodegeneration diseases [1, 45-48].

Due to the importance of protein S-nitrosylation, several methods have been developed to detect nitrosylated proteins in biological samples. These approaches can be generally divided into two branches: direct methods and indirect methods.

Direct detection of protein S-nitrosylation includes immunohistochemistry by the use of a SNO-specific antibody to detect *in vivo* protein S-nitrosylation [23].

Conventional methods such as immunoprecipitation, 2D-gel electrophoresis or western blot are generally not preferable for protein S-nitrosylation because the S-NO bond is degraded in the SDS-PAGE step [24]. However, the use of biotin switch assay coupled

with these methods can indirectly detect the changes in protein S-nitrosylation status under different biological conditions [25].

Currently, a number of indirect methods are being used for the nitrosothiols quantitative measurement, which either requires cleavage of the S-NO bond followed with NO level measurement or replaces the S-NO with another detectable tag. One widely utilized method is the saville assay [17]. The mechanism of this method is to replace NO⁺ from the thiol group by mercuric chloride in the presence of sulphamylamide and then react with N-(1-naphyl)-ethylenediamine. The reaction product, a colored azo dye, can be detected by spectrophotometrically at 540nm [20]. Biotin switch assay (BSA) is another widely used method for detecting protein S-nitrosylation [25]. It utilizes a sulphhydryl-specific biotinylation agent to react with free cysteine that is created from nitrosothiol group (S-NO) to form the biotin tag. Then this method can couple with immunoblotting, 2D-gel electrophoresis, or fluorescence gel electrophoresis to detect changes in protein S-nitrosylation status under different biological conditions. Such a method can effectively determine the total level of protein S-nitrosylation present in the biological sample, but they are unable to identify specific S-nitrosylated proteins.

For the identification of nitrosylated proteins sites in the complex biological samples, mass spectrometry (MS)-based approaches are required. Due to the lability to this type of modification, the direct detection of MS is still quite problematic. A couple of indirect methods have been developed for protein identification. The previously widely used method is the biotinylated proteins purified by avidin affinity chromatography after BSA and then followed by 2D-gel electrophoresis (2-DE) for MS analysis [5, 7, 26-30]. Few S-nitrosylation proteins have been identified by this approach due to its low

abundance and to the low recovery of S-nitrosylated peptides from in-gel digestion. A new method, SNO Site Identification (SNO), introduced a proteolytic digestion step before avidin capture [31]. It allows the selective isolation of peptides that previously contained S-nitrosylated Cys residues. Sixty eight S-nitrosylated peptides from 56 rat cerebellar proteins were identified in this study. In this way, only the modified peptides are enriched and eluted for the following identification by MS: this is a fundamental improvement because only the localization of the modified residue can confer high confidence as to the results. However, two disadvantages are shown in this method. First, the identification of a protein depends on MS/MS-based sequence information inferred from a single peptide ion. Second, the relative large amount (1g) of starting tissue/cells required. Camerini et al. used an N-terminally modified His-tag to selectively label the thiol group (SH) reduced by nitrosothiol group (SNO) instead of biotin tag [32]. From this approach, the author got 28 modified Cysteine moieties from 19 proteins. Forrester et al. recently developed a method named S-nitrosothiol resin-assisted capture (SNO-RAC) which required fewer steps because it combines the labeling and pull down steps from the BSA into one step [33]. This approach can detect 44 novel SNO sites in *E. coli*. The reporter pointed out that this method appeared to be more sensitive than the BSA for high mass proteins, and at least as sensitive as the BSA for proteins smaller than 100 kDa. However, Liu et al. revealed that both the BSA and RAC approaches were not effective at S-nitrosylation site identification [24]. They did not address the issue of accurate site localization, especially when more than one cysteine was present in an identified peptide sequence. They presented a novel and robust method for site-specific high-throughput identification of protein S-nitrosylation (SHIPS) in complex protein mixtures. The SHIPS

approach utilized a cysteinyl affinity resin to pull down ascorbate reduced S-nitrosylated peptides, rather than S-nitrosylated proteins. Two commonly used alkylation agents, acrylamide and iodoacetamide, were employed to differentiate free and disulfide-bonded cysteine from reduced S-nitrosylated cysteine [24]. A total of 162 S-nitrosylation sites were identified, and an S-nitrosylation motif was revealed in this study.

Cancer is commonly referred to as a genetic disease. However, the functional product, the protein, is what determines the signaling events that lead to cancer progression. A number of alterations can occur at the posttranslational level to affect function (i.e., phosphorylation, carbonylation, S-nitrosylation). Cancer chemotherapeutic agents inhibit cancer cell proliferation, but also cause damage to these cells and normal cells by inducing oxidative stress. Menadione (MQ), a redox cycling quinone used with cancer chemotherapeutic agents, results in oxidative protein S-nitrosylation damage in human colon adenocarcinoma cells (HT-29) [78]. MQ has been used in conjunction with cancer chemotherapeutic agents to treat various cancers [93]. MQ has the redox-cycling capacity to acrylate cellular nucleophiles such as DNA and proteins, with mitochondrion considered as the main redox site [52-54, 93]. Proteins in cellular and subcellular members and in the cytoskeleton may be altered by MQ [93]. Thus, MQ is proposed to initiate a cascade of ROS formation which leads to cell injury and death (Figure 5-1).

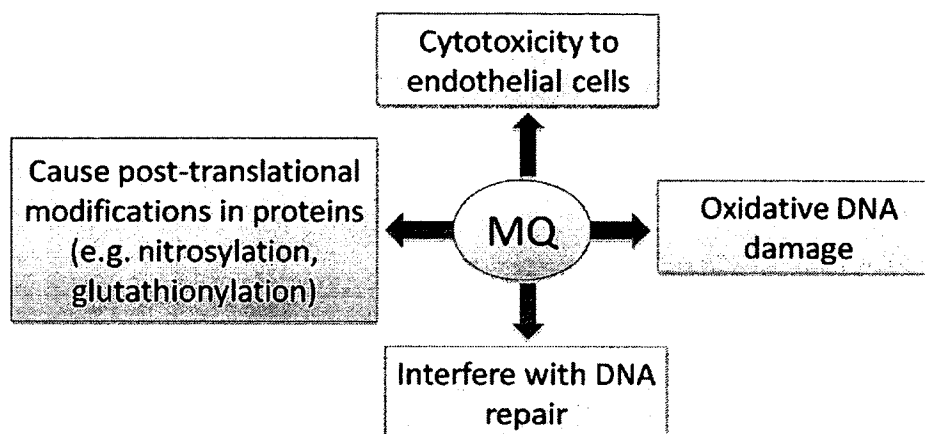


Figure 5-1: The potential damage MQ induced in cells.

Oxidative protein nitrosylation damage mediated by menadione (MQ) was monitored. To extend the capability of the biotin-switch method, a proteolytic digestion step before avidin capture was introduced. This changed step provides for the selective isolation of peptides that previously contained SNO-Cys residues, rather than intact SNO proteins in the original biotin-switch method [31]. Then, liquid chromatography tandem MS (LC-MS/MS) was exploited for high-throughput peptide identification, thereby describing the set of SNO-Cys sites on proteins. Among the 20 S-nitrosylated proteins identified in the MQ-treated HT-29 cells, 17 of them are novel targets of S-nitrosylation. The identification of these novel S-nitrosylated proteins may benefit the oncology community in treatment.

5.2 Material and Methods

5.2.1 Materials and Reagents

Biotin-HPDP and streptavidin-agarose were purchased from Pierce. Acetone was purchased from VWR International. Other materials and reagents were previously listed in Section 3.2.1.

5.2.2 *In Vitro* Nitrosylation of BSA and SNO Quantification by Saville-Griess Assay

An internal control experiment was performed to confirm that the same amount of sample and control was added. The procedure was previously described in Section 3.2.3.

5.2.3 Labelling of S-nitrosylated Proteins by the Biotin Switch Assay

The biotin switch assay was performed as described by Jaffrey and Snyder [25] (Figure 5-2). Briefly, the protein concentration was adjusted to $0.8 \mu\text{g}/\mu\text{L}$ using HEN Buffer (250 mM HEPES/NaOH pH 7.7, 1 mM EDTA, 0.1 mM neocuproine) and then incubated at 50 °C for 30 minutes in Blocking buffer (nine volumes of HEN buffer, one volume of SDS (25% w/v in H₂O) and a final concentration of 20 mM MMTS) with frequent vortexing. Acetone precipitation was performed to remove MMTS. The protein pellet was re-suspended in 0.1 mL HENS solution (HEN Buffer in 1% SDS) per mg protein, followed by incubation with 2 mM biotin-HPDP and 2 mM ascorbate for 1 hour at 25 °C. Until this point, all operations were carried out in the dark. After biotinylation to label S-nitrosylated proteins, biotin-HPDP was removed by acetone precipitation and centrifugation, and the pellet was resuspended in 0.5 mL HENS buffer.

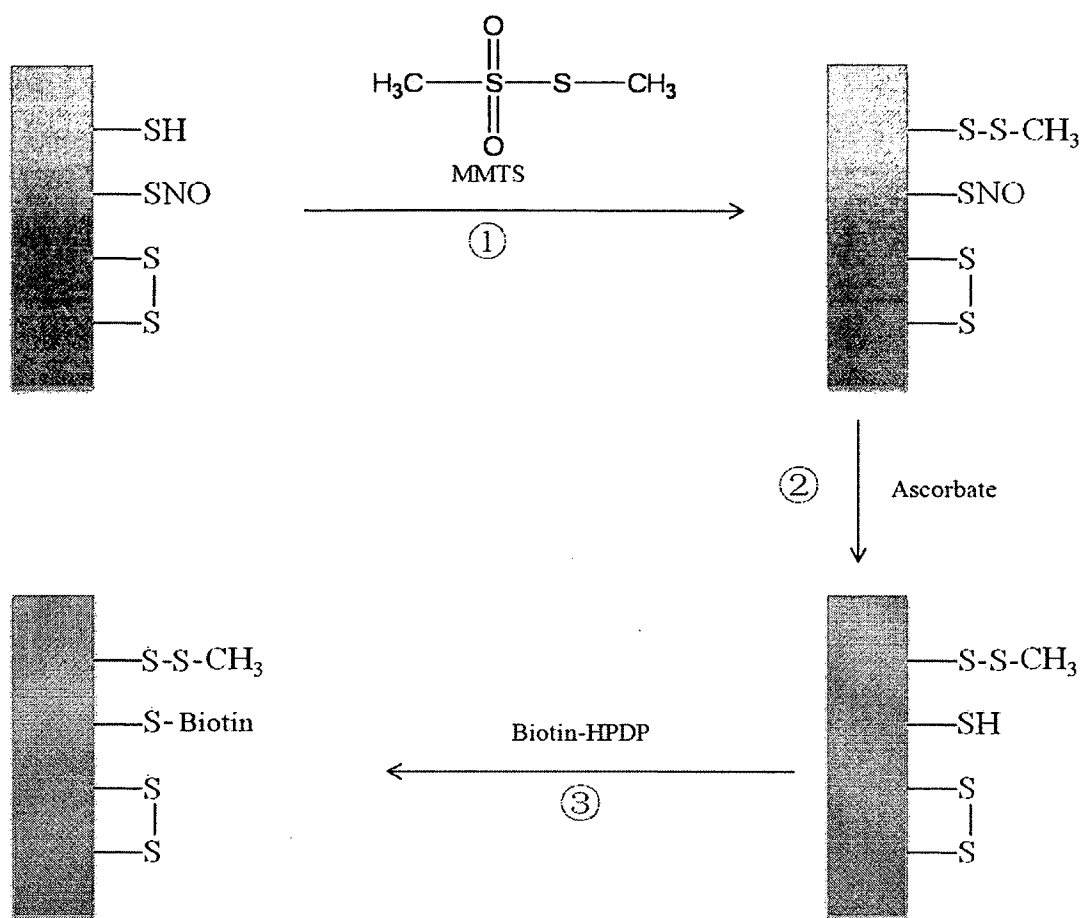


Figure 5-2: Schematic of the biotin switch assay technique following the track of protein S-nitrosylation.

5.2.4 Purification of S-nitrosylated Proteins for Proteomics

The biotinylated proteins were incubated with trypsin (1: 10 enzyme/ protein ratio) at 37 °C for overnight. The peptides were recovered and incubated with 50 μL of streptavidin-agarose beads per mg of initial protein for 30 minutes with gentle mixing. Samples were centrifuged at $5,000 \times g$ for five minutes, and the supernatants were discarded. The beads were washed five times with ten volumes of 1 M ammonium bicarbonate, followed by five washes with ten volumes of deionized water. Between washes, samples were centrifuged at $1,000 \times g$ for one minute. Elution buffer containing

70% formic acid (FA) was incubated with the beads for 30 minutes with gentle mixing. The captured peptides were recovered by centrifuging beads at $5,000 \times g$ for four minutes and collected the supernatant. To ensure complete removal of streptavidin-agarose, the samples were centrifuged again. The supernatant was collected and was further purified with a mixed-mode cation exchange column prior to liquid chromatography-tandem mass spectrometry (LC-MS/MS) analysis [6].

5.2.5 Analysis by LC-MS/MS

Liquid chromatography-tandem mass spectrometry (LC-MS/MS) analysis was performed as described in previous report [94, 95]. Briefly, the peptide fragments extracted from streptavidin were separated and analyzed using a capillary LC system coupled with a nanospray quadrupole time-of-flight micro mass spectrometer (Waters Corp., Milford, MA). The MS was operated in a data-dependent acquisition mode. Then a full survey MS scan was followed by three MS/MS scans using normalized collision energy. The instrument was set up in positive ion mode, with an electrospray voltage of 3.5 kV, sample cone voltage of 40 V, and extraction cone voltage of 1.5 V. The peaklist (pkl) files were generated using ProteinLynx Global Server 2.2.5 (PLGS 2.2.5, Waters Corp.) Tandem mass spectra were analyzed using the PLGS 2.2.5 (Waters Corp.) and MASCOT (version 2.2, Matrix Science, Cambridge, MA) software against a Swiss-Prot database (release 57.3, 468 851 sequences) [95]. For both PLGS and MASCOT, the database search settings included variable modifications of biotin-HPDP of cysteine residues (+428 atomic mass units); precursor-ion mass tolerance, 200 ppm; fragment-ion mass tolerance. MQ oxidation of protein was allowed as a variable modification in the databank search query in PLGS and MASCOT, and automodification query was selected

to identify peptides with further post-translational modifications in PLGS. The top ranking hits (score 8-13 for PLGS and $p < 0.05$ for Mascot assignment of identity) were scrutinized based on molecular weight, pI, and sequence coverage. Spectra were also examined carefully to verify that the spectra included a good number of consecutive “y” ions with high mass accuracy. If peptides matched to multiple members of protein family with similar sequences, the protein identified was the one with the highest number of matched peptides and score [94].

5.3 Results

5.3.1 Proteomic Analysis of S-nitrosylated Proteins in MQ Treated HT-29 Cells

To determine the proteomic profile of S-nitrosylated proteins in HT-29 cells, the biotin-switch method was used combined with a proteomic approach. S-nitrosylated proteins extracted from HT-29 cells undergoing MQ exposure were subjected to the biotin-switch method, digested overnight, purified by affinity chromatography on a streptavidin-agarose matrix and then separated by LC-MS/MS. Four biological replicates were carried out for the data analysis. Twenty proteins were detected and included in the analysis of MQ treated HT-29 cells (Table 5-1). Among the 20 proteins, ten of them are identified in the untreated HT-29 cells (Table 5-2). The proteins identified were members of specific functional families including folding proteins, chaperones, metabolic proteins, signaling proteins, cytoskeleton proteins, and membrane proteins. Three of these, Elongation factor 2, Elongation factor 1 A-1 and L-lactate dehydrogenase B chain, have been previously reported to be S-nitrosylated in other systems [6, 28, 29].

Table 5-1: S-nitrosylated proteins identified by LC-MS/MS in HT-29 cells preincubated with MQ.

Number (NO.)	Protein ID (MQ treated HT-29 cells)	Description	Accession NO.	Molecular Mass (kDa)	PI
Protein folding					
1	RS7_HUMAN	40S ribosomal protein S7 OS Homo sapiens GN RPS7 PE 1 SV 1		22.1	10.6
Chaperones					
2*	HSP77_HUMAN	Putative heat shock 70 kDa protein 7 OS Homo sapiens GN HSPA7 PE 5 SV 2	P48741	40.2	7.9
Metabolism					
3	LDHB_HUMAN	L lactate dehydrogenase B chain OS Homo sapiens GN LDHB PE 1 SV 2	P07195	36.6	5.6
4*	LDHA_HUMAN	L lactate dehydrogenase A chain OS Homo sapiens GN LDHA PE 1 SV 2	P00338	36.7	8.4
5*	GSTO1_HUMAN	Glutathione S transferase omega 1 OS Homo sapiens GN GSTO1 PE 1 SV 2	P78417	27.5	6.2
6*	PGK1_HUMAN	Phosphoglycerate kinase 1 OS Homo sapiens GN PGK1 PE 1 SV 3	P00558	44.6	8.1

Table 5-1 (continued): S-nitrosylated proteins identified by LC-MS/MS in HT-29 cells preincubated with MQ.

Translation and posttranslational modification					
7	VE2_HP63	Regulatory protein E2 OS Human papillomavirus type 63 GN E2 PE 3 SV 1	Q07850	45.4	10.0
Redox-related proteins					
8	CX064_HUMAN	Uncharacterized protein CXorf64 OS Homo sapiens GN CXorf64 PE 2 SV 1	B1ATL7	31.9	7.3
9	KDM7_HUMAN	Lysine specific demethylase 7 OS Homo sapiens GN JHDM1D PE 1 SV 2	Q6ZMT4	106.5	8.0
10	TSH1_HUMAN	Teashirt homolog 1 OS Homo sapiens GN TSHZ1 PE 2 SV2	Q6ZSZ6	117.8	6.6
11	DPOL_ADE07	DNA polymerase OS Human adenovirus B serotype 7 GN POL PE 3 SV 1	P05664	128.6	6.3
12*	HNRPU_HUMAN	Heterogeneous nuclear ribonucleoprotein U OS Homo sapiens GN HNRNPU PE 1 SV 6	Q00839	90.5	5.6
Translation					
13*	RS20_HUMAN	40S ribosomal protein S20 OS Homo sapiens GN RPS20 PE 1 SV 1	P60866	13.4	10.4

Table 5-1(continued): S-nitrosylated proteins identified by LC-MS/MS in HT-29 cells preincubated with MQ.

Regulation of the colloidal osmotic pressure of blood					
14*	ALBU_HUMAN	Serum albumin OS Homo sapiens GN S100A10 PE 1 SV 2	P02768	69.3	5.9
Signaling proteins					
15*	EF2_HUMAN	Elongation factor 2 OS Homo sapiens GN EEF2 PE 1 SV 4	P13639	95.3	6.4
16	EF1A1_HUMAN	Elongation factor 1 alpha 1 OS Homo sapiens GN EEF1A1 PE 1 SV 1	P68104	50.1	9.3
17*	S10AA_HUMAN	Protein S100 A10 OS Homo sapiens GN S100A10 PE 1 SV 2	P60903	11.2	7.3
18	MARK2_HUMAN	Serine threonine protein kinase MARK2 OS Homo sapiens GN MARK2 PE 1 SV 2	Q7KZI7	87.9	10.1
Cytoskeleton proteins					
19*	ACTB_HUMAN	Actin cytoplasmic 1 OS Homo sapiens GN ACTB PE 1 SV 1	P60709	41.7	5.1
Membrane proteins					
20	ECE1_HUMAN	Endothelin converting enzyme 1 OS Homo sapiens GN ECE 1 PE 1 SV 2	P42892	87.1	5.5

Table 5-2: S-nitrosylated proteins identified by LC-MS/MS analysis in untreated HT-29 cells.

Number (NO.)	Protein ID (Controls)	Description	Accession NO.	Molecular Mass (kDa)	PI
1	S10AA_HUMAN	Protein S100 A10 OS Homo sapiens GN S100A10 PE 1 SV 2	2P60903	11.2	7.3
2	RS7_HUMAN	40S ribosomal protein S7 OS Homo sapiens GN RPS7 PE 1 SV 1	2P62081	22.1	10.6
3	EF1A1_HUMAN	Elongation factor 1 alpha 1 OS Homo sapiens GN EEF1A1 PE 1 SV 1	2P68104	50.1	9.3
4	CX064_HUMAN	Uncharacterized protein CXorf64 OS Homo sapiens GN CXorf64 PE 2 SV 1	2B1ATL7	31.9	7.3
5	HSP77_HUMAN	Putative heat shock 70 kDa protein 7 OS Homo sapiens GN HSPA7 PE 5 SV 2	2P48741	40.2	7.9
6	RS20_HUMAN	40S ribosomal protein S20 OS Homo sapiens GN RPS20 PE 1 SV 1	2P60866	13.4	10.4
7	LDHB_HUMAN	L lactate dehydrogenase B chain OS Homo sapiens GN LDHB PE 1 SV 2	2P07195	36.6	5.6

Table 5-2 (continued): S-nitrosylated proteins identified by LC-MS/MS analysis in untreated HT-29 cells.

8	ALBU_HUMAN	Serum albumin OS Homo sapiens GN S100A10 PE 1 SV 2	2P02768	69.3	5.9
9	MARK2_HUMAN	Serine threonine protein kinase MARK2 OS Homo sapiens GN MARK2 PE 1 SV 2	2Q7KZI7	87.9	10.1
10	KDM7_HUMAN	Lysine specific demethylase 7 OS Homo sapiens GN JHDM1D PE 1 SV 2	2Q6ZMT4	106.5	8.0

5.3.2 Identification of Biotin Modification Sites in MQ Treated HT-29 Cells

To provide further evidence that the proteins identified by mass fingerprinting were S-nitrosylated, the biotin modification sites were also identified in HT-29 cells (Table 5-3). The MS/MS spectra of identified proteins are shown in Figure 5-3 to Figure 5-12.

Table 5-3: S-nitrosylated proteins identification of biotin modification sites in MQ treated HT-29 cells.

Number (NO.)	Protein ID (MQ treated HT-29 cells)	Description	Accession NO.	Molecular Mass (kDa)	PI
1	GSTO1_HUMAN	Glutathione S transferase omega 1 OS Homo sapiens GN GSTO1 PE 1 SV 2	2P78417	27.5	6.2
2	EEF2_HUMAN	Elongation factor 2 OS Homo sapiens GN EEF2 PE 1 SV 4	2P13639	95.3	6.4
3	HNRPU_HUMAN	Heterogeneous nuclear ribonucleoprotein U OS Homo sapiens GN HNRNPU PE 1 SV 6	2Q00839	90.5	5.6
4	LDHA_HUMAN	L lactate dehydrogenase A chain OS Homo sapiens GN LDHA PE 1 SV 2	2P00338	36.7	8.4
5	ACTB_HUMAN	Actin cytoplasmic 1 OS Homo sapiens GN ACTB PE 1 SV 1	2P60709	41.7	5.1
6	PGK1_HUMAN	Phosphoglycerate kinase 1 OS Homo sapiens GN PGK1 PE 1 SV 3	2P00558	44.6	8.1
7	S10AA_HUMAN	Protein S100 A10 OS Homo sapiens GN S100A10 PE 1 SV 2	2P60903	11.2	7.3

Table 5-3 (continued): S-nitrosylated proteins identification of biotin modification sites in MQ treated HT-29 cells.

8	HSP77_HUMAN	Putative heat shock 70 kDa protein 7 OSHomo sapiens GN HSPA7 PE 5 SV 2	2P48741	40.2	7.9
9	RS20_HUMAN	40S ribosomal protein S20 OS Homo sapiens GN RPS20 PE 1 SV 1	2P60866	13.4	10.4
10	ALBU_HUMAN	Serum albumin OS Homo sapiens GN S100A10 PE 1 SV 2	2P02768	69.3	5.9

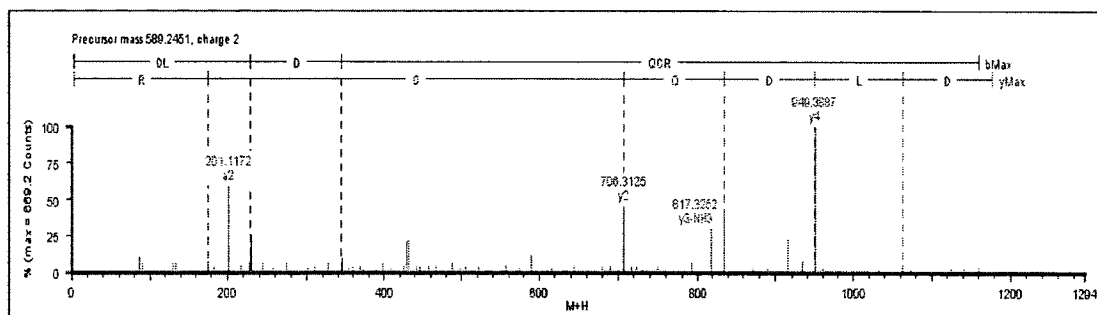


Figure 5-3: The MS/MS spectra of Protein S100 A10.

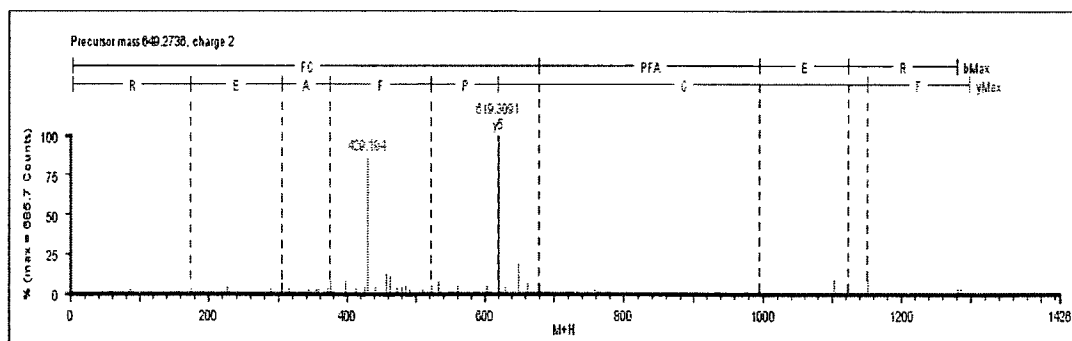


Figure 5-4: The MS/MS spectra of Glutathione S transferase.

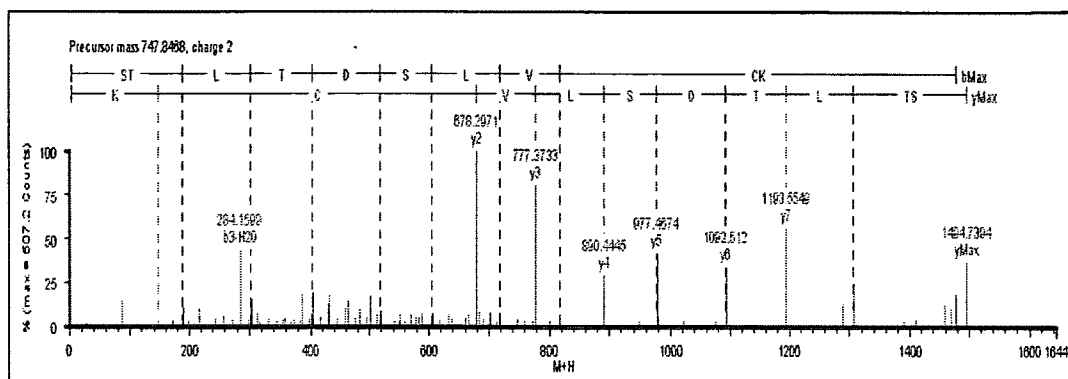


Figure 5-5: The MS/MS spectra of Enlogation factor 2.

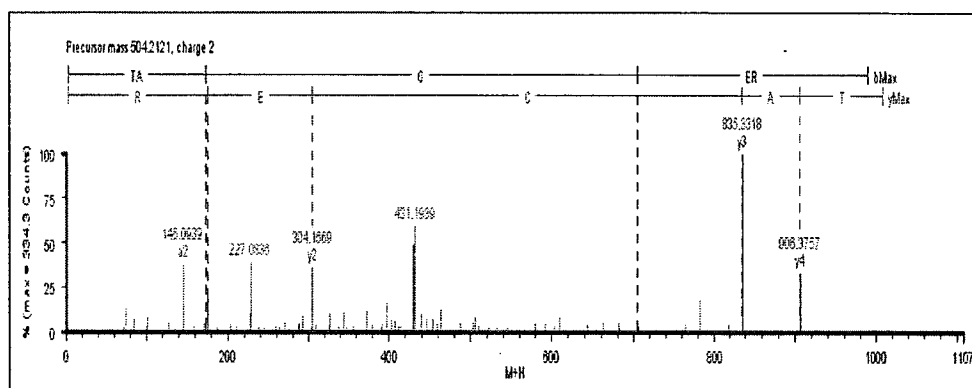


Figure 5-6: The MS/MS spectra of Putative heat shock 70 kDa protein 7.

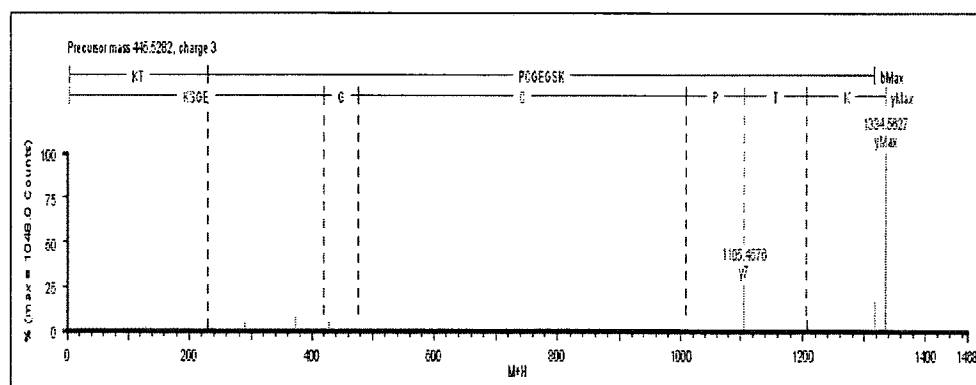


Figure 5-7: The MS/MS spectra of 40S ribosomal protein S20.

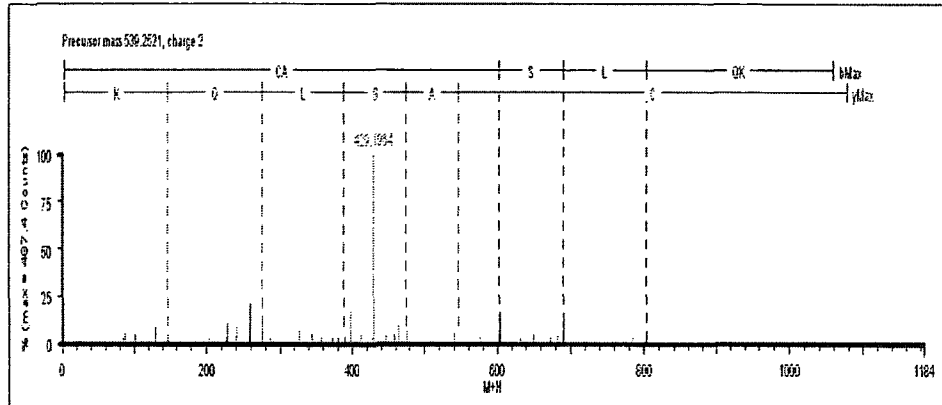


Figure 5-8: The MS/MS spectra of Serum albumin (Human).

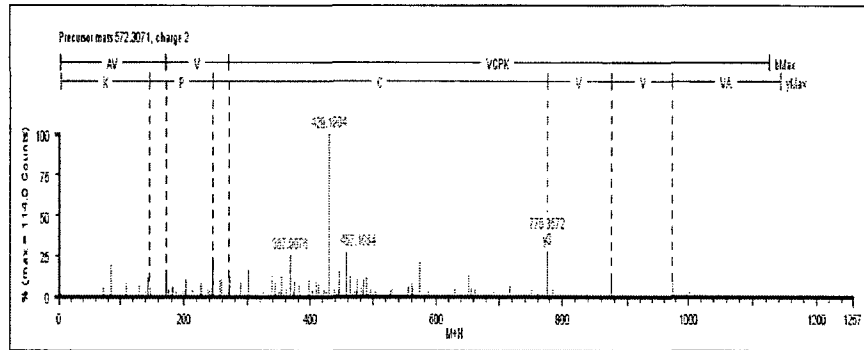


Figure 5-9: The MS/MS spectra of Heterogeneous nuclear ribonucleoprotein U.

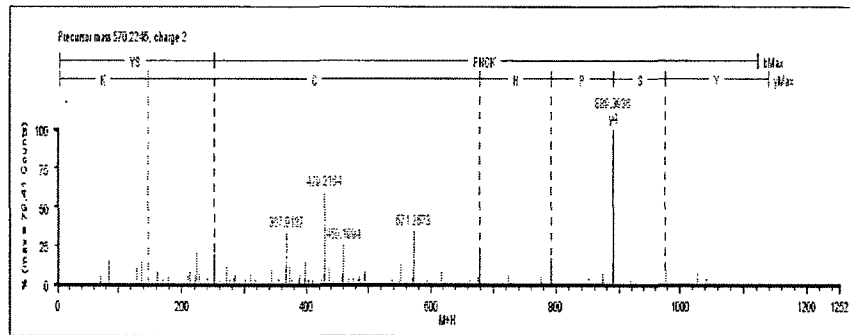


Figure 5-10: The MS/MS spectra of L lactate dehydrogenase A chain.

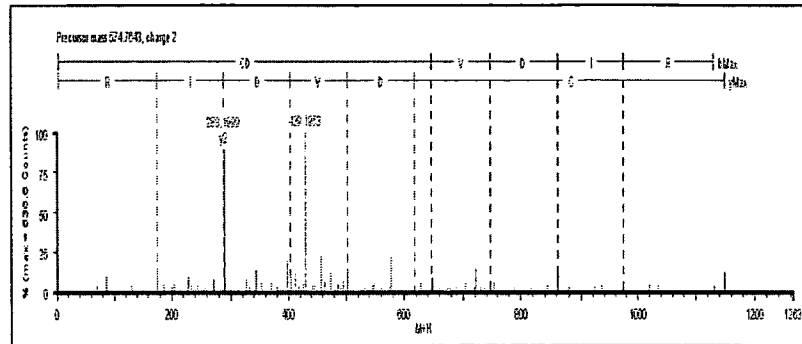


Figure 5-11: The MS/MS spectra of Actin cytoplasmic 1.

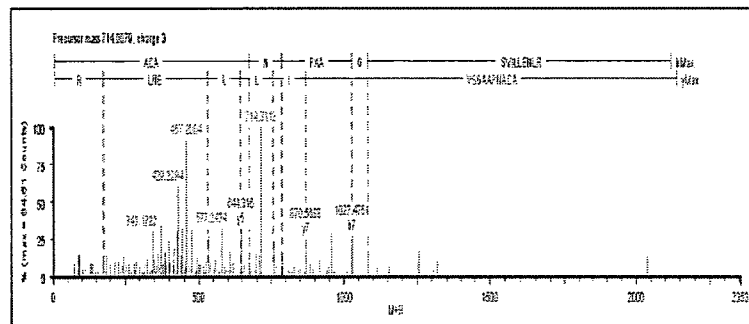


Figure 5-12: MS/MS spectra of Phosphoglycerate kinase 1.

5.4 Discussion

S-nitrosylation has become recognized as a ubiquitous, specific, and reversible regulatory reaction comparable to other protein modification. Up to current data, there are over 100 different proteins which have been described as being regulated through the protein S-nitrosylation in various systems, typically on the basis of in vitro modification or exogenous sources of NO [96]. In a previous report, the protein S-nitrosylation in both MQ treated HT-29 cells and untreated ones is quantified [78]. However, it is poorly understood how increased nitrosative stress directly affects the cells and their functions.

Therefore, this research seeks to identify S-nitrosylated proteins in MQ-exposed HT-29 cells compared to the controls.

In the current study, HT-29 cells were exposed to MQ to induce more nitrosylated proteins modification. Unlike the other studies, there was no component in which cells were exposed to a source of exogenous NO. Like the studies previously mentioned, these results indicate that a large number of proteins are S-nitrosylated in this setting. Indeed, three of the proteins identified as S-nitrosylated in MQ treated HT-29 cells, EF2, EF1A1, and L-lactate dehydrogenase B chain, have been reported to be S-nitrosylated in other systems [6, 28, 29].

Colon cancer cell lines, HT-29 cells (MQ treatment and untreated), were analyzed for their nitrosylated content. Both the sample and the control were subjected to the biotin-switch method for detection of S-nitrosylated proteins. It has been suggested that the biotin-switch method may also detect S-gluthionylated proteins [5]. However, new evidence indicates that treatments with reduced and oxidized glutathione (GSH, GSSG) did not show any differences with respect to untreated extracts. Therefore, the biotin-switch method was considered suitable for studying the protein S-nitrosylation [97]. As was expected, more nitrosylated proteins were identified in MQ treated HT-29 cells, when compared to the control. This increase in the number of S-nitrosylation observed in MQ treated HT-29 cells is probably a consequence of the exposure of these cells to MQ. These findings are in agreement with the previous study that MQ was able to accumulate the overall level of protein S-nitrosylation in HT-29 cells [78].

Initially, it was expected that differences would be seen in the pattern of S-nitrosylation between MQ treated HT-29 cells and control. However, as shown in Table

5-1 and 5-2, both the sample and the control have some of the same pattern of S-nitrosylated proteins.

At least ten proteins that were increased by exposure to MQ in their S-nitrosylation status have been identified, as shown in Table 5-1. These increased S-nitrosylated proteins can be classed as 1) cytoskeleton proteins (Actin cytoplasmic 1), 2) metabolic enzymes (L Lactate dehydrogenase A chain, Glutathione S transferase omega 1, Phosphoglycerate kinase 1), 4) signaling molecules (Elongation factor 2), 5) transcription factor (Regulatory protein E2, Teashirt homolog 1, DNA polymerase, Heterogeneous nuclear ribonucleoprotein U) and 6) membrane proteins (Endothelin converting enzyme 1). Many of these proteins are likely to undergo S-nitrosylation in other cell types. Because S-nitrosylation has been implicated in the regulation of numerous protein activities, the findings that MQ regulates protein S-nitrosylation in HT-29 cells could provide a new insight into the mechanisms underlying nitrosylation injury on the cells. The significance of these findings and the potential role of the identified S-nitrosylated proteins in apoptosis and cancer are discussed in Section 5.4.1 to 5.4.7.

5.4.1 Signaling Proteins

EF-2, a signaling protein involved in protein synthesis, catalyzes the translocation of the peptidyl-tRNA from the A site to the P site of the ribosome. Most organisms encode a single EF2 protein and its activity is regulated by EF-2 kinase resulting in phosphorylation. S-nitrosylation of EF-2 might be an alternative mechanism used to enhance protein synthesis [29].

S100A10 is a member of the S100 family of proteins, which are small acidic proteins (10-12 kDa) and constitute the largest subfamily of EF-hand proteins, with at

least 25 members [98]. A unique feature of S100A10 is its calcium insensitivity, since it contains mutations in both of the calcium-binding sites[99]. The majority of the S100A10 is found intracellularly in the cytosol or at the inner surface of the plasma membrane. However, S100A10 is also present on the extracellular surface of many cells, where it binds tissue plasminogen activator (tPA) via its C-terminal lysines [98].

5.4.2 Chaperones

MQ treated HT-29 cells also showed S-nitrosylation of specific chaperones, including Hsp70 protein 7 (Hsp77). The heat shock proteins (Hsps) are known as molecular chaperones, and help guide protein transport and folding under physiological conditions. Hsp77 is constitutively present in unstressed organisms, reflecting the housekeeping function performed under normal circumstances [100]. Although Hsp70 family members have been shown in other proteomics of nitrosylation papers, the Hsp77 has first been identified in this study. As to the role of stress-induced Hsps, more work is needed to understand the exact mechanism by which these proteins provide protection to the cell, in particular at the tissue level [101].

5.4.3 Metabolism

Tumor formation is generally linked to increased activity of glycolytic enzymes. Inhibition of glycolysis effectively kills colon cancer cells in a hypoxic environment in which the cancer cells exhibit high glycolytic activity and decreased sensitivity to anticancer drugs. Three metabolic enzymes were identified to be S-nitrosylated in MQ treated HT-29 cells, glutathione S transferase omega 1 (GSTO1), phosphoglycerate kinase 1 (PGK1) and lactate dehydrogenase A chain (LDHA). These three proteins could be potentially considered as new targets for cancer therapy.

Glutathione-S-transferases (GSTs) are a family of Phase II detoxification enzymes that catalyse the conjugation of glutathione (GSH) to a wide variety of endogenous and exogenous electrophilic compounds [102]. GSTs are divided into two distinct super-family members: the membrane-bound microsomal and cytosolic family members [102]. GSTO1 belongs to the cytosolic family members, which are subject to significant genetic polymorphisms in human populations. GSTs have emerged as a promising therapeutic target because specific isozymes are overexpressed in a wide variety of tumors [103, 104].

Phosphoglycerate kinase 1 (PGK 1), a secretable glycolytic enzyme, is known to participate in angiogenesis. A previous study identified PGK1 as a potential biomarker and/or therapeutic target for pancreatic ductal adenocarcinoma (PDAC) [105]. Given that the ability to respond to changes in oxygen tension is fundamental, in the case of the PGK to have been preserved in evolution, the possibility is raised that the oxygen-regulated control system may not only act on a wide variety of genes in mammalian cells but also have an equivalent in more primitive species. Similarly, LDH, a cellular metabolic enzyme, also show both structural and functional conservation in evolution [106].

5.4.4 Post-translational Modification

Specific RNA-binding proteins, such as the hnRNP family, regulate the mRNA processing, as well as other mRNA-related cell activities [107]. About 20 major hnRNP proteins, from A1 to U, have been described and included in the family by their capacity to bind to pre-mRNA with no unique structural motif or function [108]. HnRNP proteins are involved in variety of key cellular functions, such as mRNA splicing, stabilization,

nucleo-cytoplasmic transport, and transcriptional control [109-113]. Several authors have reported an association of hnRNP expression with actively proliferating cells [114-116]. It is still not clear whether the over-expression of the hnRNP proteins in cancer is a tumor specific event or rather it is a mere consequence of the accelerated mRNA metabolism common to highly proliferative cancer cells [108]. One of hnRNP family member, heterogeneous nuclear ribonucleoprotein U (HNRPU), may act as a scaffolding protein and mediate interactions between target mRNAs and proteins regulating mRNA expression [117].

5.4.5 Translation

The expression profiles of the individual ribosomal protein (RP) S20 mRNA exhibited a constantly down regulation in previous reports [118]. Most of the studies of the regulation of RP synthesis have been made in *Xenopus*. The regulation of RP synthesis occurs at four different levels: transcriptional, post-transcriptional, translational and stability of the proteins [119, 120]. The majority of the regulation is at the translational level, and this is achieved by modulating the fractions of RP mRNA on polysomes and stored in RNPs, respectively [118].

5.4.6 Regulation of the Colloidal Osmotic Pressure of Blood

Human serum albumin (ALBU) is the most abundant protein in the circulatory system [121]. It is synthesized in the liver, exported as a non-glycosylated protein, and is present in the blood to regulate the colloidal osmotic pressure. Previous report shows that the S-nitrosothiol fraction is largely composed of the S-nitrosothiol adduct of serum albumin [122]. The levels of S-nitroso-serum albumin change with inhibition of nitric oxide production in concert with changes in blood pressure [122].

5.4.7 Cytoskeleton Proteins

Actin is highly conserved protein which participates in a wide variety of cellular functions in eucaryotes, including muscle contraction, ameboid movement, cytokinesis, and mitotic division [123]. Cytoplasmic actin is one of the major classes of actin. All organisms thus far examined express a cytoplasmic actin form, which is usually utilized to construct the cellular microfilaments [124].

5.5 Conclusions

These results present the first proteomic profiling of S-nitrosylation related to MQ exposure in colon cancer cells (HT-29 cells). The biotin switch technique is a viable technique for identification of S-nitrosylated proteins in this study. Certainly, based on the study of these results, a total of 20 proteins were modified by nitrosylation in MQ-treated HT-29 cells and at least 10 nitrosylated proteins were increased by exposure to MQ. Among the 20 proteins, seventeen of them are never reported in other systems. In addition to identifying novel targets of S-nitrosylation, these results provide new protein targets that should facilitate future biomarker and therapy research.

CHAPTER 6

CONCLUSIONS AND FUTURE WORK

6.1 Conclusions

This dissertation provides a description of technologies that enable studies aimed at understanding the significance of protein modification in colon cancer and Alzheimer's disease. The S-nitrosothiol level increases in both 200 μ M MQ treated HT-29 cells and 5-month-old AD Tg mice model monitored by commercial CGE-LIF machine and in-house built 2D μ -CE system. The fluorescence switch method, coupled with a commercial CE machine, can detect 1.3 pM concentration of nitrosylated proteins in nanogram amounts of proteins, which is the lowest LOD reported to date. This method also demonstrated its capability in monitoring nitrosylation in both cell culture and tissue systems. Due to the small sample need, it is envisioned that the method can be extended to investigate protein nitrosylation profiles in minuscule samples of brain tissues and/or blood plasma in the disease progression of AD transgenic mouse models.

The increasing of the S-nitrosothiol level in both 200 μ M MQ treated HT-29 cells and 11-month-old AD Tg mice model is also monitored by an in-house built 2D μ -CE system. Nitrosylated proteins were profiled using a 2D μ -CGE/MEEKC polymer microchip and monitoring its expression using an LIF detector. The 2D μ -CE device achieved high peak capacity, which allows the separation of a panel of nitrosylated

proteins. In addition, the ultrasensitive assay of nitrosothiol derivatization and labeling allowed for the monitoring of these biomarkers even at a low abundance level.

Altogether, an oxidative-stress induced biomarker profiling was generated, and this application could further serve as a fingerprint to determine AD disease phenotypes from biological samples.

The identified nitrosylated proteins with an increase in nitrosylation, done by proteomics, also provide the evidence to support the central hypothesis. These results present the first proteomic profiling of S-nitrosylation related to MQ exposure in colon cancer cells (HT-29 cells). The biotin switch technique is a viable technique for identification of S-nitrosylated proteins in this study. A total of 20 proteins were modified by nitrosylation in MQ-treated HT-29 cells and at least 10 nitrosylated proteins were increased by exposure to MQ. Among the 20 proteins, seventeen of them are never reported in other systems. In addition to identifying novel targets of S-nitrosylation, these results provide new protein targets that should facilitate future biomarker and therapy research.

6.2 Future Work

The methodologies developed in this dissertation could be extended to investigate protein S-nitrosylation for all kinds of tissues and blood in different animal models or human beings. It is important to point out the potential application of early disease screening through combining these 3D landscapes of biomarkers from the AD Tg mice brain tissue of different ages and gender with multivariate analysis. Furthermore, similar applications may be found in investigating the etiologies of diseases including Alzheimer's disease, Parkinson's disease, diabetes and stroke. In addition, the in-house

built 2D μ -CE system has great potential for biomarker discovery by coupling with mass spectrometry. This technique has a wide range of applications in analysing other sub-populations of proteomes, such as phosphorylation, carbonylation, nitration and others.

6.2.1 PCA Analysis for Future Direction

Principle component analysis (PCA) is one of the most common techniques used to bring out data patterns that are not easily identified in electrophoretic profiles in the fields of biological processes, polymer materials, and food products. It does so by reducing the number of dimensions (e.g. number of data points in an electropherogram) in multidimensional datasets to fewer dimensions (i.e. principle components, PC's), while retaining the dataset's variability. In PCA, each sample has scores associated with each PC. The most important PCs can be used to define a coordinate system and their score values represent each sample in the score plot. In the score plot, the closer the distance between samples, the more similar they are in respect to the features represented by the PCs selected for the score plot.

In this work, CGE-LIF electropherograms were used as fingerprints of protein S-nitrosylation. In order to have a better understanding of age-associated change in nitrosylation profiling of the AD Tg mice model, PCA is needed to predict the relationship between the nitrosylation and aging.

6.2.2 Estimating S-Nitrosylation Levels by Fluorescence Imaging

In the previous study, it has been demonstrated that S-nitrosylation levels of proteins increase in AD Tg mice brain tissue (Chapters 3 and 4). However, the exact localization of nitrosylated proteins within the brain is still unknown (Figure 6-1). Future

studies should investigate a methodology to localize the S-nitrosylated proteins needed in AD Tg mice brain tissues.

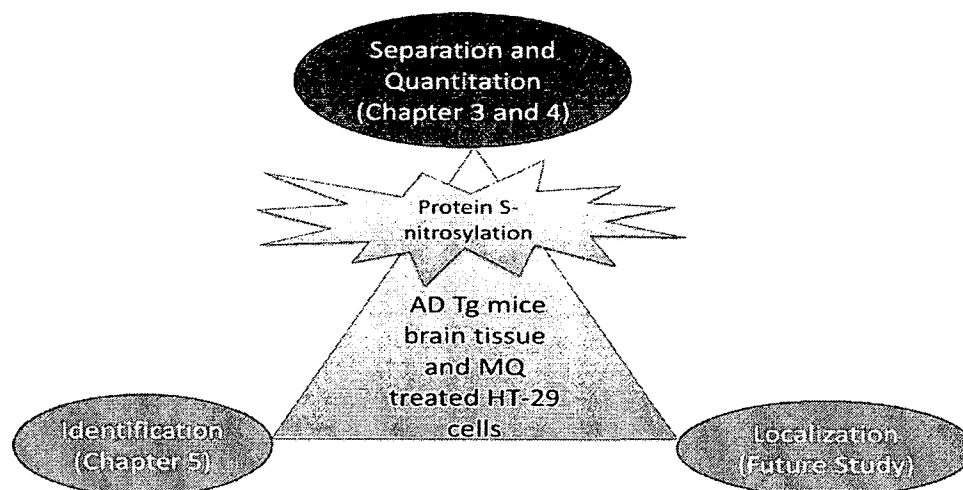


Figure 6-1: General picture of the protein S-nitrosylation study in AD Tg mice brain tissue and MQ treated HT-29 cells.

6.2.3 Integrated Microfluidic Systems with Proteomics

Microchip separation technology has great potential to integrate with proteomics since it has been successfully used in the CE study. By integrating various devices into a single microchip, dead volumes are minimized and total analysis time is reduced.

The in-house built 2D- μ CE system has great potential for biomarker discovery by coupling with mass spectrometry. In addition, this technique has a wide range of applications in analysing other sub-populations of proteomes, such as phosphorylation, carbonylation, nitration and others.

REFERENCES

- [1] I. M. Riederer, *et al.*, "Ubiquitination and cysteine nitrosylation during aging and Alzheimer's disease," *Brain Res Bull*, vol. 80, pp. 233-41, Oct 28 2009.
- [2] M. Crabtree, *et al.*, "Detection of cysteine S-nitrosylation and tyrosine 3-nitration in kidney proteins," *Methods Mol Med*, vol. 86, pp. 373-84, 2003.
- [3] K. H. Moon, *et al.*, "Inactivation of oxidized and S-nitrosylated mitochondrial proteins in alcoholic fatty liver of rats," *Hepatology*, vol. 44, pp. 1218-30, Nov 2006.
- [4] K. Ckless, *et al.*, "In situ detection and visualization of S-nitrosylated proteins following chemical derivatization: identification of Ran GTPase as a target for S-nitrosylation," *Nitric Oxide*, vol. 11, pp. 216-27, Nov 2004.
- [5] T. Kuncewicz, *et al.*, "Proteomic analysis of S-nitrosylated proteins in mesangial cells," *Mol Cell Proteomics*, vol. 2, pp. 156-63, Mar 2003.
- [6] T. M. Greco, *et al.*, "Identification of S-nitrosylation motifs by site-specific mapping of the S-nitrosocysteine proteome in human vascular smooth muscle cells," *Proc Natl Acad Sci U S A*, vol. 103, pp. 7420-5, May 9 2006.
- [7] Y. Yang and J. Loscalzo, "S-nitrosoprotein formation and localization in endothelial cells," *Proc Natl Acad Sci U S A*, vol. 102, pp. 117-22, Jan 4 2005.
- [8] P. Han and C. Chen, "Detergent-free biotin switch combined with liquid chromatography/tandem mass spectrometry in the analysis of S-nitrosylated proteins," *Rapid Commun Mass Spectrom*, vol. 22, pp. 1137-45, Apr 2008.
- [9] A. Martinez-Ruiz and S. Lamas, "S-nitrosylation: a potential new paradigm in signal transduction," *Cardiovasc Res*, vol. 62, pp. 43-52, Apr 1 2004.
- [10] S. Christen, *et al.*, "Plasma S-nitrosothiol status in neonatal calves: ontogenetic associations with tissue-specific S-nitrosylation and nitric oxide synthase," *Exp Biol Med (Maywood)*, vol. 232, pp. 309-22, Feb 2007.
- [11] C. M. Spickett, *et al.*, "Proteomic analysis of phosphorylation, oxidation and nitrosylation in signal transduction," *Biochim Biophys Acta*, vol. 1764, pp. 1823-41, Dec 2006.

- [12] N. Hogg, "The kinetics of S-transnitrosation--a reversible second-order reaction," *Anal Biochem*, vol. 272, pp. 257-62, Aug 1 1999.
- [13] Z. Liu, *et al.*, "S-Transnitrosation reactions are involved in the metabolic fate and biological actions of nitric oxide," *J Pharmacol Exp Ther*, vol. 284, pp. 526-34, Feb 1998.
- [14] J. S. Stamler, *et al.*, "S-nitrosylation of proteins with nitric oxide: synthesis and characterization of biologically active compounds," *Proc Natl Acad Sci U S A*, vol. 89, pp. 444-8, Jan 1 1992.
- [15] R. J. Singh, *et al.*, "Mechanism of nitric oxide release from S-nitrosothiols," *J Biol Chem*, vol. 271, pp. 18596-603, Aug 2 1996.
- [16] N. J. Kettenhofen, *et al.*, "Proteomic methods for analysis of S-nitrosation," *J Chromatogr B Analyt Technol Biomed Life Sci*, vol. 851, pp. 152-9, May 15 2007.
- [17] B. Saville, "A scheme for the colorimetric determination of microgram amounts of thiols," *The Analyst*, vol. 83, pp. 670-672, 1958.
- [18] A. Gow, *et al.*, "S-Nitrosothiol measurements in biological systems," *J Chromatogr B Analyt Technol Biomed Life Sci*, vol. 851, pp. 140-51, May 15 2007.
- [19] A. Doctor, *et al.*, "Hemoglobin conformation couples erythrocyte S-nitrosothiol content to O₂ gradients," *Proc Natl Acad Sci U S A*, vol. 102, pp. 5709-14, Apr 19 2005.
- [20] A. Hausladen, *et al.*, "Assessment of nitric oxide signals by triiodide chemiluminescence," *Proc Natl Acad Sci U S A*, vol. 104, pp. 2157-62, Feb 13 2007.
- [21] H. Kojima, *et al.*, "Detection and imaging of nitric oxide with novel fluorescent indicators: diaminofluoresceins," *Anal Chem*, vol. 70, pp. 2446-53, Jul 1 1998.
- [22] Y. Itoh, *et al.*, "Determination and bioimaging method for nitric oxide in biological specimens by diaminofluorescein fluorometry," *Anal Biochem*, vol. 287, pp. 203-9, Dec 15 2000.
- [23] A. J. Gow, *et al.*, "Immunohistochemical detection of S-nitrosylated proteins," *Methods Mol Biol*, vol. 279, pp. 167-72, 2004.
- [24] M. Liu, *et al.*, "Site-specific proteomics approach for study protein S-nitrosylation," *Anal Chem*, vol. 82, pp. 7160-8, Sep 1 2010.

- [25] S. R. Jaffrey and S. H. Snyder, "The biotin switch method for the detection of S-nitrosylated proteins," *Sci STKE*, vol. 2001, pp. 11, Jun 12 2001.
- [26] C. Lindermayr, *et al.*, "Proteomic identification of S-nitrosylated proteins in Arabidopsis," *Plant Physiol*, vol. 137, pp. 921-30, Mar 2005.
- [27] C. Wadham, *et al.*, "High glucose attenuates protein S-nitrosylation in endothelial cells: role of oxidative stress," *Diabetes*, vol. 56, pp. 2715-21, Nov 2007.
- [28] C. Gao, *et al.*, "Identification of S-nitrosylated proteins in endotoxin-stimulated RAW264.7 murine macrophages," *Nitric Oxide*, vol. 12, pp. 121-6, Mar 2005.
- [29] M. Dall'Agnol, *et al.*, "Identification of S-nitrosylated proteins after chronic exposure of colon epithelial cells to deoxycholate," *Proteomics*, vol. 6, pp. 1654-62, Mar 2006.
- [30] L. M. Lopez-Sanchez, *et al.*, "Alteration of S-nitrosothiol homeostasis and targets for protein S-nitrosation in human hepatocytes," *Proteomics*, vol. 8, pp. 4709-20, Nov 2008.
- [31] G. Hao, *et al.*, "SNOSID, a proteomic method for identification of cysteine S-nitrosylation sites in complex protein mixtures," *Proc Natl Acad Sci U S A*, vol. 103, pp. 1012-7, Jan 24 2006.
- [32] S. Camerini, *et al.*, "A novel approach to identify proteins modified by nitric oxide: the HIS-TAG switch method," *J Proteome Res*, vol. 6, pp. 3224-31, Aug 2007.
- [33] M. T. Forrester, *et al.*, "Proteomic analysis of S-nitrosylation and denitrosylation by resin-assisted capture," *Nat Biotechnol*, vol. 27, pp. 557-9, Jun 2009.
- [34] O'Farrell P. H., "High resolution two-dimensional electrophoresis of proteins," *J Biol Chem*, vol. 250, pp. 4007-4021, May 25 1975.
- [35] Service R. F., "Proteomics. High-speed biologists search for gold in proteins," *Science*, vol. 294, pp. 2074-2077, Dec 7 2001.
- [36] Marko-Varga G and Fehniger T. E., "Proteomics and disease--the challenges for technology and discovery," *J Proteome Res*, vol. 3, pp. 167-178, Mar-Apr 2004.
- [37] J. K. Osiri, *et al.*, "Integrated multifunctional microfluidics for automated proteome analyses," *Top Curr Chem*, vol. 304, pp. 261-94, 2011.
- [38] H. Shadpour and S. A. Soper, "Two-dimensional electrophoretic separation of proteins using poly(methylmethacrylate) microchips," *Anal Chem*, vol. 78, pp. 3519-27, Jun 1 2006.

- [39] J. K. Osiri, *et al.*, "Generating high peak capacity 2-D maps of complex proteomes using PMMA microchip electrophoresis," *Electrophoresis*, vol. 29, pp. 4984-92, Dec 2008.
- [40] J. K. Osiri, *et al.*, "Ultra-fast two-dimensional microchip electrophoresis using SDS micro-CGE and microemulsion electrokinetic chromatography for protein separations," *Anal Bioanal Chem*, vol. 398, pp. 489-98, Sep 2010.
- [41] M. C. Broillet, "S-nitrosylation of proteins," *Cell Mol Life Sci*, vol. 55, pp. 1036-42, Jul 1999.
- [42] S. R. Jaffrey, *et al.*, "Protein S-nitrosylation: a physiological signal for neuronal nitric oxide," *Nat Cell Biol*, vol. 3, pp. 193-7, Feb 2001.
- [43] S. C. Huber and S. C. Hardin, "Numerous posttranslational modifications provide opportunities for the intricate regulation of metabolic enzymes at multiple levels," *Curr Opin Plant Biol*, vol. 7, pp. 318-22, Jun 2004.
- [44] D. T. Hess, *et al.*, "Protein S-nitrosylation: purview and parameters," *Nat Rev Mol Cell Biol*, vol. 6, pp. 150-66, Feb 2005.
- [45] F. Mangialasche, *et al.*, "Biomarkers of oxidative and nitrosative damage in Alzheimer's disease and mild cognitive impairment," *Ageing Res Rev*, vol. 8, pp. 285-305, Oct 2009.
- [46] M. W. Foster, *et al.*, "S-nitrosylation in health and disease," *Trends Mol Med*, vol. 9, pp. 160-8, Apr 2003.
- [47] M. R. Hara, *et al.*, "Neuroprotection by pharmacologic blockade of the GAPDH death cascade," *Proc Natl Acad Sci U S A*, vol. 103, pp. 3887-9, Mar 7 2006.
- [48] S. A. Lipton, "Pathologically-activated therapeutics for neuroprotection: mechanism of NMDA receptor block by memantine and S-nitrosylation," *Curr Drug Targets*, vol. 8, pp. 621-32, May 2007.
- [49] C. J. Yu, *et al.*, "On-line concentration of proteins by SDS-CGE with LIF detection," *Electrophoresis*, vol. 29, pp. 483-90, Jan 2008.
- [50] L. Santhanam, *et al.*, "Selective fluorescent labeling of S-nitrosothiols (S-FLOS): a novel method for studying S-nitrosation," *Nitric Oxide*, vol. 19, pp. 295-302, Nov 2008.
- [51] D. Tello, *et al.*, "A "fluorescence switch" technique increases the sensitivity of proteomic detection and identification of S-nitrosylated proteins," *Proteomics*, vol. 9, pp. 5359-70, Dec 2009.

- [52] M. L. Circu, *et al.*, "Contribution of mitochondrial GSH transport to matrix GSH status and colonic epithelial cell apoptosis," *Free Radic Biol Med*, vol. 44, pp. 768-78, Mar 1 2008.
- [53] M. Okouchi, *et al.*, "Preservation of cellular glutathione status and mitochondrial membrane potential by N-acetylcysteine and insulin sensitizers prevent carbonyl stress-induced human brain endothelial cell apoptosis," *Curr Neurovasc Res*, vol. 6, pp. 267-78, Nov 2009.
- [54] M. L. Circu, *et al.*, "Contribution of glutathione status to oxidant-induced mitochondrial DNA damage in colonic epithelial cells," *Free Radic Biol Med*, vol. 47, pp. 1190-8, Oct 15 2009.
- [55] J. Feng, *et al.*, "Principal component analysis reveals age-related and muscle-type-related differences in protein carbonyl profiles of muscle mitochondria," *J Gerontol A Biol Sci Med Sci*, vol. 63, pp. 1277-88, Dec 2008.
- [56] J. Feng and E. A. Arriaga, "Quantification of carbonylated proteins in rat skeletal muscle mitochondria using capillary sieving electrophoresis with laser-induced fluorescence detection," *Electrophoresis*, vol. 29, pp. 475-82, Jan 2008.
- [57] S. Basu, *et al.*, "Hemoglobin effects in the Saville assay," *Nitric Oxide*, vol. 15, pp. 1-4, Aug 2006.
- [58] P. Han, *et al.*, "On-gel fluorescent visualization and the site identification of S-nitrosylated proteins," *Anal Biochem*, vol. 377, pp. 150-5, Jun 15 2008.
- [59] F. Torta, *et al.*, "Proteomic analysis of protein S-nitrosylation," *Proteomics*, vol. 8, pp. 4484-94, Nov 2008.
- [60] L. M. Lopez-Sanchez, *et al.*, "Detection and proteomic identification of S-nitrosated proteins in human hepatocytes," *Methods Enzymol*, vol. 440, pp. 273-81, 2008.
- [61] J. Feng, *et al.*, "Quantitative proteomic profiling of muscle type-dependent and age-dependent protein carbonylation in rat skeletal muscle mitochondria," *J Gerontol A Biol Sci Med Sci*, vol. 63, pp. 1137-52, Nov 2008.
- [62] P. J. Kersey, *et al.*, "The International Protein Index: an integrated database for proteomics experiments," *Proteomics*, vol. 4, pp. 1985-8, Jul 2004.
- [63] D. Giustarini, *et al.*, "Is ascorbate able to reduce disulfide bridges? A cautionary note," *Nitric Oxide*, vol. 19, pp. 252-8, Nov 2008.
- [64] M. T. Forrester, *et al.*, "Detection of protein S-nitrosylation with the biotin-switch technique," *Free Radic Biol Med*, vol. 46, pp. 119-26, Jan 15 2009.

- [65] P. C. Jocelyn, "The standard redox potential of cysteine-cystine from the thiol-disulphide exchange reaction with glutathione and lipoic acid," *Eur J Biochem*, vol. 2, pp. 327-31, Oct 1967.
- [66] D. Njus and P. M. Kelley, "Vitamins C and E donate single hydrogen atoms in vivo," *FEBS Lett*, vol. 284, pp. 147-51, Jun 24 1991.
- [67] M. T. Forrester, *et al.*, "Assessment and application of the biotin switch technique for examining protein S-nitrosylation under conditions of pharmacologically induced oxidative stress," *J Biol Chem*, vol. 282, pp. 13977-83, May 11 2007.
- [68] W. W. Wells and D. P. Xu, "Dehydroascorbate reduction," *J Bioenerg Biomembr*, vol. 26, pp. 369-77, Aug 1994.
- [69] S. Chesne, *et al.*, "Effects of oxidative modifications induced by the glycation of bovine serum albumin on its structure and on cultured adipose cells," *Biochimie*, vol. 88, pp. 1467-77, Oct 2006.
- [70] P. Rondeau, *et al.*, "Oxidative stresses induced by glycoxidized human or bovine serum albumin on human monocytes," *Free Radic Biol Med*, vol. 45, pp. 799-812, Sep 15 2008.
- [71] M. Oblak, *et al.*, "Thiol-reactive clenbuterol analogues conjugated to bovine serum albumin," *Z Naturforsch C*, vol. 59, pp. 880-6, Nov-Dec 2004.
- [72] K. Oettl and R. E. Stauber, "Physiological and pathological changes in the redox state of human serum albumin critically influence its binding properties," *Br J Pharmacol*, vol. 151, pp. 580-90, Jul 2007.
- [73] J. R. Burgoyne and P. Eaton, "A rapid approach for the detection, quantification, and discovery of novel sulfenic acid or S-nitrosothiol modified proteins using a biotin-switch method," *Methods Enzymol*, vol. 473, pp. 281-303, Jul 2010.
- [74] J. R. Laver, *et al.*, "Bacterial nitric oxide detoxification prevents host cell S-nitrosothiol formation: a novel mechanism of bacterial pathogenesis," *FASEB J*, vol. 24, pp. 286-95, Jan 2010.
- [75] A. J. Gow, *et al.*, "Basal and stimulated protein S-nitrosylation in multiple cell types and tissues," *J Biol Chem*, vol. 277, pp. 9637-40, Mar 22 2002.
- [76] Y. Zhang and N. Hogg, "Formation and stability of S-nitrosothiols in RAW 264.7 cells," *Am J Physiol Lung Cell Mol Physiol*, vol. 287, pp. L467-74, Sep 2004.
- [77] J. Chen, *et al.*, "Method development and validation for the simultaneous determination of four coumarins in *Saussurea superba* by capillary zone electrophoresis," *J AOAC Int*, vol. 93, pp. 1410-5, Sep-Oct 2010.

- [78] Wang S, *et al.*, "Highly sensitive detection of S-nitrosylated proteins by capillary gel electrophoresis with laser induced fluorescence," *J Chromatogr A*, vol. 1218, pp. 6756-6762, Sep 23 2011.
- [79] J. E. MacNair, *et al.*, "Ultrahigh-pressure reversed-phase capillary liquid chromatography: isocratic and gradient elution using columns packed with 1.0-micron particles," *Anal Chem*, vol. 71, pp. 700-8, Feb 1 1999.
- [80] D. Wu, *et al.*, "Electrophoretic separations on microfluidic chips," *J Chromatogr A*, vol. 1184, pp. 542-59, Mar 14 2008.
- [81] J. C. Giddings, "Two-dimensional separations: concept and promise," *Anal Chem*, vol. 56, pp. 1258A-1260A, 1262A, 1264A passim, Oct 1984.
- [82] H. Chen and Z. H. Fan, "Two-dimensional protein separation in microfluidic devices," *Electrophoresis*, vol. 30, pp. 758-65, Mar 2009.
- [83] Y. Li, *et al.*, "Integration of isoelectric focusing with parallel sodium dodecyl sulfate gel electrophoresis for multidimensional protein separations in a plastic microfluidic [correction of microfluidic] network," *Anal Chem*, vol. 76, pp. 742-8, Feb 1, 2004.
- [84] S. Yang, *et al.*, "Microfluidic 2-D PAGE using multifunctional in situ polyacrylamide gels and discontinuous buffers," *Lab Chip*, vol. 9, pp. 592-9, Feb 21 2009.
- [85] R. D. Rocklin, *et al.*, "A microfabricated fluidic device for performing two-dimensional liquid-phase separations," *Anal Chem*, vol. 72, pp. 5244-9, Nov 1 2000.
- [86] J. D. Ramsey, *et al.*, "High-efficiency, two-dimensional separations of protein digests on microfluidic devices," *Anal Chem*, vol. 75, pp. 3758-64, Aug 1 2003.
- [87] N. Gottschlich, *et al.*, "Two-dimensional electrochromatography/capillary electrophoresis on a microchip," *Anal Chem*, vol. 73, pp. 2669-74, Jun 1 2001.
- [88] Ford S. M, *et al.*, "Micromachining in plastics using X-ray lithography for the fabrication of microelectrophoresis devices," *J Biomech Eng*, vol. 121, pp. 13-21, Feb 1999.
- [89] H. Shadpour, *et al.*, "Physiochemical properties of various polymer substrates and their effects on microchip electrophoresis performance," *J Chromatogr A*, vol. 1111, pp. 238-51, Apr 14 2006.

- [90] S. Wang, *et al.*, "Highly sensitive detection of S-nitrosylated proteins by capillary gel electrophoresis with laser induced fluorescence," *J Chromatogr A*, vol. 1218, pp. 6756-62, Sep 23 2011.
- [91] J. R. Petersen, *et al.*, "Laser induced resonance energy transfer--a novel approach towards achieving high sensitivity in capillary electrophoresis. I. Clinical diagnostic application," *J Chromatogr A*, vol. 744, pp. 37-44, Sep 13 1996.
- [92] A. E. Herr, *et al.*, "On-chip coupling of isoelectric focusing and free solution electrophoresis for multidimensional separations," *Anal Chem*, vol. 75, pp. 1180-7, Mar 1 2003.
- [93] W. C. McAmis, *et al.*, "Menadione causes endothelial barrier failure by a direct effect on intracellular thiols, independent of reactive oxidant production," *Biochim Biophys Acta*, vol. 1641, pp. 43-53, Jun 17 2003.
- [94] I. Kheterpal, *et al.*, "Proteome of human subcutaneous adipose tissue stromal vascular fraction cells versus mature adipocytes based on DIGE," *J Proteome Res*, vol. 10, pp. 1519-27, Apr 1 2011.
- [95] J. P. DeLany, *et al.*, "Proteomic analysis of primary cultures of human adipose-derived stem cells: modulation by Adipogenesis," *Mol Cell Proteomics*, vol. 4, pp. 731-40, Jun 2005.
- [96] Y. W. Lam, *et al.*, "Comprehensive identification and modified-site mapping of S-nitrosylated targets in prostate epithelial cells," *PLoS One*, vol. 5, p. e9075, 2010.
- [97] M. C. Romero-Puertas, *et al.*, "Proteomic analysis of S-nitrosylated proteins in *Arabidopsis thaliana* undergoing hypersensitive response," *Proteomics*, vol. 8, pp. 1459-69, Apr 2008.
- [98] P. Svenningsson and P. Greengard, "p11 (S100A10)--an inducible adaptor protein that modulates neuronal functions," *Curr Opin Pharmacol*, vol. 7, pp. 27-32, Feb 2007.
- [99] V. Gerke and K. Weber, "The regulatory chain in the p36-kd substrate complex of viral tyrosine-specific protein kinases is related in sequence to the S-100 protein of glial cells," *EMBO J*, vol. 4, pp. 2917-20, Nov 1985.
- [100] A. Piano, *et al.*, "Hsp70 expression in thermally stressed *Ostrea edulis*, a commercially important oyster in Europe," *Cell Stress Chaperones*, vol. 7, pp. 250-7, Jul 2002.
- [101] L. E. Hightower, *et al.*, "Tissue-level cytoprotection," *Cell Stress Chaperones*, vol. 5, pp. 412-4, Nov 2000.

- [102] D. M. Townsend and K. D. Tew, "The role of glutathione-S-transferase in anti-cancer drug resistance," *Oncogene*, vol. 22, pp. 7369-75, Oct 20 2003.
- [103] K. D. Tew, "Glutathione-associated enzymes in anticancer drug resistance," *Cancer Res*, vol. 54, pp. 4313-20, Aug 15 1994.
- [104] R. A. Zakharyan, *et al.*, "Human monomethylarsonic acid (MMA(V)) reductase is a member of the glutathione-S-transferase superfamily," *Chem Res Toxicol*, vol. 14, pp. 1051-7, Aug 2001.
- [105] H. Li, *et al.*, "Induction of phosphoglycerate kinase 1 gene expression by hypoxia. Roles of Arnt and HIF1alpha," *J Biol Chem*, vol. 271, pp. 21262-7, Aug 30 1996.
- [106] J. D. Firth, *et al.*, "Oxygen-regulated control elements in the phosphoglycerate kinase 1 and lactate dehydrogenase A genes: similarities with the erythropoietin 3' enhancer," *Proc Natl Acad Sci U S A*, vol. 91, pp. 6496-500, Jul 5 1994.
- [107] G. Dreyfuss, *et al.*, "Messenger-RNA-binding proteins and the messages they carry," *Nat Rev Mol Cell Biol*, vol. 3, pp. 195-205, Mar 2002.
- [108] I. Pino, *et al.*, "Altered patterns of expression of members of the heterogeneous nuclear ribonucleoprotein (hnRNP) family in lung cancer," *Lung Cancer*, vol. 41, pp. 131-43, Aug 2003.
- [109] C. W. Smith and J. Valcarcel, "Alternative pre-mRNA splicing: the logic of combinatorial control," *Trends Biochem Sci*, vol. 25, pp. 381-8, Aug 2000.
- [110] A. N. Chkheidze, *et al.*, "Assembly of the alpha-globin mRNA stability complex reflects binary interaction between the pyrimidine-rich 3' untranslated region determinant and poly(C) binding protein alphaCP," *Mol Cell Biol*, vol. 19, pp. 4572-81, Jul 1999.
- [111] W. M. Michael, "Nucleocytoplasmic shuttling signals: two for the price of one," *Trends Cell Biol*, vol. 10, pp. 46-50, Feb 2000.
- [112] T. Tomonaga and D. Levens, "Activating transcription from single stranded DNA," *Proc Natl Acad Sci U S A*, vol. 93, pp. 5830-5, Jun 11 1996.
- [113] H. Habelhah, *et al.*, "ERK phosphorylation drives cytoplasmic accumulation of hnRNP-K and inhibition of mRNA translation," *Nat Cell Biol*, vol. 3, pp. 325-30, Mar 2001.
- [114] P. Minoo, *et al.*, "Loss of proliferative potential during terminal differentiation coincides with the decreased abundance of a subset of heterogeneous ribonuclear proteins," *J Cell Biol*, vol. 109, pp. 1937-46, Nov 1989.

- [115] G. Biamonti, *et al.*, "Human hnRNP protein A1 gene expression. Structural and functional characterization of the promoter," *J Mol Biol*, vol. 230, pp. 77-89, Mar 5 1993.
- [116] J. Zhou, *et al.*, "Purification and characterization of a protein that permits early detection of lung cancer. Identification of heterogeneous nuclear ribonucleoprotein-A2/B1 as the antigen for monoclonal antibody 703D4," *J Biol Chem*, vol. 271, pp. 10760-6, May 3 1996.
- [117] S. J. Cok, *et al.*, "The proximal region of the 3'-untranslated region of cyclooxygenase-2 is recognized by a multimeric protein complex containing HuR, TIA-1, TIAR, and the heterogeneous nuclear ribonucleoprotein U," *J Biol Chem*, vol. 278, pp. 36157-62, Sep 19 2003.
- [118] M. Bevort and H. Leffers, "Down regulation of ribosomal protein mRNAs during neuronal differentiation of human NTERA2 cells," *Differentiation*, vol. 66, pp. 81-92, Oct 2000.
- [119] W. H. Mager, "Control of ribosomal protein gene expression," *Biochim Biophys Acta*, vol. 949, pp. 1-15, Jan 25 1988.
- [120] P. Pierandrei-Amaldi and F. Amaldi, "Aspects of regulation of ribosomal protein synthesis in *Xenopus laevis*. Review," *Genetica*, vol. 94, pp. 181-93, 1994.
- [121] S. Curry, *et al.*, "Crystal structure of human serum albumin complexed with fatty acid reveals an asymmetric distribution of binding sites," *Nat Struct Biol*, vol. 5, pp. 827-35, Sep 1998.
- [122] J. S. Stamler, *et al.*, "Nitric oxide circulates in mammalian plasma primarily as an S-nitroso adduct of serum albumin," *Proc Natl Acad Sci U S A*, vol. 89, pp. 7674-7, Aug 15 1992.
- [123] P. Gunning, *et al.*, "Isolation and characterization of full-length cDNA clones for human alpha-, beta-, and gamma-actin mRNAs: skeletal but not cytoplasmic actins have an amino-terminal cysteine that is subsequently removed," *Mol Cell Biol*, vol. 3, pp. 787-95, May 1983.
- [124] R. D. Goldman, *et al.*, "Cytoplasmic fibers in mammalian cells: cytoskeletal and contractile elements," *Annu Rev Physiol*, vol. 41, pp. 703-22, 1979.